Nonequilibrium single electron transport in solvated molecular junctions

Dissertation
zur Erlangung des Doktorgrades
an der Fakultät für Mathematik, Informatik und Naturwissenschaften
Fachbereich Physik
der Universität Hamburg

vorgelegt von

Gregor Gurski

Hamburg

2023

Gutachter der Dissertation:	Prof. Dr. Michael Thorwart Prof. Dr. Peter Nalbach
Zusammensetzung der Prüfungskommission:	Prof. Dr. Michael Thorwart Prof. Dr. Peter Nalbach Prof. Dr. Daniela Pfannkuche Prof. Dr. Henning Moritz Prof. Dr. Michael Potthoff
Vorsitzender der Prüfungskommission:	Prof. Dr. Michael Potthoff
Datum der Disputation:	08.12.2023
Vorsitzender Fach-Promotionsausschuss PHYSIK:	Prof. Dr. Markus Drescher
Leiter des Fachbereichs PHYSIK:	Prof. Dr. Wolfgang J. Parak
Dekan der Fakultät MIN:	Prof. Dr.-Ing. Norbert Ritter

Zusammenfassung

In der vorliegenden Dissertation wird das Zusammenspiel zwischen der molekularen elektronischen Leitfähigkeit und der Reaktion einer Solvens-Umgebung untersucht. Wir stellen ein theoretisches Modell einer molekularen Brücke bereit, welche sich in einem polaren Solvens befindet, das als dielektrisches Kontinuum beschrieben wird. Letzteres bildet eine bosonische Umgebung aus fluktuierenden Polarisationsmoden, welche an ein einzelnes überschüssiges Elektron in der molekularen Brücke zwischen den beiden metallischen Elektroden koppeln. Unsere Schwerpunkte liegen dabei einerseits bei der Untersuchung von reinen Solvenzien und mischbaren binären Solvens-Gemischen, und andererseits bei der Einbindung einer Hydrathülle. Die Hydrathülle besteht aus der ersten Wasserschicht, welche das überbrückende Molekül umgibt und welche andere Eigenschaften besitzt als der Bulk-Solvens.

Mithilfe einer quantenmechanischen, diagrammatischen Realzeit-Technik berechnen wir den elektrischen Ladungsstrom der Brücke in dem sequentiellen Tunnel-Regime, welches eine schwache Kopplung zwischen dem Molekül und den Zuleitungen erfordert. Diese Technik basiert auf der Liouville-Von-Neumann-Gleichung und erlaubt das Lösen der Quanten-Master-Gleichung der reduzierten Dichtematrix des Mölekuls in störungstheoretischer Weise in der Tunnel-Kopplung, bei nichtperturbativer Einbeziehung der elektrostatischen Molekül-Solvens Kopplung bei der Einelektronenübertragung. Um den Solvens zu beschreiben, verwenden wir den Ansatz von Gilmore und McKenzie, welcher auf dem Solvatationsmodell von Onsager basiert. Dieser Ansatz bietet ein probates Mittel zur Bestimmung der Spektraldichte des Solvens, welche in die irreduzible Selbstenergie der Quanten-Master-Gleichung einfließt. Zur Beschreibung von Solvens-Gemischen nutzen wir den Gladstone-Dale-Ansatz, um eine effektive dielektrische Funktion zu bestimmen und einen Ausdruck für die resultierende Spektraldichte von den Polarisationsfluktuationen von binären Solvens-Gemischen aufzustellen. Mit dieser Methode berechnen wir den Leitwert der Brücke in Abhängigkeit von dem Anteil der Solvens-Komponenten und deren chemischer Eigenschaften. Bei Inbezugnahme der gemessenen dielektrischen Konstanten und Debye Relaxationszeiten von reinen Solvenzien sowie der Anpassung des Volumenanteils haben wir eine sehr gute Übereinstimmung zwischen den mithilfe des Modells berechneten und experimentell ermittelten Werten für den nichtlinearen differentiellen Leitwert erhalten. Dieser Ansatz kann ohne Weiteres auf komplexere Solvens-Gemische verallgemeinert werden und bietet somit die Möglichkeit für eine technische Anwendung als Konzentrationssensor auf molekularer Ebene.

Zur Untersuchung der Hydrathülle führen wir eine zeitabhängige Wechselspannung ein. Diese erlaubt es uns im linearen Transport-Regime zu bleiben (lineare Antwort auf ein kleines, externes Potenzial) und einen anderen Kontrollparameter als die Gleich-

spannung für die Untersuchung des Solvens sowohl mit als auch ohne Hydrathülle zu verwenden. Wir führen eine Fourier-Entwicklung der Quanten-Master-Gleichung durch und berechnen die Fourier-Komponenten des Stroms in Abhängigkeit von der Wechselspannungsfrequenz. In Analogie zum Gleichstromfall bei den binären Solvens-Gemischen, zeigen wir, dass der Einfluss der Hydrathülle auf den elektrischen Strom anhand der Spektraldichte beschrieben werden kann, wo die Eigenschaften der Hülle, wie die Dicke oder die dielektrische Funktion, direkt einfließen. Somit bietet der Ansatz ein probates Mittel, um die Dicke der Hülle anhand des Stromes zu bestimmen. Insgesamt haben wir eine theoretische Methode aufgestellt, welche als molekularer Sensor zur Bestimmung der Dicke einer Hydrathülle oder zur Bestimmung des Volumenanteils eines Solvens-Gemisches mit hoher Sensitivität genutzt werden kann.

Abstract

In this thesis, the interplay between molecular electronic conduction and the response of a solvent environment is investigated. We propose a theoretical model of a molecular junction in a polar solvent described as a dielectric continuum. The latter forms a bosonic environment of fluctuating polarization modes which couple to a single excess electron in the molecular junction between two metallic electrodes. Our focus areas are, on the one hand, the investigation of pure solvents and miscible binary solvent mixtures, and on the other hand, the incorporation of a hydration shell. The hydration shell consists of the first water layer surrounding the bridging molecule in the junction and has distinct properties different from the bulk solvent.

Using a quantum mechanical real-time diagrammatic technique, we calculate the junction's electric charge current in the sequential tunneling regime which requires a weak coupling between the molecule and the leads. This technique is based on the Liouville-von Neumann equation and allows to solve the quantum master equation of the reduced density matrix of the molecule in a perturbative manner in the tunnel coupling to the metallic leads, while including the electrostatic molecule-solvent coupling in the single electron transfer nonperturbatively. In order to describe the solvent, we employ an approach by Gilmore and McKenzie which is based on the Onsager model of solvation. This approach presents a valid means to determine the spectral density of the solvent which enters the irreducible self-energy of the quantum master equation. For the description of solvent mixtures, we use the Gladstone-Dale approach to determine an effective dielectric function and propose an expression for the resulting spectral density of the polarization fluctuations of binary solvent mixtures. With this methodology, we calculate the junction's conductance in dependence on the fractional ratio of the solvent constituents and their respective chemical properties. Utilizing the measured dielectric constants of pure solvents as well as their respective Debye relaxation times together with tuning the volumetric fraction, we have obtained a very good agreement of the nonlinear differential conductance either calculated by the proposed model and experimentally measured conductance values. The approach can readily be generalized to more complicated mixtures of solvents, giving rise to technical applications as concentration sensors on the molecular scale.

For the investigation of the hydration shell, we introduce a time-dependent ac voltage. This allows us to stay in the linear transport regime (linear response to a small external potential) and use a different control parameter than the applied dc voltage to study the influence of the solvent with and without hydration shell. We Fourier expand the quantum master equation and calculate the Fourier components of the current in dependence of the ac frequency. In analogy to the dc case for binary solvent mixtures, we show that the influence of the hydration shell on the electric current can

be captured by a spectral density where the shell properties, i.e., its thickness or its dielectric function, directly enter. Interestingly, the Fourier components of the charge current for different applied ac voltage frequencies portray a nonlinear behavior when altering the thickness of the hydration shell. Therefore, the approach provides a valid means to determine the thickness of the shell through the current. In total, we have established a theoretical methodology that may be applied for a molecular sensor to determine the thickness of a hydration shell or the volume fraction of a solvent mixture with high sensitivity.

Contents

Chapter 1.

Introduction

The miniaturization of electronic devices remains an enormous challenge. To this end, the field of molecular electronics has made considerable progress in recent years where it is now routinely possible to wire an organic molecule, an object as small as 1 nm, between two metallic leads and measure its electronic transport characteristics [1]. Generally, the concept of electrons moving through single molecules comes in two different guises. The first involves a charge moving from one end of the molecule to the other and the second involves current passing through a single molecule that is strung between electrodes. The two are closely related because they both attempt to answer the same fundamental question: How do electrons move through molecules [2]? Understanding the motion of electrons to and through a single molecule is central to the field of molecular electronics. The field dates back to 1974, when Aviram and Ratner first proposed the idea of utilizing single organic molecules as rectifiers [3]. Since then, there have been dramatic advances toward the realization of electronic transistors integrated on the molecular scale [4]. As a vital component of molecular electronics, single molecular junctions have attracted significant attention both in theory and experiment [1, 5]. Experimentally and theoretically, it has been shown that there are two limiting cases of charge transfer through molecular junctions according to the two mentioned guises. (1) Charge transmission via elastic coherent scattering from one lead to the other [6–11]. (2) Charge transfer via sequential tunneling due to strong localization induced by a thermal environment and the decoherence of the electron's wave function. The second has vital applications in single molecular junctions in electrochemical environments at room temperature while recent studies investigate the partial decoherence of the electron wave function combining both limiting cases [12,13].

Not only was the first single-molecule transistor fabricated already in 2000 [14] but single-molecule junctions have been realized as rectifiers [15], switches [16], sensors [17, 18] and have recently attracted much attention due to their promising thermoelectric properties [19–21]. Moreover, single molecular junctions provide a unique platform for simultaneous investigation, manipulation, detection, and stimulation of chemical reactions [22]. Usual realizations of electro-chemical charge transmission consider single molecular junctions as immersed in solution. The inclusion of the bridging molecule into the (bulk) solvent alters the interacting network between the solvent molecules in proximity of the introduced molecule. Thus, the solvent molecules must build stronger bonds among each other and/or the junction molecule and form a sol-

vation shell with distinct properties different from the bulk solvent [23–25]. Therefore, on the one hand, the type of the surrounding solvent can play a significant role on the transport properties of single-molecule junctions [26–28]. On the other hand, the formation of a solvation shell can further drastically change the electronic conductance of a metal-molecule-metal junction by up to two orders of magnitude [29].

Theoretical description of the influence of the solvent on the transmission properties has so far relied on utilizing density functional theory (DFT) calculations for the molecular orbitals when placing few, i.e., 1-2, water molecules in the vicinity of the bridging molecule [29]. Their rigorous but calculationally involved outcome have predicted the influence of polar solvents and the hydration shell on the charge transmission through molecular junctions [29, 30]. Contrary to these numerically expensive calculations, the present thesis aims to provide a theoretical model based on few coarse grained solvent and shell parameters, like the dielectric properties and the shell thickness, to determine the role of a solvent, and mixtures thereof, as well as the solvation shell on charge transport properties of a molecular junction.

The transport theory presented here is based on a real-time diagrammatic approach [31–35] closely related to path-integral methods formulated in connection with dissipation [36–38]. The idea is to integrate out the environment degrees of freedom and to set up a formally exact quantum master equation for the reduced density matrix of the molecule. The kernel of this integro-differential equation is represented as a sum over all irreducible diagrams and can be calculated in a systematic perturbation expansion in tunneling [35]. The lowest order of this perturbation expansion represents the sequential tunneling regime. It describes single-electron tunneling processes through molecule states and is valid when the coupling between the molecule and the electrodes is weak. It is important to notice that the master equation within the sequential tunneling regime is a perturbative approach only in the coupling to the electrodes, but it includes the electrostatic molecule-solvent coupling non-perturbatively [35]. The overall goal of this theoretical framework is to find a valid means by which characteristics of the solvent surrounding the molecule will be made visible via electron transport properties, e.g., via the tunneling current or the differential conductance. Such a tool in turn gives rise to possible applications of a molecular junction acting as a sensor model measuring, e.g., the volume fraction of solvent mixtures or the thickness of a hydration shell.

Having this in mind, we present in Section 1.1 a brief overview of the experimental techniques that led up to the establishment of molecular electronics as a solid field of science and that are currently being used to fabricate both atomic-scale wires and molecular junctions. In the subsequent Section 1.2, we collect theoretical approaches utilized for the description of transport mechanisms in nanoscale systems. In the last section of this introduction we outline the structure of this thesis.

1.1. Experimental techniques

As for many other fields in nanoscience, the invention of the scanning tunneling microscope (STM) by Gerd Binnig and Heinrich Rohrer (at IBM Zurich) in 1981 [39, 40], for

which they were awarded the Nobel prize in 1986, changed the panorama for molecular electronics. The STM was the first tool that provided a practical way to 'visualize' and manipulate matter at the atomic scale. Soon after its invention, it became clear that the STM could provide a realistic way to address single molecules and to study their electronic transport properties [41]. The discovery of the STM has also inspired many related scanning probe microscopy tools, which measure a great variety of properties with atomic resolution [42]. The most important probe is the Atomic Force Microscope (AFM).

While in the application of an STM a fine metallic tip is held at a distance from a counter electrode (in general a metallic surface) by making use of the exponential distance dependence of the tunneling current, an AFM uses the distance dependence of the force between tip and surface instead of the tunnel current. Depending on the chemical nature of both the tip and the surface this force consists of several contributions and its distance dependence may be complex and even nonmonotonic [41]. One advantage of AFM as compared to STM is that it allows the study of poorly conducting or isolating surfaces. It has also been used for the study of such problems as the forces required for unfolding an individual protein molecule [43]. The latter example also illustrates an important aspect of these tools: Apart from imaging atoms at the surface of a solid, it is possible to manipulate individual atoms and molecules [44]. In 1992 in Leiden [45] a new technique was introduced by Muller et al. dedicated to the study of atomic sized junctions, baptized the Mechanically Controllable Break Junction (MCBJ) technique, based on an earlier design by Moreland and Ekin [44,46]. The principle of this technique is schematically illustrated in Fig. 1.1.

Different groups showed that the STM and the MCBJ technique could be used to fabricate metallic wires of atomic dimensions [44]. Since then these nanowires have become an endless source of new physical phenomena and have played a crucial role in the fields of mesoscopic physics and nanoelectronics. The relevance of these systems for molecular electronics is two-fold. On the one hand, they provide the basis to contact individual molecules with dimensions on the range of a few nanometers, which is out of the scope of conventional lithographies. On the other hand, the atomic contacts have allowed establishing the connection between the quantum properties of single atoms and the macroscopic electrical properties of the circuits in which they are embedded, which is an important lesson for molecular electronics [41].

At the end of the 1990's and the beginning of the 21st century new experimental techniques were introduced and additional results were reported showing that molecules can indeed mimic the behavior of ordinary microelectronics components [41]. Thus for instance, the so-called nanopore technique was utilized to show that junctions based on certain organic molecules can exhibit, for example, a very pronounced negative differential resistance [47]. Techniques like electromigration [48], which were specially designed to contact single molecules, made possible to incorporate a gate electrode in single-molecule junctions and thus, to mimic the measurements performed in solid state devices like transistors or in nanostructures like quantum dots. The term electromigration denotes a process in which ions are moved due to high electrical current densities. It has been understood that several effects contribute to the total force

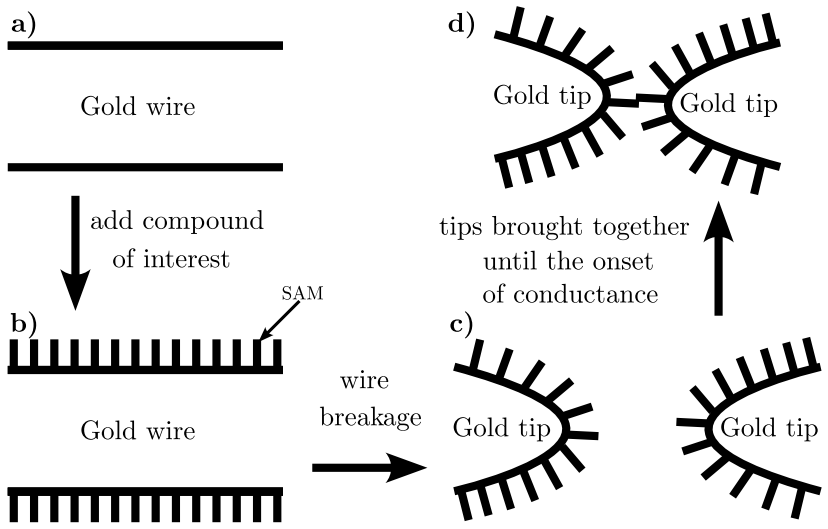

Figure 1.1.: Schematics of the principles of the mechanically controllable break junction (MCBJ) technique. a) The gold wire of the break junction before breaking and tip formation. b) After addition of the compound of interest, self-assembled monolayers (SAMs) form on the gold wire surfaces. c) Mechanical breakage of the wire produces two opposing gold contacts that are SAM-covered. d) The gold contacts are slowly moved together until the onset of conductance is achieved [41].

acting on a metal atom which forms the conductor, the two most important being the so-called direct force due to the electric field. It causes the electrical current and thus points into the direction of the field. The second one is caused by momentum transfer of the conduction electrons onto the ions. It has opposite sign and is called the wind force. When the total force overcomes the binding force of the ions, they start to diffuse but can be pinned again at defects or positions where the current density and driving force falls below this threshold value [41].

An important difference to STM techniques and MCBJs is the fact that the wire forming the contact is in solid contact with a substrate. The advantage lies in the fact that no particular requirements exist for the properties of the substrate, besides the fact that it should be sufficiently insulating. Often silicon - the standard substrate in microelectronics - is used. With suitable doping it can be used as back-gate for inducing an electric potential and building a three-terminal device [41]. The fabrication process of a three-terminal device needs to ensure that the gate couples only electrostatically to the molecule. This can be achieved by electrically insulating the gate from the source/drain electrodes and from the molecule. However, parasitic currents caused by various mechanisms (quantum tunneling, electron hopping, etc.) can lead to a current between the gate and the drain. This gate leakage can overshadow the molecular signature, and should therefore be kept as low as possible [49]. A further drawback of the electromigration technique is the fact that it is a single-shot experiment: Once an atomic contact has been established there is only limited possibility to fine tune its atomic configuration, in particular coming back to a larger contact

is almost impossible. After burning through the wire it cannot be closed again. A combination of electromigration with the lithographic MCBJ technique can overcome the latter problem: A thin-film MCBJ is thinned-out by electromigration to a narrow constriction with a cross section of a few nanometers. The substrate is then bent carefully for completely breaking the wire or arranging single-atom contacts. This last step is reversible and repeatable for studying small contacts or trapped nanoobjects [41].

However, the technical challenges remain for the integration of an additional gate electrode due to current leakage. To address this issue, solvent gating has been considered as a potentially simple method to continuously fine-tune the charge transport through single-molecule junctions. A strong influence of the surrounding solvent on the charge transport was recently reported for certain organic molecular junctions with different anchoring groups in various solvent environments using the MCBJ technique [27]. The molecular conductance was shown to be tunable by nearly an order of magnitude by varying the polarity of solvent. Furthermore, gating efficiency due to solvent-molecule interactions was found to depend on the choice of the anchor group.

With the use of the introduced experimental techniques it was possible to show, for example, that single-molecule junctions can exhibit physical phenomena like Coulomb blockade or the Kondo effect [50], which are well-known in the context of other nanoscopic structures. Manifold variations of these techniques exist (in addition to other, not mentioned techniques in this brief overview) that are permanently improved and extended to study various additional properties related to molecular electronics [41].

1.2. Theoretical approaches

The theoretical treatment of transport at nanoscale requires the combined use of different approaches and approximations, where we will briefly outline some of the main concepts following Ref. [51].

The Landauer-Büttiker (LB) [6–11] method (also known as the scattering method) establishes the relation between the wave functions (scattering amplitudes) of electrons in a quantum junction and the conducting properties of this junction. The method can be applied to find the current through a noninteracting system or through an effectively noninteracting system, for example if the meanfield description is valid and the inelastic scattering is not essential. Such type of an electron transport is called coherent, because there is no phase-breaking and quantum interference is preserved during the electron motion across the system [51].

The notion of coherent or incoherent transport pertains to an independent particle description of the electrons where they occupy one-particle orbitals. In the case of coherent transport, the phase of the orbitals evolves deterministically. In the case of incoherent processes, the phase changes in an unpredictable way due to interactions which are not contained in the independent particle Hamiltonian. Such interactions can be electron–electron interaction, or electron–phonon interaction, or the interaction between the electrons and an electromagnetic field. If the electrons spend a long

time on the molecule, which happens when the couplings to the leads are weak, the decoherence will be complete. Only for short traversal times, the phase will be well preserved. Another distinction is that between elastic and inelastic transport. In the latter case, interactions may cause energy loss or gain of the electrons flowing through the device. This energy change may be caused by the same interactions as those causing decoherence. Note, however, that incoherent transport can still be elastic [52].

Coherence is assumed in many ab-initio based transport methods using the DFT and Landauer approach, so that the LB method is now routinely applied to any basic transport calculation through nanosystems and single molecules. Besides, it is directly applicable in many semiconductor quantum dot systems with weak electron-electron interactions. Due to simplicity and generality of this method, it is now widely accepted and is in the base of our understanding of coherent transport [51].

However, the peculiarity of single-molecule transport is the essential role of electron-electron and electron-phonon interactions, so that the LB method is usually not enough to describe essential physics even qualitatively. During last years many new methods were developed to describe transport at finite voltage, with focus on correlation and inelastic effects, in particular in the cases when Coulomb blockade, Kondo effect and vibronic effects take place. Among others, there are two very well established theoretical frameworks that can be used to study quantum transport with interactions and at finite voltage: Quantum master equation and nonequilibrium Green function techniques.

The quantum master equation (QME) [38] describes the time evolution of the reduced density matrix or density operator of the molecule and is usually formulated in the basis of the eigenstates of the molecule. It gives a fairly complete description of sequential tunneling, the main features of Coulomb blockade and even can capture Kondo physics for temperatures of the order of or larger than the Kondo temperature [34]. The QME technique leads to more simple "classical" master equations in the case where (i) the electrode-system coupling can be considered as a weak perturbation, and (ii) off-diagonal elements of the reduced density matrix in the eigenstate representation (coherences) can be neglected due to very short coherence times [51].

The nonequilibrium Green function (NGF) formalism was developed independently by Kadanoff and Baym [53] and Keldysh [54] about 60 years ago. It is able to deal with a very broad variety of physical problems related to quantum transport. Since its appearance, it has been used successfully in the theory of nonequilibrium superconductivity [55], and later was proposed as a standard approach in mesoscopic physics and molecular electronics. In particular, an elegant approach was formulated by Meir, Wingreen and Jauho [56–58], who derived an exact expression for nonequilibrium current through an interacting nanosystem placed between large noninteracting leads in terms of the nonequilibrium Green functions of the nanosystem. Still, the problem of calculation of these Green functions is not trivial [51].

Both approaches, the QME and NGF techniques, can yield formally exact expressions for many observables. For noninteracting systems, one can even solve many models analytically. However, once interactions are introduced—and these are the most

interesting cases containing a very rich physics—different approximation schemes have to be introduced to make the problems tractable [51].

We apply the QME for the investigation of the current and the nonlinear differential conductance through a molecular junction which is embedded in a polar solvent. We use a weak coupling approximation between the leads and the molecule but we do not neglect off-diagonal elements of the reduced density matrix. Our approach is based on the Liouville-von Neumann equation and was developed by König, Schoeller and Schön [31–34] in the middle of the 1990's. They formulated a real-time diagrammatic technique which allows a systematic application of the QME in a perturbative scheme in the tunneling. Each tunneling process can thereby be represented as a diagram where the number of inseparable tunneling processes corresponds to the order of tunneling. With this technique they calculated, for example, the conductance through a single-electron transistor by incorporating second-order tunneling, i.e., cotunneling, and found quantitative agreement with experiments [59, 60].

In order to take the influence of the solvent surrounding the molecule into account we use a reduced description based on the Onsager continuum model of solvation. In 1936, Lars Onsager was the first who has effectively described the polarization of the solvent as back action on the solute dipole moment by means of a fluctuating force field, the reaction field [61]. His concept of molecular dipole moments acting on the continuum dipolar solvent with a resulting back action opened up the way to describe the solute dynamics quantum mechanically, e.g., as a two level system with distinct dipole moments for the ground and excited states [62,63]. Central macroscopic properties such as the dielectric constants and the relaxation time of the solvent, which are all experimentally measurable, enter in that model. Although this model does not include the microscopic details of the solvent, it captures the essential low-energy physics of the solvation process in the regime of long polarization wavelengths [62, 64, 65]. In order to describe binary solvent mixtures we exploit the simplest approach of Gladstone and Dale [66] for its effective dielectric function which includes the relative concentrations of a host and an inclusive solvent together with the respective dielectric permittivities. With this approach we derive a spectral density of the solvent mixture on the basis of the calculations by Gilmore and McKenzie [62]. They determined the spectral density within the Onsager continuum model of solvation and also extended this model to include a thin shell of bound water, the hydration shell [67].

The concept of a hydration shell has been employed to describe the peculiar properties of water directly next to biomolecules and biomolecular ensembles such as membranes. The hydration shell consists of the first water layer–or sometimes the first few water layers–surrounding the biomolecule and interacting with it or at least noticeably influenced by it. The structure and function of biomolecules are strongly influenced by their hydration shells. Structural fluctuations and molecular excitations of hydrating water molecules cover a broad range in space and time, from individual water molecules to larger pools and from femtosecond to microsecond time scales [68]. Therefore, the solvent molecules close to the junction molecule display distinct properties different from the bulk solvent [23–25]. On the other hand, the aqueous environment "sufficiently" far from the biomolecular surface should display properties of bulk-like

water [68]. We show that the influence of the hydration shell on the electric current through a solvated molecular junction can be captured by a spectral density where the shell properties, i.e., its thickness or its dielectric function, directly enter.

We emphasize that the list of theoretical methods mentioned so far is far from exhaustive and, like in the case of experimental techniques, many variations and adaptations of these methods exist which are constantly improved and extended to incorporate the description of additional properties related to molecular electronics.

1.3. Structure of this thesis

The outline of this thesis is as follows. Chapter 2 is an introduction to the general concept of charging effects in transport through nanoscale devices. We discuss the circumstances and relevant scales, such as the size of the nanodevice or the temperature, for observing effects due to the discrete nature of charge. To this end, we use a description of electronic circuits which include the single-molecule device. After we have identified the conditions for the occurrence of charging effects, we introduce the starting point, given by a model Hamiltonian, of our description of a molecular junction immersed in a solvent in Chapter 3. There we present a suitable theoretical description to characterize the main properties of the involved constituents and their interactions contributing to the current through the junction. A real-time transport theory adapted to our model is then derived in Chapter 4. We use a diagrammatic technique in which each diagram can be interpreted physically as a particular tunneling process. With this technique we solve the quantum master equation in the sequential tunneling regime and derive an expression for the stationary tunneling current.

In Chapter 5 we focus on the dielectric solvation dynamics involving charged and polar solutes in dielectric environments. We consider a polar solvent characterized by its dielectric response function. We describe the relaxation process due to a sudden change in the charge distribution inside the solvent in terms of this dielectric function. To do so, we use linear dielectric response theory and utilize the Debye model. For homogeneous and isotropic systems we recapitulate the relations between the polarization, displacement and electric field from textbook. Furthermore we show how polar solvents can be modeled as harmonic environments in which the harmonic modes are motions of the polarization field. We also derive the spectral density both for a single solvent and solvent mixtures by describing the solvation process by the Onsager model and the concept of Gilmore and McKenzie. For solvent mixtures we additionally incorporate the approach of Gladstone and Dale for an effective dielectric function. In the last section of this chapter we present the results generated on the basis of the theoretical analysis described to this point. We begin by reproducing well-known results within the field of electron transport theory in order to give an overview of possible observations with our model. Then we demonstrate how pure solvents affect the current as well as the nonlinear differential conductance. Additionally, we investigate the temperature dependence of the differential conductance. Our main results in this chapter are differential conductance calculations for binary solvent mixtures,

including a promising comparison to experimental data [69].

Chapter 6 is devoted to the description of time-dependent transport. In order to investigate novel transport characteristics while staying in the linear transport regime (linear response to a small external potential), we introduce a time-dependent ac voltage. By Fourier expanding the quantum master equation, the electric current can then be expressed by its Fourier components. Our goal is to incorporate the influence of the hydration shell on the transport characteristics. Similar to the solvation description of solvent mixtures, the spectral density of the hydration shell can be captured via an extended Onsager model. Here our main results are calculations of the Fourier components of the current with respect to the hydration shell thickness [70]. We also find the same qualitative behavior for the first Fourier component with respect to the volume fraction of a solvent mixture as for the nonlinear differential conductance in the dc case. The main difference is that we are here in the linear transport regime and still find that the current is highly sensitive to both the volume fraction and the individual solvents themselves. These results can be easily extended to photon-assisted electron transport in molecular wires given its mathematical form as under ac driving.

Finally, Chapter 7 concludes the thesis and provides an outlook. Two Appendices A and B are included containing a detailed analysis of a contour integration needed in Chapter 4 and a table of the experimentally measured dielectric solvent parameters used for the numerical results, respectively.

Chapter 2.

Theoretical background

In this chapter we describe the fundamental physical principles and theoretical prerequisites underlying the modeling of single molecules that are trapped between two or three electrodes, as laid out in Refs. [35, 41, 52, 71–76]. The modeling concept is based on the assumption that the accumulation of charge on the single molecule can be represented by a capacitive circuit model. To make modeling possible on the level of circuits, we have to translate the physical or electrochemical quantities–such as charge, Coulomb energy, electrostatic charging energy, addition energy, or energy levels–to the circuit quantities, charge, voltage difference, potential, current, and energy [75]. To this end, we consider in the following single-electron transport through a tunnel barrier, i.e., quantum tunneling, and Coulomb blockade physics.

2.1. Quantum tunneling and Coulomb blockade

We examine a single molecule connected between a source and a drain electrode, while a third electrode–the gate electrode–is only capacitively coupled to the molecule, see Fig. 2.1 for a schematic sketch. The gate electrode enables us to tune the energy level spectrum of the molecule and in turn allows us to control the current that flows through the system by an external field, very much like in the case of field-effect transistors in microelectronics. Due to this analogy and also to the fact that the transport is usually dominated by single-electron processes, these systems are known as single-molecule transistors (SMTs) or single-electron transistors (SETs), when a quantum dot is located between source and drain instead of a molecule [41]. A quantum dot is, e.g., a semiconductor nanostructure with very small spatial dimension, therefore exhibiting a discrete energy spectrum just like that of an atom or molecule. Now, an important and distinguishing property of single molecules in solid-state devices is the strength of the coupling between the electrons in the electrodes (or leads) and the electrons in the molecule. If the coupling is weak, it is possible to describe all electrical properties of the system with well-defined energy levels and well-defined voltages across the molecule and the respective electrodes [75].

It is important to mention that any modeling effort of real devices involves a theoretical framework on a certain level. At the lowest modeling level, the transport of electrons from the source to the molecule and from the molecule to the drain can be described by quantum mechanical tunneling. There, the interface between the leads

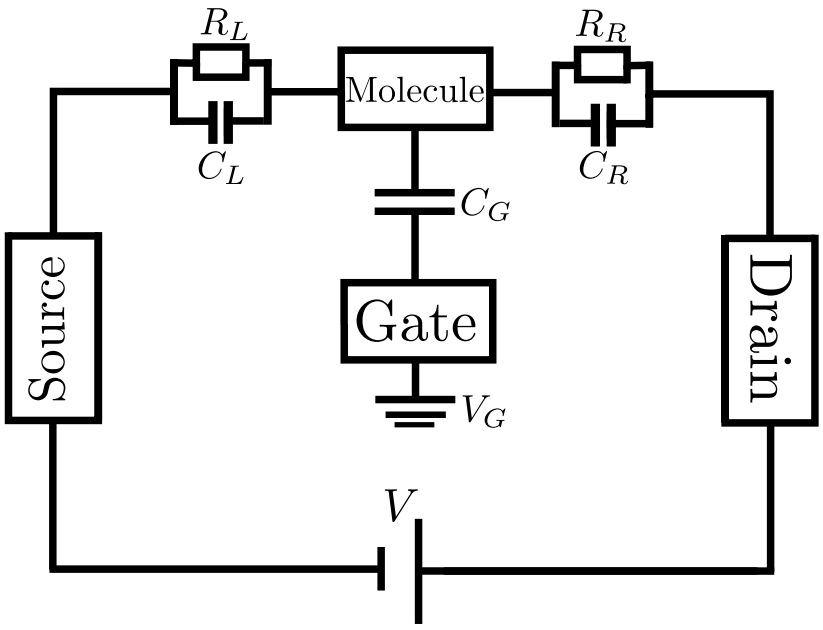

Figure 2.1.: A schematic three-terminal molecular junction or single-molecule transistor, made of a molecule that is connected between a source and a drain electrode, with a third electrode that functions as a gate.

and the molecule acts as tunneling barriers. Due to their wave nature, electrons can tunnel through these potential tunneling barriers, even if the total energy of an electron is smaller than the energy needed to overcome the barrier in a classical way. By tunneling through the barriers from source to drain, the electrons create a current flow when a sufficiently large voltage is applied. Weak coupling allows a description in terms of a two-step process in which an electron first tunnels from the source to the molecule, and then tunnels from the molecule to the drain [75]. This is called sequential tunneling or single-electron tunneling.

At the modeling level above this, phenomena are described by classical physics, such as thermodynamics. This is the level at which Coulomb blockade can be described as a condition that relies on the reduction in the free (electrostatic) energy of the system as a result of the tunneling event [75]. Coulomb blockade is an electronic phenomenon that describes the suppression of current flow through the molecule due to the electrostatic (Coulomb) repulsion between electrons occupying the molecule. This phenomenon is generally associated with the quantization of charge, i.e., tunneling can be done only by whole electrons. To overcome the Coulomb blockade, the so-called addition energy E_{add} has to be provided by energy sources in the electronic circuitry that excites the trapped molecule. The expression for the addition energy consists of two terms: The first term is the charging energy E_{ce} associated with the energy necessary to bring a single electron on a classical metallic island in between the leads. The second term is the quantum kinetic energy ΔE due to the fact that we are dealing with a molecule having well-separated energy levels instead of the dense spectrum of

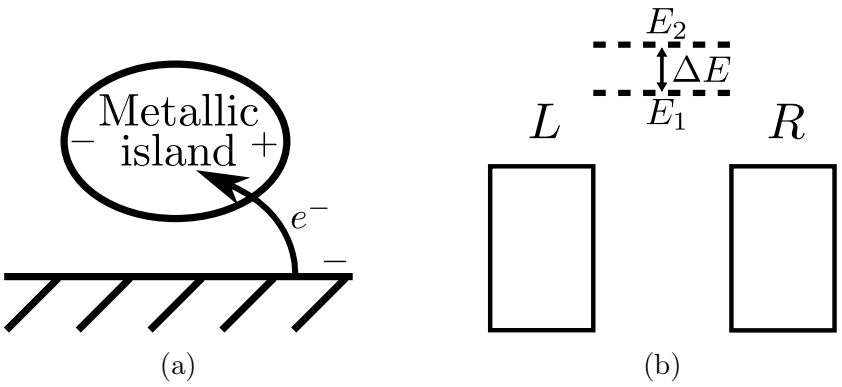

Figure 2.2.: (a) Tunneling of an electron toward an isolated metallic island. (b) Two-level model to illustrate the transport characteristics in the Coulomb blockade regime as presented in Ref. [41].

a large metallic island [75]. The addition energy then is

$$E_{add} = E_{ce} + \Delta E\,. \tag{2.1}$$

In order to determine the charging energy E_{ce} let us consider an isolated metallic island embedded in an insulating medium, see Fig. 2.2 (a). The number of elementary particles in the island must be integer. Thus, its charge Q must be an integer amount of elementary charges, $Q = eN$, with N being the number of excess electrons in the island [73]. We can view the system as a single capacitance C, in which the island forms one electrode of this capacitor and the environment forms the other electrode. Both sides of the capacitor are not connected [75]. The induced electrostatic capacitive charge for a capacitor is given by

$$q = CV\,, \tag{2.2}$$

where V is the voltage between both sides of the capacitor. Notice that the induced charge q is not the charge of a particle and therefore, in contrast to the charge transfer from and to the molecule or its occupation number, is not a quantized number [74]. Transporting additional charge (dq) to another plate of a capacitor requires the electrostatic work

$$E_{pot} = \int V dq = \int \frac{q}{C} dq \tag{2.3}$$

against the applied voltage [35, 76]. For the total charge Q, the work performed can be determined as

$$E_{pot} = \frac{1}{C}\int_0^Q q dq = \frac{Q^2}{2C} = \frac{e^2}{2C}N^2 = E_C N^2\,. \tag{2.4}$$

The increase in energy when an electron is added to this island, to which already N electrons have been tunneled, is called the single-electron charging energy $E_{ce}(N)$ [75].

$$E_{ce}(N) = \frac{((N+1)e)^2}{2C} - \frac{(Ne)^2}{2C} = \frac{e^2}{2C}(2N+1)\,. \tag{2.5}$$

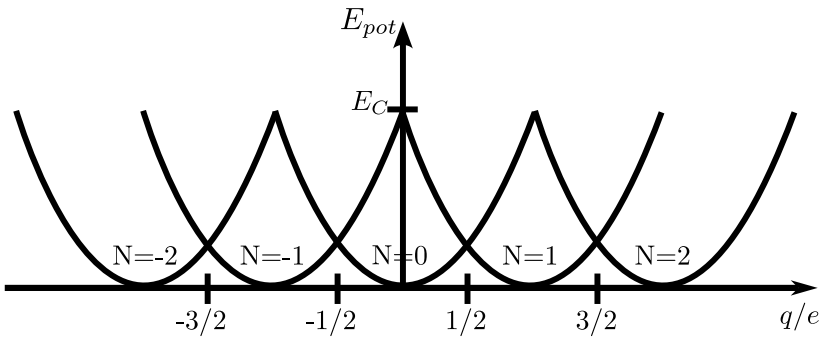

Figure 2.3.: The electrostatic energy within the capacitive circuit model for different particle numbers N as presented in Ref. [35]. At the intersection point of two adjacent parabolas transport is possible.

For initially uncharged islands, the expression for the single-electron charging energy $E_{ce}(N = 0)$ is called the Coulomb energy E_C:

$$E_C = \frac{e^2}{2C} \,. \tag{2.6}$$

Often the Coulomb energy is interpreted as the energy barrier felt by a single electron moving onto an electrically neutral island. That is, tunneling is forbidden until this barrier can be surmounted when an energy source is applied that provides enough energy during tunneling. A Coulomb blockade exists if enough energy is not supplied [75].

Let us return to our three-terminal molecular junction from Fig. 2.1. There, the total capacitance of the SMT is given by $C = C_L + C_R + C_G$, where C_L, C_R and C_G are the capacitances of the source, drain and gate electrode, respectively. The induced charge in this case is $q = C_L V_L + C_R V_R + C_G V_G$, where V_L, V_R and V_G denote the potential shift for the source, drain and gate electrode, respectively. The electrostatic work required then becomes [35, 74]

$$E_{pot}(Q = eN) = E_C(N - q/e)^2 \,. \tag{2.7}$$

The system tries to minimize its electrostatic energy. Therefore, the integer particle number N tends to be as close as possible to the continuous variable q/e. As a consequence, the particle number can be controlled in discrete units by varying q/e via the gate voltage V_G. For half-integer values of q/e, two adjacent particle numbers $N = q/e \pm 1/2$ lead to the same electrostatic energy and transport is possible, see Fig. 2.3. Away from the degeneracy points, transport is suppressed up to smearing due to temperature, bias voltage and quantum fluctuations [35]. This is again the Coulomb blockade phenomenon. The system is called transistor since by tuning the gate voltage V_G the current can be switched on and off [72].

So far we have considered only the Coulomb interaction and neglected the energy level spacing ΔE, i.e., the separation between discrete energy states, of the molecule.

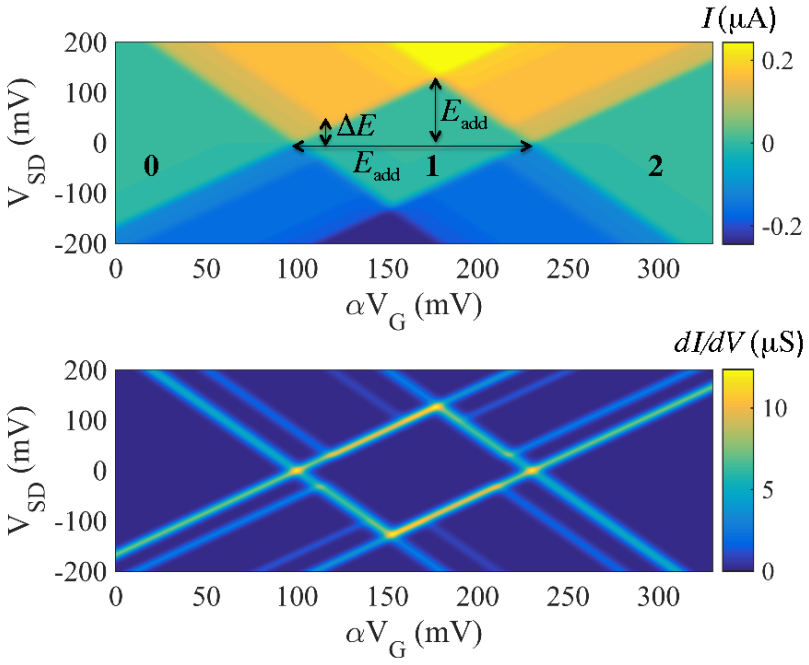

Figure 2.4.: Calculated stability diagrams corresponding to the two-level system of Fig. 2.2 (b). Top: Current vs. gate voltage and source-drain (or bias) voltage. Bottom: Differential conductance vs. gate voltage and source-drain voltage. The picture is taken from Ref. [41].

In order to illustrate the consequences from the single-particle states of the molecule let us have a look at an example of a two-level system as presented in Ref. [41]. The system has two non-degenerate single-particle levels with energies $E_1 = 50$ meV and $E_2 = 80$ meV, which are measured with respect to the equilibrium chemical potential of the leads (set to zero), see Fig. 2.2 (b). The charging energy is assumed to be $e^2/C = 100$ meV, which in this case is larger than the excitation energy $\Delta E = E_2 - E_1 = 30$ meV. The temperature is $k_\mathrm{B}T = 2.5$ meV (i.e., $T \approx 30$ K) and the tunnel barriers are identical for the left (L) and right (R) lead.

When we consider the energy configuration illustrated in Fig. 2.2 (b), the current is suppressed, in the weak coupling regime and at low temperature, when all chemical potential levels lie outside of the bias window. As we can tune the location of these levels using the gate voltage V_G, it is interesting to study the current I and the differential conductance dI/dV of the device as a function of the bias voltage V_{SD} and V_G. A two-dimensional plot of the current or conductance as a function of the two voltages is often referred to as stability diagram [41]. Figure 2.4 shows the stability diagrams of the two-level system from Fig. 2.2 (b). Each level resonance generates two straight lines in the V_{SD}-V_G plane, separating regions of suppressed current from those with finite current. The resulting diamond-shaped regions are traditionally called Coulomb diamonds, as they are often studied in the context of metallic dots, where

the chemical potential difference of the levels is mainly made up of the Coulomb energy. The name is also used in molecular transport, although this is strictly speaking not justified since in this case the level spacing can be of the same order as the Coulomb interaction [41].

Nevertheless, one can infer valuable information from the Coulomb diamond picture. Thus for instance, the addition energy, see Eq. 2.1, can be read off from the height of the diamond or from the distance of the degeneracy points. Additionally, excitations appear as lines running parallel to the Coulomb diamond edges. At such a line, a new excited state enters the bias window, creating an additional transport channel. The result is a step-wise increase of the current and a corresponding peak in the differential conductance. The energy of an excitation, ΔE in Fig. 2.4, can be determined by reading off the bias voltage of the intersection point between the excitation line and the Coulomb diamond edge [41]. The width of the lines in the dI/dV plot (or, equivalently, the voltage range over which the step-wise increase in the current occurs) is determined by temperature and the coupling strength between the leads and the two-level system [52]. There are other important issues like the size of the diamonds or the role of the asymmetry in the coupling that can be discussed at a qualitative level. We refer to Refs. [41, 52] for more details.

In this thesis we focus on the level spacing of the molecule, in particular on the energy difference between the highest occupied molecular orbital (HOMO) and the lowest unoccupied molecular orbital (LUMO). The excitation energy ΔE will be simply a single-level energy ε_d given with respect to the Fermi energy of the leads. Furthermore, we will neglect electron-electron interactions. Our focus lies on the determination of solvent and solvation shell influences on the electron transport through the molecule. Therefore, our stability diagrams will not contain the Coulomb diamonds, see Fig. 5.3 (a) in the Results and discussion chapter. However, given the electrostatic interaction between solvent molecules and conducting molecule, the solvent can shift the level energy ε_d and, thus, can have the same effect as a gate potential.

2.2. Charging effects in transport through nanoscale devices and higher order tunneling

In this section we examine the circumstances under which single-electron charging effects are important in the transport through small devices. In other words, following Refs. [41,71] we want to address the following question: How small and how cold should a conductor be so that adding or subtracting a single electron has a measurable effect? To answer this question, let us consider again the three-terminal molecular junction from Fig. 2.1, where we have already established the charging energy $\propto e^2/C$ with the total capacitance C. The charging energy becomes important when it exceeds the thermal energy $k_{\mathrm{B}}T$ [41, 71].

A second requirement to observe charging effects is that the barriers are sufficiently opaque such that the electrons are located either in the source, in the drain, or on the

molecule. This means that quantum fluctuations in the number N due to tunneling through the barriers are much less than one over the time scale of the measurement. (This time scale is roughly the electron charge divided by the current.) This requirement translates to a lower bound for the tunnel resistances R_t of the barriers. To see this, consider the typical time to charge or discharge a capacitor $\Delta t = R_t C$. The Heisenberg uncertainty relation: $\Delta E \Delta t = (e^2/C) R_t C > h$ implies that R_t should be much larger than the resistance quantum $h/e^2 = 25.813$ kΩ in order for the energy uncertainty to be much smaller than the charging energy [41, 71]. To summarize, the two conditions for observing effects due to the discrete nature of charge are [41, 71]

$$R_t \gg h/e^2 \quad \text{and} \quad e^2/C \gg k_\mathrm{B}T\,. \tag{2.8}$$

The first criterion can be met by weakly coupling the small object to the source and drain leads. The second criterion can be met by making the object small or by lowering the temperature [41, 71]. Let us recall that the capacitance of an object scales with its radius r and for a sphere, $C = 4\pi\varepsilon_0 r$. Thus for instance, the charging energy of a C_{60} molecule, which has a radius of $r \sim 4$Å, can be estimated to be $e^2/4\pi\varepsilon_0 r \sim 3.6$ eV. This indicates that charging effects can in principle be readily observed in single-molecule junctions even at room temperature ($k_\mathrm{B}T = 25$ meV), as long as the molecules are weakly coupled to the electrodes [41, 71].

As discussed in the previous section, when it comes to charging effects, an important energy scale is the energy level spacing ΔE in the molecule, i.e., the separation between the discrete energy states of the small conductor. To be able to resolve these levels, the spacing must be much larger than $k_\mathrm{B}T$. In the case of molecular junctions, the spacing ΔE, which is basically the HOMO-LUMO gap, is typically of the order of several electronvolts. Therefore, level quantization should be easily observable in SMTs even at room temperature [41].

Now that we have identified the relevant scales for the occurrence of charging effects, we will briefly discuss some phenomena occurring when the requirements for single-electron charging effects are not met. For example, when the temperature is not sufficiently low enough, small but finite currents can appear inside of the Coulomb diamonds due to thermal fluctuations [74]. There is, however, a further effect which can lead to finite currents in the blocked region. The origin of this effect are cotunneling and higher-order tunneling processes. Even though we have used classical arguments for the charging energy, the SMT is a quantum mechanical system. While a single electron is bound to the law of energy conservation, it is possible for two or more electrons to tunnel simultaneously [74]. The tunneling electrons then do not need to conserve energy individually but only as a whole, thereby giving rise to new contributions to the charge current. These are called cotunneling contributions and are of higher order in the system-lead interaction than the sequential tunneling contributions we have discussed so far. In this thesis, we will concentrate on sequential tunneling only. It is however important to be aware of the existence of cotunneling effects. They become important for strong molecule-lead interactions or when all other transitions are forbidden. In order to stay in the sequential tunneling regime, it is

therefore necessary to ensure that the molecule-lead interaction is weak compared to all other energy scales in the problem [74]. For larger tunnel coupling or low temperature and transport voltage higher-order processes will have significant effects on the transport characteristics and in general need to be taken into account under these conditions [72].

Chapter 3.

The model of a molecular nanojunction in solution

We consider a molecule in a polar solvent coupled to two leads under the influence of an external voltage. The system is illustrated in Fig. 3.1. We want to investigate how the solvent influences the current through the molecule when a voltage is applied between the source and the drain. The goal is to find a relation between the applied voltage and the resulting electron current depending on different solvents such that in the end it is possible to deduce from the measured current the properties of the solvent in which the molecule is present. To this extent, we have to find a suitable theoretical description to characterize the main properties of the involved constituents contributing to the current which we will present in the following.

3.1. The molecule

We model the molecule in terms of a quantum dot. A quantum dot is a semiconductor nanostructure that confines the motion of conduction band electrons, valence band holes, or excitons (bound pairs of conduction band electrons and valence band holes) in all three spatial directions [77]. Due to this confinement the charge and energy of a quantum dot have a discrete quantized spectrum just like that of an atom or molecule. Hence, quantum dots are sometimes referred to as artificial atoms [78, 79] and thus are used to describe the central interacting region in our model. In general, experimentally realizable quantum dots contain a lot of levels. If the level splitting is larger than temperature and bias voltage, then at most one level participates in transport [72]. Hence, we limit our consideration to two molecular electronic states, describing an oxidized state with N and a reduced state with $N + 1$ electrons on the molecule. This standard assumption of strong Coulomb repulsion pushes states with other electronic occupations in energy regimes that are not accessible under the experimental conditions [27, 80]. The Hamiltonian of the molecule is then given by

$$H_{\mathrm{mol}} = \varepsilon_d d^\dagger d \ . \tag{3.1}$$

Here $d^\dagger$ and d are the creation and annihilation operators of an electron on the molecule with energy ε_d, respectively. We also neglect the spin degree of freedom since we

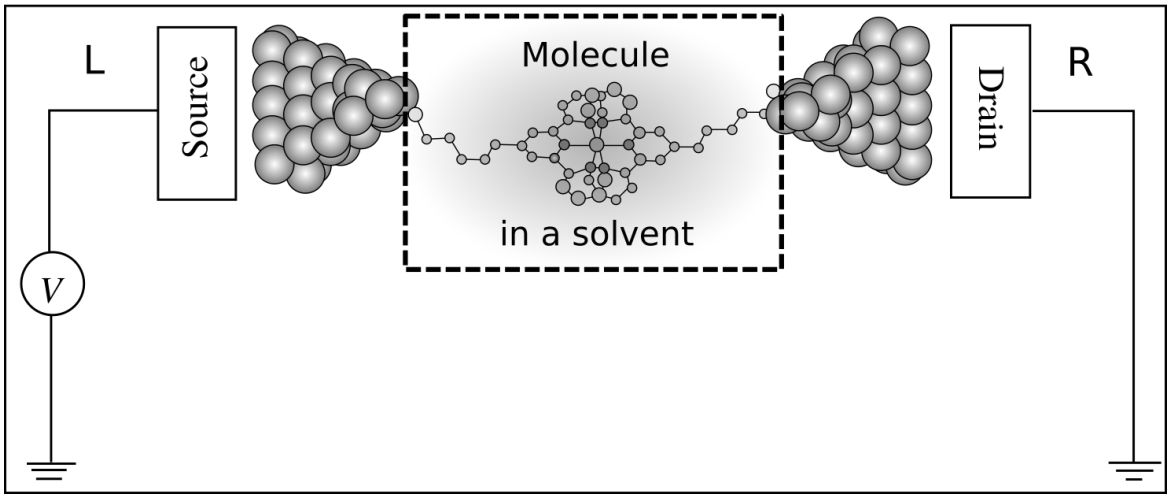

Figure 3.1.: Illustration of the model of the system given by a molecule in a solvent, which is in contact with two leads, the source (L) and the drain (R), respectively. The picture is adapted from Ref. [64].

are mainly interested in the charge current regardless of the spin of the electrons. Furthermore, our model does not include the electron-electron interaction needed to describe, e.g., Coulomb blockade effects, but focuses on the study of the inelastic effects of the electron-phonon interaction [81].

3.2. The leads

Guided by the typical experimental geometry in which the leads rapidly broaden into metallic contacts, we view electrons in the leads as noninteracting except for an overall self-consistent chemical potential μ_r [58], where the index $r = \mathrm{L}$ (R) labels the left (right) lead. The Hamiltonian takes the form of a free electron Fermi gas

$$H_{\text{leads}} = \sum_{r,k} (\varepsilon_{k,r} - \mu_r) c^\dagger_{k,r} c_{k,r} \ . \tag{3.2}$$

The creation (annihilation) operators of an electron in the leads with momentum k are denoted by $c^\dagger_{k,r}$ ($c_{k,r}$). The bias voltage is symmetrically applied around the Fermi energy $\varepsilon_F \equiv 0$, i.e., $\mu_{\mathrm{L}} = -\mu_{\mathrm{R}} = eV/2$. Furthermore, we set $\hbar \equiv 1$ and $k_B \equiv 1$.

3.3. The solvent

We assume the solvent to consist of polar molecules interacting with the central molecule when an electron is present on the latter one. Polar molecules contain polar bonds due to a difference in electronegativity between the bonded atoms. This means

that the negative charges from the electrons are not evenly distributed among the polar molecules, which causes a dipole moment. Thus, polar molecules interact through dipole–dipole intermolecular forces. A classic example of a polar bond is the bond in water between hydrogen and oxygen. Due to their relatively large net dipole moments caused by the opposing partial charges water molecules exhibit hydrogen bonds which is a common form of a dipole-dipole interaction where the partial charge of one water molecule interacts with the opposing charge of a neighboring water molecule and creates the H-bond. Hydrogen bonds are much weaker than covalent bonds within a molecule. However, a single water molecule can exhibit several H-bonds and as a result the influence of hydrogen bonds is in total significantly large. The dipole-dipole interactions can be attributed as fluctuations or phonons of the electrodynamic environment surrounding the central molecule. We characterize these fluctuations as bosonic modes ω_m and describe the polar solvent by the Hamiltonian [64, 65]

$$H_{\text{solv}} = \sum_m \omega_m a_m^\dagger a_m \ . \tag{3.3}$$

Here $a_m^\dagger$ (a_m) creates (destroys) a polarization excitation which we denote as phonon in mode m. Although we assume the bosonic modes stemming from fluctuations of the electrodynamic environment, i.e., the solvent, the specific kind of the modes ω_m can be adjusted accordingly to the bosonic environment [33]. Polar solvents can be modeled as harmonic environments in which the harmonic modes are motions of the polarization field [64]. In Section 5.3 we show in more detail how the dielectric response of a polar medium can be described in terms of the Hamiltonian (3.3).

3.4. Coupling between leads and molecule

In order to couple the leads and the molecule, we introduce tunneling. This is done in a perturbative way by considering the overlap between the lead states and the states of the molecule. This overlap is parametrized by tunneling amplitudes $t_{k,r}$ that enter in the tunneling Hamiltonian [75]

$$H_{\text{tun}} = \sum_{r,k} \left(t_{k,r} c_{k,r}^\dagger d + \text{H.c.} \right) \ . \tag{3.4}$$

This tunneling Hamiltonian describes charge transfer processes of single electrons tunneling from the leads to the molecule and vice-versa. We will assume that the tunneling amplitudes are free parameters that we can tune as we wish, but in principle one can compute them from overlap integrals between orbital wave functions of the lead and the molecule [75].

3.5. Coupling between solvent and molecule

Finally, we have the last interaction taken into account which represents the coupling between the phonon modes of the solvent and the electron at the resonant level of the

molecule given by the Hamiltonian [82]

$$H_{\text{mol-solv}} = \sum_m g_m d^\dagger d(a_m^\dagger + a_m) \ , \tag{3.5}$$

where g_m describes an electron-phonon coupling constant. The Hamiltonian describes the lowest-order coupling between electrons and phonons derived from linear response theory [82].

3.6. Polaron transformation

We write the full Hamiltonian of our system model as

$$\begin{aligned} H &= H_0 + H_{\text{tun}} \, , \\ H_0 &= H_{\text{mol}} + H_{\text{leads}} + H_{\text{solv}} + H_{\text{mol-solv}} \ . \end{aligned} \tag{3.6}$$

The reason why we choose this notation becomes apparent in the following. In the real-time diagrammatic technique, which we introduce in the next chapter to calculate the current through the molecule, we change to the interaction picture. To this extent, it is useful to have a Hamiltonian which contains the free parts of the partial subsystems and a separate single interacting part. This can be obtained by a unitary transformation [83, 84] given by $U = \exp\left(-id^\dagger d\varphi\right)$ and $\varphi = i\sum_m \frac{g_m}{\omega_m}\left(a_m^\dagger - a_m\right)$. This transformation is called Lang-Firsov or polaron transformation [83, 84] and yields the transformed Hamiltonian

$$\bar{H} = UHU^{-1} = \bar{H}_0 + \bar{H}_{\text{tun}} \, , \tag{3.7}$$

where

$$\bar{H}_0 = \bar{H}_{\text{mol}} + H_{\text{leads}} + H_{\text{solv}} \, , \tag{3.8}$$

with

$$\bar{H}_{\text{mol}} = \left(\varepsilon_d - \sum_m \frac{g_m^2}{\omega_m}\right) d^\dagger d \, , \tag{3.9}$$

and

$$\bar{H}_{\text{tun}} = \sum_{r,k} \left(t_{k,r} c_{k,r}^\dagger d e^{i\varphi} + \text{H.c.}\right) . \tag{3.10}$$

The essential building block of the calculation consists of exploiting the Baker-Campbell-Hausdorff formula for two operators X and Y, which reads [85]

$$e^X Y e^{-X} = \sum_{n=0}^{\infty} \frac{1}{n!} \left[X, Y\right]_n = Y + [X, Y] + \frac{1}{2}\left[X, [X, Y]\right] + \frac{1}{6}\left[X, [X, [X, Y]]\right] + \cdots \, , \tag{3.11}$$

where $[X,Y]_n = \big[X,[X,Y]_{n-1}\big]$, and $[X,Y]_0 = Y$. With $X = d^\dagger d \sum_m \frac{g_m}{\omega_m}\left(a_m^\dagger - a_m\right)$, we thus obtain for the transformation of the relevant operators

$$
\begin{aligned}
\bar{d} &= e^X d e^{-X} = \sum_{n=0}^{\infty} \frac{\left(\sum_m \frac{g_m}{\omega_m}\left(a_m^\dagger - a_m\right)\right)^n}{n!} \left[d^\dagger d, d\right]_n = d e^{\sum_m \frac{g_m}{\omega_m}\left(a_m - a_m^\dagger\right)} = d e^{-i\varphi}\,, \\
\bar{d}^\dagger &= d^\dagger e^{i\varphi}\,, \\
\bar{a}_m &= e^X a_m e^{-X} = \sum_{n=0}^{\infty} \frac{\left(d^\dagger d\right)^n}{n!} \left[\sum_{m'} \frac{g_{m'}}{\omega_{m'}}\left(a_{m'}^\dagger - a_{m'}\right), a_m\right]_n = a_m - \frac{g_m}{\omega_m} d^\dagger d\,, \\
\bar{a}_m^\dagger &= a_m^\dagger - \frac{g_m}{\omega_m} d^\dagger d\,, \\
\bar{c}_{k,r} &= c_{k,r}\,, \\
\bar{c}_{k,r}^\dagger &= c_{k,r}^\dagger\,.
\end{aligned}
\tag{3.12}
$$

Here, we have used $\left[d^\dagger d, d\right]_n = (-1)^n d$, and $\left[a_{m'}^\dagger - a_{m'}, a_m\right] = -\delta_{m',m}$. The consequences of this transformation are that the electron-phonon interaction renormalizes the level position of the molecule, i.e., $\bar{\varepsilon}_d = \left(\varepsilon_d - \sum_m \frac{g_m^2}{\omega_m}\right)$, and the tunneling term acquires phase factors $e^{\pm i\varphi}$ [72]. These phase factors describe the effect of boson-assisted tunneling caused by the solvent. Without tunneling the problem is now solved, i.e., the interaction between the molecule and the solvent can be treated exactly in the absence of the fermionic leads. The tunneling term is still nontrivial and therefore the real-time diagrammatic technique set up in the following chapter is based on an expansion in the tunneling vertex [35]. Operatorwise we have a part of the Hamiltonian $\bar{H}_0$ containing the free subsystems and a single interacting part $\bar{H}_{\text{tun}}$ containing all the interactions between the three subsystems. This separation also comes in handy for the upcoming derivation of the real-time diagrammatics. For convenience we drop the bar on all operators and imply implicitly that all operators $O \equiv \bar{O} = UOU^{-1}$ are the transformed ones after the polaron transformation [35]. Furthermore, from here on we refer to the renormalized level position of the molecule as ε_d.

Chapter 4.

Quantum master equation and real-time diagrammatic technique

A full description of the molecule and its environment is, in most cases, impossible due to the size of the environment. It is, however, possible to describe the dynamics of only the molecule by integrating out the environment. An approach based on this technique is the quantum master equation. The master equation describes the evolution of the reduced density matrix of the molecule via transition rates between the molecule and the environment [74]. The total transformed Hamiltonian of our system consists of an environment, including the leads and the solvent, the molecule part, and the tunneling part. The latter describes the coupling between environment and molecule and will drive the molecule system out of equilibrium. Therefore, we formulate the nonequilibrium problem in the following way. For $t \leq t_0$, we assume the tunneling part of the Hamiltonian to vanish, and the environment to be in equilibrium. This means that the initial density matrix for the total system (ρ) factorizes into parts for the molecule (ρ_{mol}), the leads (ρ^{eq}_{leads}), and the solvent (ρ^{eq}_{solv}), i.e.,

$$\rho(t) = \rho_{\text{mol}}(t)\rho^{eq}_{\text{leads}}\rho^{eq}_{\text{solv}} \qquad \text{for } t \leq t_0 \ , \tag{4.1}$$

where

$$\rho^{eq}_{\text{leads}} = \frac{e^{-\beta H_{\text{leads}}}}{\text{Tr}_{\text{leads}}\left[e^{-\beta H_{\text{leads}}}\right]} \quad \text{and} \quad \rho^{eq}_{\text{solv}} = \frac{e^{-\beta H_{\text{solv}}}}{\text{Tr}_{\text{solv}}\left[e^{-\beta H_{\text{solv}}}\right]} \, . \tag{4.2}$$

The reduced density matrix of the molecule is given by

$$\rho_{\text{mol}}(t) = \text{Tr}_{\text{leads}}\text{Tr}_{\text{solv}}\left[\rho(t)\right] \ , \tag{4.3}$$

with Tr_{leads} and Tr_{solv} being the trace over the lead and solvent degrees of freedom, respectively [35]. We further assume that the molecule, the leads, and the solvent are at the same temperature T leading to the same inverse temperature $\beta = 1/T$. The master equation can now be derived starting from the Liouville-von Neumann equation

$$\frac{\partial}{\partial t}\rho(t) = -i\left[H, \rho(t)\right] \ , \tag{4.4}$$

which describes how the full density operator evolves in time in the Schrödinger picture. As mentioned earlier we want to change to the interaction picture in order

to utilize the real-time diagrammatic technique. To this extent, we use the definition of an arbitrary Schrödinger operator in the interaction picture which is given by $O(t)_I = e^{iH_0(t-t_0)}O(t)e^{-iH_0(t-t_0)}$, where the subscript I denotes the interaction picture. By differentiating the full density operator $\rho(t) = e^{-iH_0(t-t_0)}\rho(t)_I e^{iH_0(t-t_0)}$ with respect to t and using Eq. (4.4) we get the interaction picture Liouville-von Neumann equation

$$\frac{\partial}{\partial t}\rho(t)_I = -i\left[H_{\mathrm{tun}}(t)_I, \rho(t)_I\right] \ , \tag{4.5}$$

which describes the time evolution of the density operator in the interaction picture and resembles the form of the Liouville-von Neumann equation in the Schrödinger picture, however, with the tunneling Hamiltonian $H_{\mathrm{tun}}(t)_I$ in the interaction picture instead of the full Hamiltonian H. The formal solution of Eq. (4.5) can be found by integration, i.e.,

$$\rho(t)_I = \rho(t_0)_I - i\int_{t_0}^{t} \mathrm{d}t' \left[H_{\mathrm{tun}}(t')_I, \rho(t')_I\right] \ . \tag{4.6}$$

Reinserting the formal solution into the right-hand side of Eq. (4.5) leads to

$$\frac{\partial}{\partial t}\rho(t)_I = -i\left[H_{\mathrm{tun}}(t)_I, \rho(t_0)_I\right] - \int_{t_0}^{t} \mathrm{d}t' \left[H_{\mathrm{tun}}(t)_I, \left[H_{\mathrm{tun}}(t')_I, \rho(t')_I\right]\right] \ . \tag{4.7}$$

Since we want to derive an equation of motion for the reduced density matrix, the next step is to trace out the lead and solvent degrees of freedom. Before we proceed with this step, we first calculate the time derivative of the density matrix from the interaction picture definition of an operator, i.e.,

$$\frac{\partial}{\partial t}\rho(t)_I = e^{iH_0(t-t_0)}\left(i\left[H_0, \rho(t)\right] + \frac{\partial}{\partial t}\rho(t)\right)e^{-iH_0(t-t_0)} \ . \tag{4.8}$$

It will become apparent below why this switch to the Schrödinger picture will be useful. Now, let us proceed with the calculation of the trace over the lead and solvent degrees of freedom. We get from Eq. (4.7)

$$\frac{\partial}{\partial t}\rho_{\mathrm{mol}}(t)_I = \mathrm{Tr}_{\mathrm{leads}}\mathrm{Tr}_{\mathrm{solv}}\left[\frac{\partial}{\partial t}\rho(t)_I\right] = -\mathrm{Tr}_{\mathrm{leads}}\mathrm{Tr}_{\mathrm{solv}}\left[\int_{t_0}^{t} \mathrm{d}t' \left[H_{\mathrm{tun}}(t)_I, \left[H_{\mathrm{tun}}(t')_I, \rho(t')_I\right]\right]\right] \ . \tag{4.9}$$

Due to our consideration that the environment is initially at its equilibrium and thus its density matrix is diagonal in the corresponding energy basis we see that the first term on the right hand side of Eq. (4.7) vanishes under the trace of the environment, i.e., $\mathrm{Tr}_{\mathrm{leads}}\mathrm{Tr}_{\mathrm{solv}}\big(\left[H_{\mathrm{tun}}(t)_I, \rho(t_0)_I\right]\big) = 0$, because the tunneling Hamiltonian H_{tun} is non-diagonal in the eigenbasis of the environment. We write a matrix element of the reduced density matrix of the molecule in the Schrödinger picture as $P^{\psi_1}_{\psi_2}(t) = \langle\psi_1|\rho_{\mathrm{mol}}(t)|\psi_2\rangle$, where $|\psi_i\rangle$ are eigenstates of the molecule, i.e., $H_{\mathrm{mol}}|\psi_i\rangle = \varepsilon_{\psi_i}|\psi_i\rangle$. By using the equality of Eq. (4.7) and Eq. (4.8) as well as the performed trace over the

lead and solvent degrees of freedom, we arrive at the quantum master equation for a matrix element of the reduced density matrix of the molecule, given by

$$\begin{aligned}\frac{\partial}{\partial t}P_{\psi_2}^{\psi_1}(t) =& i\left(\varepsilon_{\psi_2}-\varepsilon_{\psi_1}\right)P_{\psi_2}^{\psi_1}(t) \\ &- e^{i\left(\varepsilon_{\psi_2}-\varepsilon_{\psi_1}\right)(t-t_0)}\langle\psi_1|\mathrm{Tr}_{\mathrm{leads}}\mathrm{Tr}_{\mathrm{solv}}\left[\int_{t_0}^{t}\mathrm{d}t'\left[H_{\mathrm{tun}}(t)_I,\left[H_{\mathrm{tun}}(t')_I,\rho(t')_I\right]\right]\right]|\psi_2\rangle\ .\end{aligned} \tag{4.10}$$

Notice, how the left-hand side and the first term of the right hand side stems from the switch to the Schrödinger picture from Eq. (4.8). In this way it is possible to describe the coherent dynamics separately from the dissipative one. Thus, the first term on the right-hand side governs the dynamics of the isolated molecule system in the absence of tunneling, whereas the second term encloses all effects of the fermionic leads and the bosonic solvent [86]. The quantum master equation can be written in a short hand notation [72]

$$\frac{\partial}{\partial t}P_{\psi_2}^{\psi_1}(t) = i\left(\varepsilon_{\psi_2}-\varepsilon_{\psi_1}\right)P_{\psi_2}^{\psi_1}(t) - \sum_{\psi_1',\psi_2'}\int_{t_0}^{t}\mathrm{d}t' P_{\psi_2'}^{\psi_1'}(t')\Sigma_{\psi_2'\psi_2}^{\psi_1'\psi_1}(t',t)\ , \tag{4.11}$$

where the so-called irreducible self-energy part $\Sigma_{\psi_2'\psi_2}^{\psi_1'\psi_1}(t',t)$ contains all the tunneling processes between the molecule and the environment stemming from the tunneling Hamiltonian H_{tun}. We will explain in the next section how we get from Eq. (4.10) to Eq. (4.11) and how we can calculate the self-energy as well as why it is called irreducible. Before we do so, we want to make two major approximations. Notice, that up to this point, the quantum master equation is formally exact since all orders of the system-environment interaction are included either explicitly in form of the interaction Hamiltonian or implicitly in the density matrix [74].

We have stated that $\rho(t)$ factorizes for $t \leq t_0$. At later times, correlations between the environment and the molecule may arise due to the tunneling term H_{tun}. However, for a weak coupling, at all times $\rho(t)$ should only show deviations of order H_{tun} from an uncorrelated state [86]. Therefore, we assume that the environment is at thermal equilibrium at all times. In order for this assumption to be valid two conditions need to be fulfilled: First, the equilibration times of the environment need to be fast compared to the time between two tunneling processes. Second, the environment needs to be very large compared to the molecule. Since we are discussing the transfer of single electrons between a nanosystem, i.e., the molecule, and its environment typically given by solids and solvents, both of which having macroscopic dimensions, these conditions are satisfied [74]. Now, because the molecule-environment interaction is assumed to be small, we treat the interaction in the self-consistent Born approximation, where only the lowest order self-energies are kept [81]. This means that we will neglect terms of higher than second order in H_{tun} in Eq. (4.10).

The next assumption we want to perform is the Markov approximation. The dissipative part of the quantum master equation depends on the evolution of the density

matrix from the initial time t_0 to the evaluation time t, including memory effects in the dynamics [86]. Depending on the form of the environment surrounding the system of interest, it is possible that a calculation of the systems dynamics requires to take into account the previous dynamics up to a certain memory time. The dynamics of such a system is then called non-Markovian. For Markovian systems, the memory time is assumed to be much shorter than any system or environment time scale [74]. Due to the Markov approximation we can replace $\rho(t')_I$ by $\rho(t)_I$ in Eq. (4.10) which leads to a replacement of $P^{\psi_1'}_{\psi_2'}(t')$ by $P^{\psi_1'}_{\psi_2'}(t)$ in Eq. (4.11) yielding the Markov quantum master equation

$$\frac{\partial}{\partial t}P^{\psi_1}_{\psi_2}(t) = i\left(\varepsilon_{\psi_2} - \varepsilon_{\psi_1}\right)P^{\psi_1}_{\psi_2}(t) - \sum_{\psi_1',\psi_2'}\int_{t_0}^{t} \mathrm{d}t' P^{\psi_1'}_{\psi_2'}(t)\Sigma^{\psi_1'\psi_1}_{\psi_2'\psi_2}(t',t) \ . \tag{4.12}$$

What remains to be specified and calculated is the irreducible self-energy part $\Sigma^{\psi_1'\psi_1}_{\psi_2'\psi_2}(t',t)$. We will continue with this calculation in the following.

4.1. Calculation of the self-energy Σ to leading order in the tunnel coupling

In general, the irreducible self-energy $\Sigma^{\psi_1'\psi_1}_{\psi_2'\psi_2}(t',t)$ contains all orders of the interactions between the molecule and the environment happening between the times t' and t. These interactions can be represented in diagrams (see Fig. 4.1), which are similar to Feynman diagrams, and for which J. König *et al.* have developed calculation rules presented in Ref. [87]. The self-energy part $\Sigma^{\psi_1'\psi_1}_{\psi_2'\psi_2}(t',t)$ is called irreducible, because it contains the sum of all diagrams in which any vertical cut through them crosses at least one tunneling line [72]. Due to our assumption that the coupling between the molecule and the environment is sufficiently weak, it is reasonable to assume that only the lowest order of the interaction is important for the system's dynamics [74]. The lowest non-vanishing order term of the self-energy, which is of second order in H_{tun}, is called the transition rate of sequential tunneling. It corresponds to the physical situation where all tunneling processes are incoherent. The next non-vanishing term, which is of forth order in H_{tun}, is called the cotunneling transition rate. It means that at least two tunneling processes are coherent allowing for coherent transport through the molecule [35]. Again, within the Born approximation we will focus on the lowest order transition rate in the sequential tunneling regime. In order to identify the lowest order self-energy, let us expand the double commutator in Eq. (4.10) and insert identities $1 = \sum_{\psi_i} |\psi_i\rangle\langle\psi_i|$ between the operators, so that, together with the Markov

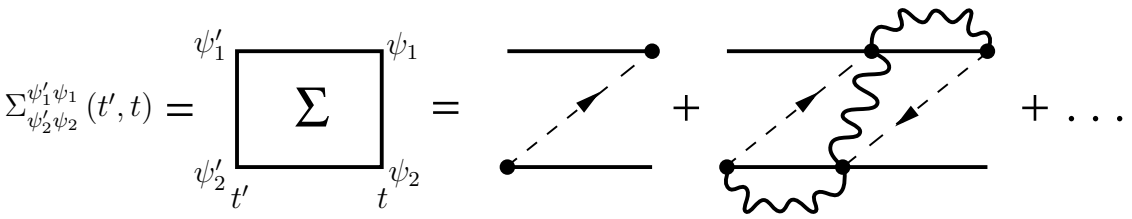

Figure 4.1.: Visualization of the full irreducible self-energy on the Keldysh contour containing all orders of the tunneling Hamiltonian H_{tun}. The dashed lines represent fermionic interactions between the molecule and the leads whereas the wiggled lines represent bosonic interactions stemming from the solvent. The picture is adapted from Ref. [35].

approximation ($\rho(t')_I \to \rho(t)_I$), we get

$$\begin{aligned}\frac{\partial}{\partial t}P^{\psi_1}_{\psi_2}(t) = i\left(\varepsilon_{\psi_2}-\varepsilon_{\psi_1}\right)P^{\psi_1}_{\psi_2}(t) - \sum_{\psi_1',\psi_2'}\int_{t_0}^{t}\mathrm{d}t' e^{i\left(\varepsilon_{\psi_2}-\varepsilon_{\psi_1}\right)(t-t_0)}\times \\ \mathrm{Tr}_{\text{leads}}\mathrm{Tr}_{\text{solv}}\Bigg[\underbrace{\langle\psi_1|H_{\text{tun}}(t')_I|\psi_1'\rangle\langle\psi_1'|\rho(t)_I|\psi_2'\rangle\langle\psi_2'|H_{\text{tun}}(t)_I|\psi_2\rangle}_{(i)} \\ + \underbrace{\langle\psi_1|H_{\text{tun}}(t)_I|\psi_1'\rangle\langle\psi_1'|\rho(t)_I|\psi_2'\rangle\langle\psi_2'|H_{\text{tun}}(t')_I|\psi_2\rangle}_{(ii)} \\ - \sum_{\psi_3'}\underbrace{\langle\psi_1|H_{\text{tun}}(t)_I|\psi_3'\rangle\langle\psi_3'|H_{\text{tun}}(t')_I|\psi_1'\rangle\langle\psi_1'|\rho(t)_I|\psi_2'\rangle}_{(iii)}\delta_{\psi_2'\psi_2} \\ - \sum_{\psi_3'}\underbrace{\langle\psi_1'|\rho(t)_I|\psi_2'\rangle\langle\psi_2'|H_{\text{tun}}(t')_I|\psi_3'\rangle\langle\psi_3'|H_{\text{tun}}(t)_I|\psi_2\rangle}_{(iv)}\delta_{\psi_1'\psi_1}\Bigg] .\end{aligned} \tag{4.13}$$

We want to end up in a form resembling Eq. (4.12). To this extent, we insert the tunneling Hamiltonian from Eq. (3.10) and switch once again from the interaction picture of the density matrix and molecule operators to the Schrödinger picture in order for the free molecule Hamiltonian to act upon its eigenstates. Furthermore, we know how the fermionic operators of the leads evolve in time, i.e., $c_{k,r}(t)_I = e^{-i\varepsilon_{k,r}(t-t_0)}c_{k,r}$. Since the tunneling Hamiltonian consists of two terms and appears twice in each of the four terms (i)–(iv) in Eq. (4.13) this would lead to a total number of sixteen terms. However, half of them do not contribute due to particle number conservation. Together with the assumption that the density matrix of the total system (molecule

+ environment) factorizes at all times, we end up with

$$\begin{aligned}\frac{\partial}{\partial t}P^{\psi_1}_{\psi_2}(t) = i\left(\varepsilon_{\psi_2}-\varepsilon_{\psi_1}\right)P^{\psi_1}_{\psi_2}(t) - \sum_{\psi_1',\psi_2'}\int_{t_0}^{t}\mathrm{d}t' P^{\psi_1'}_{\psi_2'}(t)\sum_{k,r}|t_{k,r}|^2 \\ \times\Bigg\{ e^{i(\varepsilon_{\psi_1'}-\varepsilon_{\psi_1})\tau}e^{-W(+\tau)}\Big[e^{-i\varepsilon_{k,r}\tau}f_r^-(\varepsilon_{k,r})\langle\psi_1|d|\psi_1'\rangle\langle\psi_2'|d^\dagger|\psi_2\rangle \\ +e^{+i\varepsilon_{k,r}\tau}f_r^+(\varepsilon_{k,r})\langle\psi_1|d^\dagger|\psi_1'\rangle\langle\psi_2'|d|\psi_2\rangle\Big] \\ +e^{i(\varepsilon_{\psi_2}-\varepsilon_{\psi_2'})\tau}e^{-W(-\tau)}\Big[e^{+i\varepsilon_{k,r}\tau}f_r^-(\varepsilon_{k,r})\langle\psi_1|d|\psi_1'\rangle\langle\psi_2'|d^\dagger|\psi_2\rangle \\ +e^{-i\varepsilon_{k,r}\tau}f_r^+(\varepsilon_{k,r})\langle\psi_1|d^\dagger|\psi_1'\rangle\langle\psi_2'|d|\psi_2\rangle\Big] \\ -\sum_{\psi_3'}e^{i(\varepsilon_{\psi_1'}-\varepsilon_{\psi_3'})\tau}e^{-W(+\tau)}\Big[e^{+i\varepsilon_{k,r}\tau}f_r^+(\varepsilon_{k,r})\langle\psi_1|d|\psi_3'\rangle\langle\psi_3'|d^\dagger|\psi_1'\rangle \\ +e^{-i\varepsilon_{k,r}\tau}f_r^-(\varepsilon_{k,r})\langle\psi_1|d^\dagger|\psi_3'\rangle\langle\psi_3'|d|\psi_1'\rangle\Big]\delta_{\psi_2'\psi_2} \\ -\sum_{\psi_3'}e^{i(\varepsilon_{\psi_3'}-\varepsilon_{\psi_2'})\tau}e^{-W(-\tau)}\Big[e^{-i\varepsilon_{k,r}\tau}f_r^+(\varepsilon_{k,r})\langle\psi_2'|d|\psi_3'\rangle\langle\psi_3'|d^\dagger|\psi_2\rangle \\ +e^{+i\varepsilon_{k,r}\tau}f_r^-(\varepsilon_{k,r})\langle\psi_2'|d^\dagger|\psi_3'\rangle\langle\psi_3'|d|\psi_2\rangle\Big]\delta_{\psi_1'\psi_1}\Bigg\}\,,\end{aligned} \tag{4.14}$$

where the Fermi-Dirac distribution $f_r^{\pm}(\varepsilon_{k,r}) = \left[1+e^{\pm\beta(\varepsilon_{k,r}-\mu_r)}\right]^{-1}$ of lead r with chemical potential μ_r stems from the trace over the leads, i.e.,

$$f_r^+(\varepsilon_{k,r}) = \mathrm{Tr}_{\mathrm{leads}}\left[\rho^{eq}_{\mathrm{leads}}c^\dagger_{k,r}c_{k,r}\right] \quad \text{and} \quad f_r^-(\varepsilon_{k,r}) = \mathrm{Tr}_{\mathrm{leads}}\left[\rho^{eq}_{\mathrm{leads}}c_{k,r}c^\dagger_{k,r}\right]\,. \tag{4.15}$$

The exponential factor $e^{-W(\pm\tau)}$ comes from the trace over the solvent, which can be calculated using Feynman's disentangling method [84], and together with the time difference $\tau = t - t'$ results in

$$e^{-W(+\tau)} = \mathrm{Tr}_{\mathrm{solv}}\left[\rho^{eq}_{\mathrm{solv}}e^{\pm i\varphi(t)_I}e^{\mp i\varphi(t')_I}\right] \quad \text{and} \quad e^{-W(-\tau)} = \mathrm{Tr}_{\mathrm{solv}}\left[\rho^{eq}_{\mathrm{solv}}e^{\pm i\varphi(t')_I}e^{\mp i\varphi(t)_I}\right]\,. \tag{4.16}$$

The latter factor is most interesting to our investigation, because it contains the influence of the solvent on the molecule. The exponent $W(\tau)$ is referred to as the time-dependent reservoir correlation function [65] or line shape function [88] and can be written as [35, 65, 88]

$$W(\tau) = \frac{1}{\pi}\int_0^\infty \mathrm{d}\omega\frac{J(\omega)}{\omega^2}\left\{(1-\cos(\omega\tau))\coth\left(\frac{\beta\omega}{2}\right)+i\sin(\omega\tau)\right\}\,, \tag{4.17}$$

where $J(\omega)$ is the spectral density of the solvent and in general is defined as [35, 65, 88]

$$J(\omega) = \pi\sum_m g_m^2\delta(\omega-\omega_m)\,. \tag{4.18}$$

Although the spectral density in Eq. (4.18) is defined in terms of a sum of delta functions, any macroscopic system will in practice have a continuous spectral density [65]. Depending on the type of the solvent, the spectral density can assume various kinds of possible forms. Since we consider a polar solvent, we assume the spectral density to be in the so-called Debye form, i.e., [89]

$$J(\omega) = 2\eta \frac{\omega\omega_c}{\omega^2 + \omega_c^2} \ . \tag{4.19}$$

This spectral density is linear (Ohmic) for small frequencies but has a Lorentzian cutoff. It is sometimes also referred to as an Ohmic spectral density with Drude cutoff. It describes a solvent exhibiting Debye dielectric relaxation. The two parameters which characterize the spectral density, the characteristic cutoff frequency ω_c and the coupling strength η, are related to other physical quantities: $1/\omega_c = \tau_E$ is related to the Debye relaxation time of the solvent and η is the reorganization energy [89]. In Section 5.4, we will exploit in more detail how the spectral density can be derived utilizing the Onsager model of solvation and how it differs for various polar solvents. Let us, at the moment, return to the calculation of the self-energy. By comparing Eq. (4.12) and Eq. (4.14), we can directly read off the lowest order self-energy $\Sigma^{(1)\psi_1'\psi_1}_{\psi_2'\psi_2}(t', t)$ which consists of eight terms representing eight diagrams, where each only contains one tunneling line. We label each of these diagrams according to Fig. 4.2. We see, that all the diagrams only depend on the time difference $\tau = t - t'$. For example, the first two diagrams $S^{\psi_1'\psi_1}_{\psi_2'\psi_2}(\tau)$ and $T^{\psi_1'\psi_1}_{\psi_2'\psi_2}(\tau)$ are stemming from the term (i) of Eq. (4.14), where it can be observed, that from the tunneling Hamiltonian at time t' between the states ψ_1' and ψ_1 an electron on the molecule is either annihilated (in case of diagram S) or created (in diagram T). This annihilation and creation process of an electron on the molecule is indicated by the direction of the arrow between the time points on the upper and lower contour, where an arrow pointing away from (onto) a time point means, that an electron is being annihilated (created) on the molecule. In Fig. 4.2 we have only visualized the interaction between the molecule and the leads illustrated by the dashed line. However, between the two indicated time points of each diagram, there can be, in principle, infinitely many connecting bosonic lines coming from the interaction between the molecule and the solvent due to the appearing factor $e^{-W(\pm\tau)}$.

What one can further deduce from the diagrams, is, that in contrast to the directional fermionic tunneling lines the bosonic interactions for the diagrams S and T are the same, i.e., they are direction-independent and, consequently, the factor $e^{-W(+\tau)}$ is equal for both of these diagrams. In a similar manner, the interactions between the molecule and the environment are represented in the diagrams U and V. Here, only the times at which the creation and annihilation processes take place are interchanged. In the remaining diagrams W, X, Y, and Z tunneling processes are only taking place on either the upper or the lower contour, which means, that the state of the molecule does not change on the respective free propagating contour line, leading to a $\delta_{\psi_i'\psi_i} = \langle\psi_i'|\psi_i\rangle$. In between tunneling processes on the non-free propagating contour part the molecule is in the state ψ_3' which stems from the additional identity $1 = \sum_{\psi_3'} |\psi_3'\rangle\langle\psi_3'|$ included in Eq. (4.13).

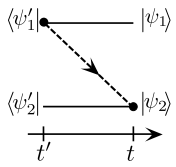

$$= S^{\psi_1'\psi_1}_{\psi_2'\psi_2}(\tau) = +\sum_{rk} |t_{rk}|^2 e^{i(\varepsilon_{\psi_1'}-\varepsilon_{\psi_1})\tau} e^{-W(+\tau)} e^{-i\varepsilon_{rk}\tau} f_r^-(\varepsilon_{rk}) \langle\psi_1|d|\psi_1'\rangle\langle\psi_2'|d^\dagger|\psi_2\rangle$$

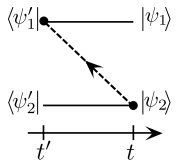

$$= T^{\psi_1'\psi_1}_{\psi_2'\psi_2}(\tau) = +\sum_{rk} |t_{rk}|^2 e^{i(\varepsilon_{\psi_1'}-\varepsilon_{\psi_1})\tau} e^{-W(+\tau)} e^{+i\varepsilon_{rk}\tau} f_r^+(\varepsilon_{rk}) \langle\psi_1|d^\dagger|\psi_1'\rangle\langle\psi_2'|d|\psi_2\rangle$$

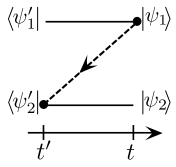

$$= U^{\psi_1'\psi_1}_{\psi_2'\psi_2}(\tau) = +\sum_{rk} |t_{rk}|^2 e^{i(\varepsilon_{\psi_2}-\varepsilon_{\psi_2'})\tau} e^{-W(-\tau)} e^{+i\varepsilon_{rk}\tau} f_r^-(\varepsilon_{rk}) \langle\psi_1|d|\psi_1'\rangle\langle\psi_2'|d^\dagger|\psi_2\rangle$$

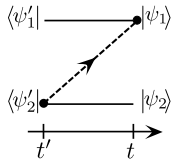

$$= V^{\psi_1'\psi_1}_{\psi_2'\psi_2}(\tau) = +\sum_{rk} |t_{rk}|^2 e^{i(\varepsilon_{\psi_2}-\varepsilon_{\psi_2'})\tau} e^{-W(-\tau)} e^{-i\varepsilon_{rk}\tau} f_r^+(\varepsilon_{rk}) \langle\psi_1|d^\dagger|\psi_1'\rangle\langle\psi_2'|d|\psi_2\rangle$$

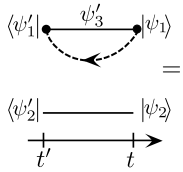

$$= W^{\psi_1'\psi_1}_{\psi_2'\psi_2}(\tau) = -\sum_{rk,\psi_3'} |t_{rk}|^2 e^{i(\varepsilon_{\psi_1'}-\varepsilon_{\psi_3'})\tau} e^{-W(+\tau)} e^{+i\varepsilon_{rk}\tau} f_r^+(\varepsilon_{rk}) \langle\psi_1|d|\psi_3'\rangle\langle\psi_3'|d^\dagger|\psi_1'\rangle\delta_{\psi_2'\psi_2}$$

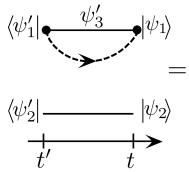

$$= X^{\psi_1'\psi_1}_{\psi_2'\psi_2}(\tau) = -\sum_{rk,\psi_3'} |t_{rk}|^2 e^{i(\varepsilon_{\psi_1'}-\varepsilon_{\psi_3'})\tau} e^{-W(+\tau)} e^{-i\varepsilon_{rk}\tau} f_r^-(\varepsilon_{rk}) \langle\psi_1|d^\dagger|\psi_3'\rangle\langle\psi_3'|d|\psi_1'\rangle\delta_{\psi_2'\psi_2}$$

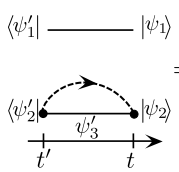

$$= Y^{\psi_1'\psi_1}_{\psi_2'\psi_2}(\tau) = -\sum_{rk,\psi_3'} |t_{rk}|^2 e^{i(\varepsilon_{\psi_3'}-\varepsilon_{\psi_2'})\tau} e^{-W(-\tau)} e^{-i\varepsilon_{rk}\tau} f_r^+(\varepsilon_{rk}) \langle\psi_2'|d|\psi_3'\rangle\langle\psi_3'|d^\dagger|\psi_2\rangle\delta_{\psi_1'\psi_1}$$

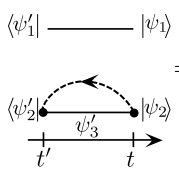

$$= Z^{\psi_1'\psi_1}_{\psi_2'\psi_2}(\tau) = -\sum_{rk,\psi_3'} |t_{rk}|^2 e^{i(\varepsilon_{\psi_3'}-\varepsilon_{\psi_2'})\tau} e^{-W(-\tau)} e^{+i\varepsilon_{rk}\tau} f_r^-(\varepsilon_{rk}) \langle\psi_2'|d^\dagger|\psi_3'\rangle\langle\psi_3'|d|\psi_2\rangle\delta_{\psi_1'\psi_1}$$

Figure 4.2.: Tunneling diagrams in first order of the self-energy.

For the calculation of the sum over all momenta k of the lead electrons we employ the wide-band approximation, where we assume that the tunnel amplitude as well as the density of states in the leads $\mathrm{D}(\varepsilon_{k,r})$ are energy independent and located around the fermi energy $\varepsilon_\mathrm{F} \equiv 0$, i.e., $t_{k,r} \to t_r$ and $\mathrm{D}(\varepsilon_{k,r}) \to \mathrm{D}(\varepsilon_\mathrm{F}) = \frac{\Gamma_r}{2\pi|t_r|^2}$, where we have introduced the tunnel coupling strength $\Gamma_r = 2\pi|t_r|^2\mathrm{D}(\varepsilon_\mathrm{F})$. This wide-band limit is justified whenever the conduction bandwidth of the leads is much larger than all other relevant energy scales [90]. We can then transform the sum over the lead states in Eq. (4.14) into a continuous energy integral, i.e., $\sum_k \to \int \mathrm{d}\varepsilon \mathrm{D}(\varepsilon_\mathrm{F}) = \mathrm{D}(\varepsilon_\mathrm{F}) \int \mathrm{d}\varepsilon$. The equation of the diagram S then looks like

$$S^{\psi_1'\psi_1}_{\psi_2'\psi_2}(\tau) = +\sum_r \frac{\Gamma_r}{2\pi} e^{i(\varepsilon_{\psi_1'} - \varepsilon_{\psi_1})\tau} e^{-W(+\tau)} \langle\psi_1|d|\psi_1'\rangle\langle\psi_2'|d^\dagger|\psi_2\rangle \int_{-\infty}^{\infty} \mathrm{d}\varepsilon e^{-i\varepsilon\tau} f_r^-(\varepsilon) \ . \tag{4.20}$$

All other diagrams change accordingly. We notice that the energy integral does not converge for positive times $\tau \geq 0$, due to the fact that the Fermi-Dirac distribution approaches zero only for one of the integral limits. Particularly, depending on the sign of the Fermi-Dirac distribution, we have for one limit $\lim_{\varepsilon\to\pm\infty} f_r^\pm(\varepsilon) = 0$, while in the other limit we have $\lim_{\varepsilon\to\mp\infty} f_r^\pm(\varepsilon) = 1$. To address this mathematical inconvenience, we observe that the replacement of the sum over the momenta of the lead electrons by an infinite integral is not fully reasonable, because the lead electrons can not have infinite energy.

Therefore, we introduce the bandwidth B of the leads, which is much larger than every other energy scale of the total system. We fix $B = 10^5\ \Gamma$ throughout this work. The sign of the bandwidth is introduced in such a way, that the energy integral approaches zero for the corresponding limit where the Fermi-Dirac distribution does not approach zero. In this way, the energy integral converges and can be calculated, e.g., utilizing the residue theorem. Depending on the sign of the Fermi-Dirac distribution and the time τ appearing in the diagrams, we get

$$\begin{aligned}
\int_{-\infty}^{\infty} \mathrm{d}\varepsilon f_r^\pm(\varepsilon) e^{+i\varepsilon\left(\tau \mp \frac{i}{B}\right)} &= \mp i\frac{\pi}{\beta} \frac{e^{i\mu_r\left(\tau \mp \frac{i}{B}\right)}}{\sinh\left(\frac{\pi}{\beta}\left(\tau \mp \frac{i}{B}\right)\right)} \ , \\
\int_{-\infty}^{\infty} \mathrm{d}\varepsilon f_r^\pm(\varepsilon) e^{-i\varepsilon\left(\tau \pm \frac{i}{B}\right)} &= \pm i\frac{\pi}{\beta} \frac{e^{-i\mu_r\left(\tau \pm \frac{i}{B}\right)}}{\sinh\left(\frac{\pi}{\beta}\left(\tau \pm \frac{i}{B}\right)\right)} \ .
\end{aligned} \tag{4.21}$$

Now that the energy part of the leads is covered, what remains to be calculated in the quantum master equation is the integration over the time. To this extent, we first have a look at the time-dependent line shape function $W(\tau)$ from Eq. (4.17). By partitioning it into its real and imaginary parts $W(\tau) = W'(\tau) + iW''(\tau)$ we have

$$W'(\tau) = \frac{1}{\pi} \int_0^\infty \mathrm{d}\omega \frac{J(\omega)}{\omega^2} \left(1 - \cos(\omega\tau)\right) \coth\left(\frac{\beta\omega}{2}\right) \tag{4.22}$$

and

$$W''(\tau) = \frac{1}{\pi} \int_0^\infty \mathrm{d}\omega \frac{J(\omega)}{\omega^2} \sin(\omega\tau) \ . \tag{4.23}$$

When we now insert the Debye spectral density from Eq. (4.19) we can recast and calculate the two parts as

$$\begin{aligned} W'(\tau) &= \frac{2\eta\omega_c}{\pi}\int_0^{\tau}\mathrm{d}\tau_2\int_0^{\tau_2}\mathrm{d}\tau_1\frac{\mathrm{d}^2}{\mathrm{d}\tau_1^2}\int_0^{\infty}\mathrm{d}\omega\frac{1}{\omega(\omega^2+\omega_c^2)}\left(1-\cos(\omega\tau_1)\right)\coth\left(\frac{\beta\omega}{2}\right) \\ &= \frac{2\eta\omega_c}{\pi}\int_0^{\tau}\mathrm{d}\tau_2\int_0^{\tau_2}\mathrm{d}\tau_1\int_0^{\infty}\mathrm{d}\omega\frac{\omega}{\omega^2+\omega_c^2}\cos(\omega\tau_1)\coth\left(\frac{\beta\omega}{2}\right) \\ &= \frac{2\eta\omega_c}{\pi}\int_0^{\tau}\mathrm{d}\tau_2\int_0^{\tau_2}\mathrm{d}\tau_1\,\mathrm{Re}\left\{\int_0^{\infty}\mathrm{d}\omega\frac{\omega}{\omega^2+\omega_c^2}e^{i\omega\tau_1}\coth\left(\frac{\beta\omega}{2}\right)\right\} \end{aligned} \tag{4.24}$$

and

$$\begin{aligned} W''(\tau) &= \frac{2\eta\omega_c}{\pi}\int_0^{\tau}\mathrm{d}\tau_1\frac{\mathrm{d}}{\mathrm{d}\tau_1}\int_0^{\infty}\mathrm{d}\omega\frac{1}{\omega(\omega^2+\omega_c^2)}\sin(\omega\tau_1) \\ &= \frac{2\eta\omega_c}{\pi}\int_0^{\tau}\mathrm{d}\tau_1\int_0^{\infty}\mathrm{d}\omega\frac{\cos(\omega\tau_1)}{\omega^2+\omega_c^2} \\ &= \frac{2\eta\omega_c}{\pi}\int_0^{\tau}\mathrm{d}\tau_1\,\mathrm{Re}\left\{\int_0^{\infty}\mathrm{d}\omega\frac{e^{i\omega\tau_1}}{\omega^2+\omega_c^2}\right\}\ . \end{aligned} \tag{4.25}$$

The integral over the frequency ω can now be performed using the residue theorem, see Appendix A. Followed by the integrals over the times τ_i, we end up with the expressions [65, 88, 91]

$$W'(\tau) = \frac{\eta}{\omega_c}\cot\left(\frac{\beta\omega_c}{2}\right)\left(e^{-\omega_c|\tau|}+\omega_c|\tau|-1\right)+\frac{4\eta\omega_c}{\beta}\sum_{n=1}^{\infty}\frac{e^{-\nu_n|\tau|}+\nu_n|\tau|-1}{\nu_n\left(\nu_n^2-\omega_c^2\right)}\ , \tag{4.26}$$

$$W''(\tau) = -\,\mathrm{sgn}(\tau)\frac{\eta}{\omega_c}\left(e^{-\omega_c|\tau|}-1\right)\ , \tag{4.27}$$

where $\nu_n = \frac{2\pi}{\beta}n$ are known as the Matsubara frequencies stemming from the complex poles of the coth function appearing in Eq. (4.24) when performing the contour integration utilizing the residue theorem and sgn is the signum function. The terms linear in τ in Eq. (4.26) can be summarized by the use of the expansion of the cot function in a series of fractions, i.e., [92]

$$\cot(\pi x) = \frac{1}{\pi x}+\frac{2x}{\pi}\sum_{n=1}^{\infty}\frac{1}{x^2-n^2}\ , \tag{4.28}$$

and we arrive at the full expression for the line shape function given by

$$W(\tau) = \frac{2\eta}{\beta\omega_c}|\tau|+\frac{4\eta\omega_c}{\beta}\sum_{n=1}^{\infty}\frac{e^{-\nu_n|\tau|}-1}{\nu_n\left(\nu_n^2-\omega_c^2\right)}+\frac{\eta}{\omega_c}\left(e^{-\omega_c|\tau|}-1\right)\left[\cot\left(\frac{\beta\omega_c}{2}\right)-i\,\mathrm{sgn}(\tau)\right]\ . \tag{4.29}$$

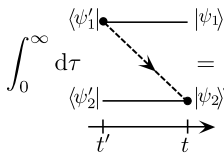

$$\int_0^\infty \mathrm{d}\tau = \int_0^\infty \mathrm{d}\tau S^{\psi_1'\psi_1}_{\psi_2'\psi_2}(\tau) = -i\sum_r \frac{\Gamma}{2\beta}\langle\psi_1|d|\psi_1'\rangle\langle\psi_2'|d^\dagger|\psi_2\rangle \int_0^\infty \mathrm{d}\tau \frac{e^{i\omega_{\psi_1'\psi_1}\tau}e^{-W(+\tau)}e^{-i\mu_r(\tau-\frac{i}{B})}}{\sinh\left(\frac{\pi}{\beta}\left(\tau-\frac{i}{B}\right)\right)}$$

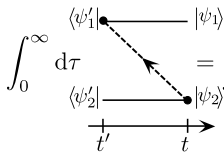

$$\int_0^\infty \mathrm{d}\tau = \int_0^\infty \mathrm{d}\tau T^{\psi_1'\psi_1}_{\psi_2'\psi_2}(\tau) = -i\sum_r \frac{\Gamma}{2\beta}\langle\psi_1|d^\dagger|\psi_1'\rangle\langle\psi_2'|d|\psi_2\rangle \int_0^\infty \mathrm{d}\tau \frac{e^{i\omega_{\psi_1'\psi_1}\tau}e^{-W(+\tau)}e^{+i\mu_r(\tau-\frac{i}{B})}}{\sinh\left(\frac{\pi}{\beta}\left(\tau-\frac{i}{B}\right)\right)}$$

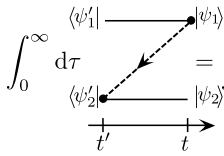

$$\int_0^\infty \mathrm{d}\tau = \int_0^\infty \mathrm{d}\tau U^{\psi_1'\psi_1}_{\psi_2'\psi_2}(\tau) = +i\sum_r \frac{\Gamma}{2\beta}\langle\psi_1|d|\psi_1'\rangle\langle\psi_2'|d^\dagger|\psi_2\rangle \int_0^\infty \mathrm{d}\tau \frac{e^{i\omega_{\psi_2\psi_2'}\tau}e^{-W(-\tau)}e^{+i\mu_r(\tau+\frac{i}{B})}}{\sinh\left(\frac{\pi}{\beta}\left(\tau+\frac{i}{B}\right)\right)}$$

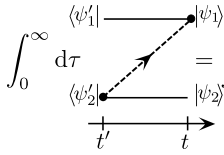

$$\int_0^\infty \mathrm{d}\tau = \int_0^\infty \mathrm{d}\tau V^{\psi_1'\psi_1}_{\psi_2'\psi_2}(\tau) = +i\sum_r \frac{\Gamma}{2\beta}\langle\psi_1|d^\dagger|\psi_1'\rangle\langle\psi_2'|d|\psi_2\rangle \int_0^\infty \mathrm{d}\tau \frac{e^{i\omega_{\psi_2\psi_2'}\tau}e^{-W(-\tau)}e^{-i\mu_r(\tau+\frac{i}{B})}}{\sinh\left(\frac{\pi}{\beta}\left(\tau+\frac{i}{B}\right)\right)}$$

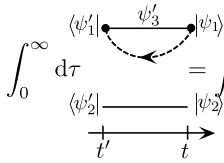

$$\int_0^\infty \mathrm{d}\tau = \int_0^\infty \mathrm{d}\tau W^{\psi_1'\psi_1}_{\psi_2'\psi_2}(\tau) = -i\sum_{r,\psi_3'} \frac{\Gamma}{2\beta}\langle\psi_1|d|\psi_3'\rangle\langle\psi_3'|d^\dagger|\psi_1'\rangle\delta_{\psi_2'\psi_2} \int_0^\infty \mathrm{d}\tau \frac{e^{i\omega_{\psi_1'\psi_3'}\tau}e^{-W(+\tau)}e^{+i\mu_r(\tau-\frac{i}{B})}}{\sinh\left(\frac{\pi}{\beta}\left(\tau-\frac{i}{B}\right)\right)}$$

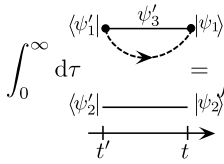

$$\int_0^\infty \mathrm{d}\tau = \int_0^\infty \mathrm{d}\tau X^{\psi_1'\psi_1}_{\psi_2'\psi_2}(\tau) = -i\sum_{r,\psi_3'} \frac{\Gamma}{2\beta}\langle\psi_1|d^\dagger|\psi_3'\rangle\langle\psi_3'|d|\psi_1'\rangle\delta_{\psi_2'\psi_2} \int_0^\infty \mathrm{d}\tau \frac{e^{i\omega_{\psi_1'\psi_3'}\tau}e^{-W(+\tau)}e^{-i\mu_r(\tau-\frac{i}{B})}}{\sinh\left(\frac{\pi}{\beta}\left(\tau-\frac{i}{B}\right)\right)}$$

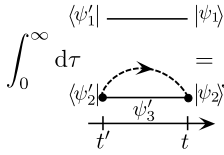

$$\int_0^\infty \mathrm{d}\tau = \int_0^\infty \mathrm{d}\tau Y^{\psi_1'\psi_1}_{\psi_2'\psi_2}(\tau) = +i\sum_{r,\psi_3'} \frac{\Gamma}{2\beta}\langle\psi_2'|d|\psi_3'\rangle\langle\psi_3'|d^\dagger|\psi_2\rangle\delta_{\psi_1'\psi_1} \int_0^\infty \mathrm{d}\tau \frac{e^{i\omega_{\psi_3'\psi_2'}\tau}e^{-W(-\tau)}e^{-i\mu_r(\tau+\frac{i}{B})}}{\sinh\left(\frac{\pi}{\beta}\left(\tau+\frac{i}{B}\right)\right)}$$

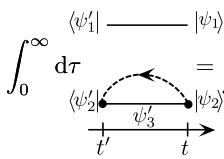

$$\int_0^\infty \mathrm{d}\tau = \int_0^\infty \mathrm{d}\tau Z^{\psi_1'\psi_1}_{\psi_2'\psi_2}(\tau) = +i\sum_{r,\psi_3'} \frac{\Gamma}{2\beta}\langle\psi_2'|d^\dagger|\psi_3'\rangle\langle\psi_3'|d|\psi_2\rangle\delta_{\psi_1'\psi_1} \int_0^\infty \mathrm{d}\tau \frac{e^{i\omega_{\psi_3'\psi_2'}\tau}e^{-W(-\tau)}e^{+i\mu_r(\tau+\frac{i}{B})}}{\sinh\left(\frac{\pi}{\beta}\left(\tau+\frac{i}{B}\right)\right)}$$

Figure 4.3.: Time integral of the tunneling diagrams.

As mentioned before, at time t_0 the tunneling between the molecule and the environment is switched on. For $t_0 \to -\infty$ this is performed adiabatically [35]. We have seen, that all diagrams depend only on the time difference $\tau = t - t'$. Thus, we replace the time variable in the integral of the quantum master equation by τ. Then, the integral runs from zero to infinity, when we set $t_0 = -\infty$. Furthermore, we set our focus on the symmetric tunneling regime, where the tunneling coupling strength of the left and right lead are set to be the same, i.e., $\Gamma = \Gamma_L = \Gamma_R$. In addition, we use the shorthand notation $\omega_{\psi_i\psi_j} = \varepsilon_{\psi_i} - \varepsilon_{\psi_j}$ for the energy difference between state ψ_i and ψ_j of the molecule. The time integral of Eq. (4.20) from the diagram S then becomes

$$\int_0^\infty \mathrm{d}\tau S^{\psi_1'\psi_1}_{\psi_2'\psi_2}(\tau) = -i\frac{\Gamma}{2\beta}\langle\psi_1|d|\psi_1'\rangle\langle\psi_2'|d^\dagger|\psi_2\rangle \sum_r \int_0^\infty \mathrm{d}\tau \frac{e^{i\omega_{\psi_1'\psi_1}\tau} e^{-W(+\tau)} e^{-i\mu_r(\tau - \frac{i}{B})}}{\sinh\left(\frac{\pi}{\beta}\left(\tau - \frac{i}{B}\right)\right)} \ . \tag{4.30}$$

In a similar manner we get the time integrated tunneling rates from the remaining diagrams, see Fig. 4.3.

4.2. Solving the quantum master equation

With the previous considerations, it follows that the quantum master equation can be written in a matrix multiplication notation given in the compact form

$$\frac{\partial}{\partial t}\mathbf{P}(t) = i\boldsymbol{\Delta\varepsilon}\mathbf{P}(t) + \boldsymbol{\Sigma}\boldsymbol{P}(t) \ , \tag{4.31}$$

where the matrix $\boldsymbol{\Delta\varepsilon}$ includes the energy difference $\varepsilon_{\psi_2} - \varepsilon_{\psi_1}$ and the time independent kernel matrix $\boldsymbol{\Sigma}$ includes the time integrated kernel elements stemming from the lowest order tunneling diagrams, i.e., $S^{\psi_1'\psi_1}_{\psi_2'\psi_2} = \int_0^\infty \mathrm{d}\tau S^{\psi_1'\psi_1}_{\psi_2'\psi_2}(\tau)$ and so on. The solution of Eq. (4.31) has the form

$$\mathbf{P}(t) = \exp(\boldsymbol{M}t)\mathbf{P}(0) \ , \tag{4.32}$$

where the matrix $\boldsymbol{M}$ consists of the sum of the matrices $\boldsymbol{\Delta\varepsilon}$ and $\boldsymbol{\Sigma}$. In principle, the matrix $\boldsymbol{M}$ is complex and non-symmetric, meaning it is in general non-diagonalizable [86]. However, there is a way to solve the quantum master equation using the right and left eigenvectors of $\boldsymbol{M}$, denoted as $\boldsymbol{r}_\lambda$ and $\boldsymbol{l}_\lambda$, respectively, and which are given by

$$\boldsymbol{M}\boldsymbol{r}_\lambda = \Lambda_\lambda \boldsymbol{r}_\lambda \ , \quad \boldsymbol{l}_\lambda^\dagger \boldsymbol{M} = \Lambda_\lambda \boldsymbol{l}_\lambda^\dagger \ , \tag{4.33}$$

where $\Lambda_\lambda = \Gamma_\lambda + i\Omega_\lambda$ is the λ-th eigenvalue of the corresponding eigenvector. The stationary solution corresponds to the eigenvector $\boldsymbol{r}_0$ with the eigenvalue $\Lambda_0 = 0$, which is the only eigenvector with a non-zero trace, i.e., $\mathrm{Tr}\,[\boldsymbol{r}_\lambda] = \delta_{\lambda 0}$ [93]. The real part of the remaining eigenvalues is always negative, i.e., $\Gamma_{\lambda\neq 0} < 0$, and describes the time scale of relaxation and decoherent processes. In addition, the asymptotic relaxation rate of the system is given by the largest non-zero real part of the eigenvalues. On the other hand, the imaginary part Ω_λ determines the time scale of coherent processes. We can

expand the initial state $\mathbf{P}(0)$ in terms of the right eigenvectors, i.e., $\mathbf{P}(0) = \sum_\lambda c_\lambda \boldsymbol{r}_\lambda$, and hence write the solution (4.32) as

$$\mathbf{P}(t) = \sum_\lambda c_\lambda \boldsymbol{r}_\lambda e^{(\Gamma_\lambda + i\Omega_\lambda)t} \ , \tag{4.34}$$

where the expansion coefficients c_λ are chosen such that Eq.(4.34) satisfies the initial condition while ensuring that the probability is conserved at all times, i.e., $\mathrm{Tr}\,[\mathbf{P}] = 1$, leading to $c_0 = 1$ [93]. Knowledge of the time evolution of the reduced density matrix then allows us to calculate expectation values of any system operator [74]. Since we are interested in the influence of the solvent on the charge current through the molecule, we investigate in the following chapter the expectation value of the stationary charge current flowing through the molecule as well as the differential conductance. In order to determine stationary quantities as well as the stationary state, which the system approaches for $t \to \infty$, we know that the stationary reduced density matrix elements $P_{\infty\psi_2}^{\psi_1} = \lim_{t\to\infty} P_{\psi_2}^{\psi_1}(t)$ do not change with time anymore and the quantum master equation simplifies to

$$\frac{\partial}{\partial t} P_{\infty\psi_2}^{\psi_1} = 0 \ . \tag{4.35}$$

We calculate the time integral appearing in (4.30) and all the other diagrams as well as the solution of the quantum master equation (4.32) numerically. To this extent, we use a *LAPACK* routine, which calculates the left and right eigenvectors and the corresponding eigenvalues of the matrix $\boldsymbol{M}$, with which we can then determine the stationary state as well as the matrix exponential and in total the solution of the quantum master equation (4.34) or (4.32). With the stationary solution we can determine the stationary tunneling current.

4.3. The stationary tunneling current

The operator of the tunneling current through lead r is given by the time derivative of the particle number operator $N_r(t) = \sum_k c_{k,r}^\dagger(t) c_{k,r}(t)$ of the respective lead multiplied by the elementary charge $e > 0$. Utilizing the Heisenberg picture we can employ the Heisenberg equation of motion and get

$$I_r(t)_\mathrm{H} = e\frac{\mathrm{d}}{\mathrm{d}t} N_r(t)_\mathrm{H} = ie\left[H, N_r\right](t)_\mathrm{H} = ie\left[H_\mathrm{tun}, N_r\right](t)_\mathrm{H} \ , \tag{4.36}$$

where we have used, that the particle number operator commutes with the free Hamiltonian H_0 and for the remaining commutators the relations $\left[c_{k,r}^\dagger c_{k,r}, c_{k,r}\right] = -c_{k,r}$ as well as $\left[c_{k,r}^\dagger c_{k,r}, c_{k,r}^\dagger\right] = c_{k,r}^\dagger$ has been applied. Inserting the expression for the tunneling Hamiltonian (3.10) yields

$$I_r(t)_\mathrm{H} = -ie \sum_k \left(t_{k,r} c_{k,r}^\dagger(t)_\mathrm{H} d(t)_\mathrm{H} - \mathrm{H.c.} \right) \ . \tag{4.37}$$

Notice that in this form the tunneling current operator resembles the tunneling Hamiltonian H_{tun} apart from the prefactor $-ie$ and the minus sign in front of the Hermitian conjugate part which creates an electron on the molecule. In order to calculate a measurable quantity we have to evaluate the expectation value of the current operator, which is given by

$$\langle I_r(t)\rangle = \mathrm{Tr}\left[\rho(t_0) I_r(t)_{\mathrm{H}}\right] = \mathrm{Tr}\left[\rho(t)_I I_r(t)_I\right] \ , \tag{4.38}$$

where we have switched again to the interaction picture in order to utilize the previous calculations of the diagrammatic technique. Inserting the integrated Liouville-von Neumann equation (4.6) then leads to

$$\langle I_r(t)\rangle = -i\mathrm{Tr}\left[\int_{t_0}^{t} \mathrm{d}t' \left[H_{\mathrm{tun}}(t')_I, \rho(t')_I\right] I_r(t)_I\right] \ , \tag{4.39}$$

where we have used again that the term with $\rho(t_0)_I$ vanishes due to the fact that the current operator is non-diagonal in the system and environment operators in the same way as H_{tun} has been for the calculation of the reduced density matrix. This equation looks also very similar to the quantum master equation (4.10) apart from the free evolution of the isolated molecule. Indeed, this equation can be written in accordance to Eq. (4.11) as [35]

$$\langle I_r(t)\rangle = -e \sum_{\psi_1'\psi_2'\psi_3} \int_{t_0}^{t} \mathrm{d}t' P^{\psi_1'}_{\psi_2'}(t') \Sigma^{I_r \psi_1' \psi_3}_{\psi_2' \psi_3}(t', t) \ , \tag{4.40}$$

where the irreducible self-energy $\Sigma^{I_r\psi_1'\psi_3}_{\psi_2'\psi_3}(t',t)$ now stems from the current operator of the lead r and thus contains the superscript I_r. In the same fashion as we have done before for the reduced density matrix, we will show how to get from Eq. (4.39) to Eq. (4.40) and identify the current rates $\Sigma^{I_r\psi_1'\psi_3}_{\psi_2'\psi_3}(t',t)$ as well as the contributing diagrams. By expanding the commutator from Eq. (4.39) and writing down the trace over the molecule eigenstates out of the full trace as well as including identities between the operators we get to the expression

$$\begin{aligned}\langle I_r(t)\rangle = -i \sum_{\psi_1'\psi_2'\psi_3} \int_{t_0}^{t} \mathrm{d}t' \mathrm{Tr}_{\mathrm{leads}}\mathrm{Tr}_{\mathrm{solv}} \Bigg[& \underbrace{\langle\psi_3|H_{\mathrm{tun}}(t')_I|\psi_1'\rangle\langle\psi_1'|\rho(t')_I|\psi_2'\rangle\langle\psi_2'|I_r(t)_I|\psi_3\rangle}_{(v)} \\ & - \underbrace{\langle\psi_1'|\rho(t')_I|\psi_2'\rangle\langle\psi_2'|H_{\mathrm{tun}}(t')_I|\psi_3\rangle\langle\psi_3|I_r(t)_I|\psi_1'\rangle}_{(vi)} \Bigg] \ .\end{aligned} \tag{4.41}$$

Applying the same steps used from Eq. (4.13) to Eq. (4.14) including the Markov approximation ($\rho(t')_I \to \rho(t)_I$) and $\tau = t - t'$ we get

$$\begin{aligned}\langle I_r(t)\rangle = &- e \sum_{\psi_1'\psi_2'\psi_3} \int_{t_0}^{t} \mathrm{d}\tau P_{\psi_2'}^{\psi_1'}(t) \sum_k |t_{k,r}|^2 \\ &\times \Big\{ e^{i(\varepsilon_{\psi_1'} - \varepsilon_{\psi_3})\tau} e^{-W(+\tau)} \Big[e^{+i\varepsilon_{k,r}\tau} f_r^+(\varepsilon_{k,r}) \langle\psi_3|d^\dagger|\psi_1'\rangle\langle\psi_2'|d|\psi_3\rangle \\ &\qquad - e^{-i\varepsilon_{k,r}\tau} f_r^-(\varepsilon_{k,r}) \langle\psi_3|d|\psi_1'\rangle\langle\psi_2'|d^\dagger|\psi_3\rangle \Big] \\ &+ e^{i(\varepsilon_{\psi_3} - \varepsilon_{\psi_2'})\tau} e^{-W(-\tau)} \Big[e^{+i\varepsilon_{k,r}\tau} f_r^-(\varepsilon_{k,r}) \langle\psi_2'|d^\dagger|\psi_3\rangle\langle\psi_3|d|\psi_1'\rangle \\ &\qquad - e^{-i\varepsilon_{k,r}\tau} f_r^+(\varepsilon_{k,r}) \langle\psi_2'|d|\psi_3\rangle\langle\psi_3|d^\dagger|\psi_1'\rangle \Big] \Big\} . \end{aligned} \tag{4.42}$$

By comparison with Eq. (4.40) we can, again, directly read off the lowest-order irreducible self-energy, this time stemming from the current operator. We recognize that there are four contributing terms coming from the two terms (v) and (vi) in Eq. (4.41). We proceed with the change to a continuous description utilizing the wide-band approximation in the symmetric tunneling regime, i.e., $\sum_k |t_{k,r}|^2 \to \frac{\Gamma}{2\pi} \int \mathrm{d}\varepsilon$ and calculate the energy integral with Eq. (4.21). Setting $t_0 \to -\infty$ and writing down the time integrated tunneling current rates $\Sigma^{I_r \psi_1' \psi_3}_{\psi_2' \psi_3} = \int_0^\infty \mathrm{d}\tau \Sigma^{I_r \psi_1' \psi_3}_{\psi_2' \psi_3}(\tau)$ we end up with the four contributing diagrams shown in Fig. 4.4. As we expected, the four diagrams resemble the first four diagrams from the reduced density matrix apart from the fact that the right vertex at time t always stems from the current operator. Therefore, the diagrams where an electron is created on the molecule at time t, i.e., where the arrow points onto the circle of the vertex stemming from the current operator, carry an additional minus sign compared to the diagrams of the reduced density matrix. This minus sign stems from the minus sign in front of the Hermitian conjugate part in Eq. (4.37). Finally, we get the stationary current $\langle I_r\rangle_\infty = \lim_{t\to\infty}\langle I_r(t)\rangle$ with the aid of the stationary reduced density matrix elements (4.35) in the following way

$$\langle I_r\rangle_\infty = -e \sum_{\psi_1'\psi_2'\psi_3} P_{\infty \psi_2'}^{\psi_1'} \Sigma^{I_r \psi_1' \psi_3}_{\psi_2' \psi_3} , \tag{4.43}$$

where we recall that the irreducible self-energy part $\Sigma^{I_r \psi_1' \psi_3}_{\psi_2' \psi_3}$ from the current operator consists of the sum of the four time-integrated diagrams depicted in Fig. 4.4. The procedure to calculate the stationary current is now as follows. First, the stationary reduced density matrix is evaluated via the left and right eigenvectors introduced in Eq. (4.33). To this extent, the time-integrated tunneling diagrams from Fig. 4.3 need to be calculated in order to solve the quantum master equation (4.31). At the same time, the integrated tunneling current diagrams from Fig. 4.4 are established. Finally, the stationary tunneling current can be calculated by means of Eq. (4.43). In Chapter 5.6 we will investigate the numerical results and discuss the influence of the solvent on the current.

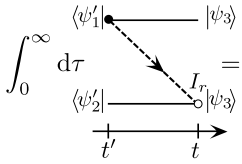

$$\int_0^\infty \mathrm{d}\tau = \int_0^\infty \mathrm{d}\tau S^{I_r \psi_1' \psi_3}_{\psi_2' \psi_3}(\tau) = +i\frac{\Gamma}{2\beta}\langle\psi_3|d|\psi_1'\rangle\langle\psi_2'|d^\dagger|\psi_3\rangle \int_0^\infty \mathrm{d}\tau \frac{e^{i\omega_{\psi_1'\psi_3}\tau} e^{-W(+\tau)} e^{-i\mu_r(\tau - \frac{i}{B})}}{\sinh\left(\frac{\pi}{\beta}\left(\tau - \frac{i}{B}\right)\right)}$$

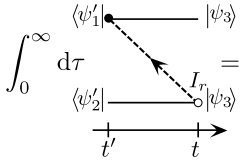

$$\int_0^\infty \mathrm{d}\tau = \int_0^\infty \mathrm{d}\tau T^{I_r \psi_1' \psi_3}_{\psi_2' \psi_3}(\tau) = -i\frac{\Gamma}{2\beta}\langle\psi_3|d^\dagger|\psi_1'\rangle\langle\psi_2'|d|\psi_3\rangle \int_0^\infty \mathrm{d}\tau \frac{e^{i\omega_{\psi_1'\psi_3}\tau} e^{-W(+\tau)} e^{+i\mu_r(\tau - \frac{i}{B})}}{\sinh\left(\frac{\pi}{\beta}\left(\tau - \frac{i}{B}\right)\right)}$$

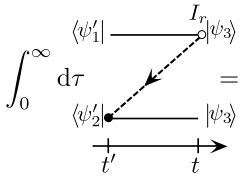

$$\int_0^\infty \mathrm{d}\tau = \int_0^\infty \mathrm{d}\tau U^{I_r \psi_1' \psi_3}_{\psi_2' \psi_3}(\tau) = +i\frac{\Gamma}{2\beta}\langle\psi_2'|d^\dagger|\psi_3\rangle\langle\psi_3|d|\psi_1'\rangle \int_0^\infty \mathrm{d}\tau \frac{e^{i\omega_{\psi_3\psi_2'}\tau} e^{-W(-\tau)} e^{+i\mu_r(\tau + \frac{i}{B})}}{\sinh\left(\frac{\pi}{\beta}\left(\tau + \frac{i}{B}\right)\right)}$$

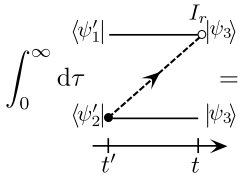

$$\int_0^\infty \mathrm{d}\tau = \int_0^\infty \mathrm{d}\tau V^{I_r \psi_1' \psi_3}_{\psi_2' \psi_3}(\tau) = -i\frac{\Gamma}{2\beta}\langle\psi_2'|d|\psi_3\rangle\langle\psi_3|d^\dagger|\psi_1'\rangle \int_0^\infty \mathrm{d}\tau \frac{e^{i\omega_{\psi_3\psi_2'}\tau} e^{-W(-\tau)} e^{-i\mu_r(\tau + \frac{i}{B})}}{\sinh\left(\frac{\pi}{\beta}\left(\tau + \frac{i}{B}\right)\right)}$$

Figure 4.4.: Time integral of the tunneling current diagrams.

Chapter 5.

Dielectric solvation dynamics

This chapter focuses on the solvation dynamics involving charged and polar solutes in dielectric environments. Our discussion follows Refs. [64, 65]. Most electron transfer reactions occur in polar solution. Here the solvent molecules such as water are characterized by permanent dipoles. By changing the type of solvent it is possible to change the magnitude of the molecular dipoles. In this manner one can control an additional external parameter (besides temperature and applied voltages) influencing the electron transfer characteristics [65].

We consider a polar solvent characterized by its dielectric response function $\varepsilon(\omega)$. Upon a sudden change in the charge distribution inside this solvent a relaxation process follows in which the solvent adjusts to the new charge distribution. We want to describe this relaxation process in terms of the dielectric response function [64]. Since the dielectric function is of central importance, we briefly recall its definition and physical meaning. If an (external) field is applied to a dielectric material, it becomes polarized. This polarization results from a deformation of the electron cloud of the molecules forming the dielectric. If these molecules possess a permanent dipole moment and if they are not very densely packed, they may also reorient in the course of time. This results in the orientational polarization. Usually a deformation of the nuclear geometry is less important. All polarization contributions can be comprised in the macroscopic vector field of the dipole density (polarization vector) $\mathbf{P}$ [65].

In a typical experiment, for instance, by photoionization, the solute charge distribution is assumed to change abruptly, at $t = 0$, say, from $\rho_1(\mathbf{r})$ to $\rho_2(\mathbf{r})$, then stays constant. This means that the dielectric displacement, related to $\rho(\mathbf{r})$ by the Poisson equation $\nabla \cdot \boldsymbol{\mathcal{D}} = 4\pi\rho$, is also switched from $\boldsymbol{\mathcal{D}}_1$ to $\boldsymbol{\mathcal{D}}_2$ at t = 0. In the process that follows the solvent structure adjusts itself to the new charge distribution. This appears as a local relaxation of the solvent polarization, which over time changes from $\mathbf{P}_1$ to $\mathbf{P}_2$ [64].

For many applications it suffices to consider two distinct contributions to the complete polarization field $\mathbf{P}$. The first contribution $\mathbf{P}_{\mathrm{el}}$ refers to the polarization of the electron cloud of the molecules. Due to the small mass of the electrons compared to that of the molecule, this polarization may respond to high-frequency external fields. It forms the high-frequency part $\mathbf{P}_\infty$ of the total polarization field, $\mathbf{P}_\infty \equiv \mathbf{P}_{\mathrm{el}}$. The second contribution is related to an orientational polarization $\mathbf{P}_{\mathrm{or}}$ that follows from an reorientation of the molecules carrying a permanent dipole moment. This type of

polarization responds much more slowly to an external disturbance than $\mathbf{P}_{\text{el}}$. Together with the electronic contribution it results in the low-frequency part $\mathbf{P}_0$, and we can set $\mathbf{P}_0 \equiv \mathbf{P}_{\text{or}} + \mathbf{P}_{\text{el}}$ [65]. These induced polarizations affect the local electrostatic field at the solute, therefore its energy. We want to relate the time evolution of this local electrostatic field to the given dielectric response function $\varepsilon(\omega)$ [64].

5.1. Dielectric relaxation and the Debye model

In linear dielectric response theory, the electrostatic displacement $\boldsymbol{\mathcal{D}}$, and the electrostatic field $\boldsymbol{\mathcal{E}}$ in a dielectric medium are related to each other by [64]

$$\boldsymbol{\mathcal{D}}(\mathbf{r},t) = \int d\mathbf{r}' \int_{-\infty}^{t} dt' \boldsymbol{\varepsilon}(\mathbf{r}-\mathbf{r}', t-t') \boldsymbol{\mathcal{E}}(\mathbf{r}', t') \,. \tag{5.1}$$

We assume that the response is local, that is, $\boldsymbol{\varepsilon}(\mathbf{r}-\mathbf{r}', t-t') = \boldsymbol{\varepsilon}(\mathbf{r}, t-t')\delta(\mathbf{r}-\mathbf{r}')$. This assumption is not really valid for dielectric response on molecular length scales, but the errors that result from it appear to be small in many cases while the mathematical simplification is considerable. Also, while in general the dielectric response $\boldsymbol{\varepsilon}$ is a tensor, we take it for simplicity to be a scalar, that is, we consider only isotropic systems. In this case, it is sufficient to consider the magnitudes $\mathcal{D}$ and $\mathcal{E}$ of $\boldsymbol{\mathcal{D}}$ and $\boldsymbol{\mathcal{E}}$ [64]. Thus, we have the local scalar relationship

$$\mathcal{D}(\mathbf{r},t) = \int_{-\infty}^{t} dt' \varepsilon(t-t') \mathcal{E}(\mathbf{r},t') \,, \tag{5.2}$$

and its Fourier transform (defining, for example, $\mathcal{E}(\omega) = \int_{-\infty}^{\infty} dt e^{i\omega t} \mathcal{E}(t)$)

$$\mathcal{D}(\omega) = \varepsilon(\omega)\mathcal{E}(\omega) \,, \tag{5.3}$$

where

$$\varepsilon(\omega) \equiv \int_{0}^{\infty} dt e^{i\omega t} \varepsilon(t) \,. \tag{5.4}$$

To account for the fast and slow components of the dielectric response, we take $\varepsilon(t)$ in the form

$$\varepsilon(t) = \varepsilon_e \delta(t) + \tilde{\varepsilon}(t) \,, \tag{5.5}$$

to get

$$\mathcal{D}(t) = \varepsilon_e \mathcal{E}(t) + \int_{-\infty}^{t} dt' \tilde{\varepsilon}(t-t') \mathcal{E}(t') \,, \tag{5.6}$$

$$\mathcal{D}(\omega) = \varepsilon_e \mathcal{E}(\omega) + \tilde{\varepsilon}(\omega)\mathcal{E}(\omega) \,. \tag{5.7}$$

The Debye model takes for the slow part of the dielectric response the form

$$\tilde{\varepsilon}(t) = \frac{\varepsilon_S - \varepsilon_e}{\tau_D} e^{-t/\tau_D} \,, \tag{5.8}$$

so that

$$\varepsilon(\omega) = \varepsilon_e + \int_0^\infty dt \frac{\varepsilon_S - \varepsilon_e}{\tau_D} e^{-t/\tau_D} e^{i\omega t} = \varepsilon_e + \frac{\varepsilon_S - \varepsilon_e}{1 - i\omega\tau_D} \,. \tag{5.9}$$

The dielectric response in this model is thus characterized by three parameters: The electronic ε_e and static ε_S response constants, and the Debye relaxation time τ_D [64]. The electronic response constant forms the high-frequency part of the dielectric function, i.e., $\varepsilon_\infty \equiv \varepsilon_e$.

When we take the time derivative of Eq. (5.6) with respect to t

$$\frac{d\mathcal{D}}{dt} = \varepsilon_e \frac{d\mathcal{E}}{dt} + \tilde{\varepsilon}(0)\mathcal{E}(t) + \int_{-\infty}^{t} dt' \left(\frac{d\tilde{\varepsilon}}{dt}\right)_{t-t'} \mathcal{E}(t') \,, \tag{5.10}$$

and use

$$\int_{-\infty}^{t} dt' \left(\frac{d\tilde{\varepsilon}}{dt}\right)_{t-t'} \mathcal{E}(t') = -\frac{1}{\tau_d} \int_{-\infty}^{t} dt' \tilde{\varepsilon}(t-t')\mathcal{E}(t') = -\frac{1}{\tau_D}(\mathcal{D}(t) - \varepsilon_e \mathcal{E}(t)) \,, \tag{5.11}$$

we get

$$\frac{d}{dt}(\mathcal{D} - \varepsilon_e \mathcal{E}) = -\frac{1}{\tau_D}(\mathcal{D} - \varepsilon_S \mathcal{E}) \,. \tag{5.12}$$

An interesting outcome of Eq. (5.12) is that the implied relaxation depends on the way the experiment is conducted [64]. When we consider an abrupt change in the solute charge distribution, as described in the previous section, it implies a jump in the dielectric displacement $\mathcal{D}$. This jump in $\mathcal{D}$ can be accounted for by the Heaviside step function $\theta(t)$ as

$$\mathcal{D}(t) = \mathcal{D}\theta(t) = \begin{cases} 0, & t < 0 \,, \\ \mathcal{D}, & t \geq 0 \,. \end{cases} \tag{5.13}$$

In this case Eq. (5.12) describes the evolution of $\mathcal{E}$ under the constant displacement $\mathcal{D}$,

$$\frac{d}{dt}\mathcal{E} = -\frac{\varepsilon_S}{\varepsilon_e \tau_D} \left(\mathcal{E} - \frac{1}{\varepsilon_S}\mathcal{D}\right) \,. \tag{5.14}$$

This implies that at equilibrium ($d\mathcal{E}/dt = 0$), $\mathcal{E} = \varepsilon_S^{-1}\mathcal{D}$. Immediately following the jump in $\mathcal{D}$, however, the electric field is $\mathcal{E}(t=0) = \varepsilon_e^{-1}\mathcal{D}$. The corresponding solution of Eq. (5.14) is then

$$\mathcal{E}(t) = \frac{1}{\varepsilon_S}\mathcal{D} + \left(\frac{1}{\varepsilon_e} - \frac{1}{\varepsilon_S}\right)\mathcal{D}e^{-t/\tau_L} \,, \tag{5.15}$$

where τ_L is the longitudinal relaxation time

$$\tau_L = \frac{\varepsilon_e}{\varepsilon_S}\tau_D \,. \tag{5.16}$$

We see that in this case the relaxation is characterized by the time τ_L which can be quite different from τ_D: For example in water $\varepsilon_e/\varepsilon_S \approx 1/20$ and while $\tau_D \approx 8$ ps, τ_L is of the order of 0.4 ps. The origin of the terms transverse and longitudinal dielectric relaxation times lies in the molecular theory of dielectric relaxation, where one finds that the decay of correlation functions involving transverse and longitudinal components of the induced polarization vector are characterized by different time constants. In a Debye fluid the relaxation times that characterize the transverse and longitudinal components of the polarization are τ_D and $\tau_L = \frac{\varepsilon_e}{\varepsilon_S}\tau_D$, respectively [64].

For what follows we want to address how an external field, e.g., induced by the charge distribution of the solute, leads to a change of the charge distribution in the solvent, characterized in terms of its polarization [63].

5.2. Dynamic response of the solvent polarization

In general, there will be a dependence of the solvent polarization field on the external field, that is, $\mathbf{P}$ becomes an (in general) nonlinear functional of the electric field. For a weak perturbation of the solvent due to the external field, a linear relation between the electric field and the polarization is justified in the form [63]

$$\mathbf{P}(\mathbf{r},t) = \int d\mathbf{r}' \int dt' \boldsymbol{\chi}(\boldsymbol{r},\boldsymbol{r}';t,t')\boldsymbol{\mathcal{E}}(\boldsymbol{r}',t') \,. \tag{5.17}$$

Here, $\boldsymbol{\chi}$ is the tensor of electric susceptibility, because the direction of $\mathbf{P}$ can differ from that of the electric field $\boldsymbol{\mathcal{E}}$. For an isotropic solvent, $\mathbf{P}$ and $\boldsymbol{\mathcal{E}}$ are parallel and the electric susceptibility becomes a scalar χ. The dependence of $\boldsymbol{\chi}(\boldsymbol{r},\boldsymbol{r}';t,t')$ on time and position reflects the fact that an applied field at a certain position at a certain time may cause a response at another position at a later time. In a homogeneous and stationary solvent the susceptibility depends only on position and time differences, i.e., $\boldsymbol{\chi}(\boldsymbol{r},\boldsymbol{r}';t,t') = \boldsymbol{\chi}(\boldsymbol{r}-\boldsymbol{r}';t-t')$. For a local susceptibility in time and position and an isotropic solvent, we even have that $\boldsymbol{\chi}(\boldsymbol{r}-\boldsymbol{r}';t-t') = \chi\delta(\boldsymbol{r}-\boldsymbol{r}')\delta(t-t')$, which implies $\mathbf{P} = \chi\boldsymbol{\mathcal{E}}$. We assume that the electric field in the solvent results from an externally controlled charge density $\rho_{ex}(\boldsymbol{r})$, i.e., from the solute molecule, and the polarization charge density of the solvent $\rho_P(\boldsymbol{r})$. Therefore, the relation for the overall electric field in the solvent $\nabla\boldsymbol{\mathcal{E}}(\boldsymbol{r}) = 4\pi(\rho_{ex}(\boldsymbol{r}) + \rho_P(\boldsymbol{r}))$ holds. The dielectric displacement field, which obeys $\nabla\boldsymbol{\mathcal{D}}(\boldsymbol{r}) = 4\pi\rho_{ex}(\boldsymbol{r})$ and where $\boldsymbol{\mathcal{D}} = \boldsymbol{\mathcal{E}} + 4\pi\mathbf{P}$, may be interpreted as the external field induced by $\rho_{ex}(\boldsymbol{r})$. For vacuum and, hence, in absence of the polarizable solvent $\boldsymbol{\mathcal{D}} = \boldsymbol{\mathcal{E}}$ [63]. Accordingly, we identify

$$\mathbf{P} = \frac{1}{4\pi}\left(\boldsymbol{\mathcal{D}} - \boldsymbol{\mathcal{E}}\right) \tag{5.18}$$

as the field induced by the dielectric solvent. With the definition of the (local) dielectric constant $\varepsilon = 1 + 4\pi\chi$, one can write the relation $\boldsymbol{\mathcal{D}} = \boldsymbol{\mathcal{E}} + 4\pi\mathbf{P}$ as $\boldsymbol{\mathcal{E}} = \varepsilon^{-1}\boldsymbol{\mathcal{D}}$. In dielectric media, $\varepsilon > 1$ holds such that the electric field $\boldsymbol{\mathcal{E}}$ inside the solvent is smaller than the applied field outside the solvent which we identify by the dielectric displacement vector $\boldsymbol{\mathcal{D}}$. This reduction of the field is a clear signature of the polarization of the solvent [63].

If the charge distribution of the solute varies appreciably during a time period, the response of the microscopic solvent particles, i.e., molecules, atoms or electrons, will not be sufficiently rapid to build up a new equilibrium polarization, such that the actual polarization $\mathbf{P}$ of the continuous solvent will lag behind the changing charge distribution and the corresponding displacement field $\boldsymbol{\mathcal{D}}$ of the solute [63]. The function mediating the linearized dependence (in analogy to Eqs. (5.1) and (5.17)) between $\mathbf{P}$ and $\boldsymbol{\mathcal{D}}$ is known as the linear molecular polarizability α [65]. For an isotropic and homogeneous solvent which is local in position, the polarizability is given according to the applied external field $\boldsymbol{\mathcal{D}} = \varepsilon^{-1}\boldsymbol{\mathcal{D}} + 4\pi\mathbf{P}$ outside as [63]

$$\mathbf{P}(t) = \frac{1}{4\pi}\int_{-\infty}^{t} dt'[\delta(t-t') - \varepsilon^{-1}(t-t')]\boldsymbol{\mathcal{D}}(t') \equiv \frac{1}{4\pi}\int_{-\infty}^{t} dt'\alpha(t-t')\boldsymbol{\mathcal{D}}(t')\,. \tag{5.19}$$

The assumption of locality is valid if the spatial variation of the actual external electric field $\boldsymbol{\mathcal{D}}(t)$ is small on the scale of atomic or molecular extensions inducing the polarization [63]. Carrying out a Fourier transform of Eq. (5.19), we get $\mathbf{P}(\omega) = \alpha(\omega)\boldsymbol{\mathcal{D}}(\omega)$. Together with the Fourier transform of Eqs. (5.1) and (5.17) for homogeneous and isotropic systems we have the relations

$$\begin{aligned} \mathbf{P}(\omega) &= \alpha(\omega)\boldsymbol{\mathcal{D}}(\omega)\,, \\ \boldsymbol{\mathcal{D}}(\omega) &= \varepsilon(\omega)\boldsymbol{\mathcal{E}}(\omega)\,, \\ \mathbf{P}(\omega) &= \chi(\omega)\boldsymbol{\mathcal{E}}(\omega)\,, \end{aligned} \tag{5.20}$$

with

$$\begin{aligned} \alpha(\omega) &= \frac{1}{4\pi}(1 - \varepsilon^{-1}(\omega))\,, \\ \chi(\omega) &= \frac{1}{4\pi}(\varepsilon(\omega) - 1)\,. \end{aligned} \tag{5.21}$$

The frequency-domain function of the polarizability $\alpha(\omega)$, as well as the time-domain version enclosed in Eq. (5.19), contains the response of the solvent polarization to an externally applied time-dependent field.

We briefly comment on the relation between the low- and high-frequency limits of the dielectric function (5.9) and the corresponding components of the polarization field, as laid out in Ref. [65]. Suppose that the external field $\boldsymbol{\mathcal{D}}$ is monochromatic. If it oscillates with a low frequency ω_{low} we write

$$\boldsymbol{\mathcal{D}}(t) = \boldsymbol{\mathcal{D}}_{\text{low}} e^{-i\omega_{\text{low}}t} + \boldsymbol{\mathcal{D}}^{*}_{\text{low}} e^{i\omega_{\text{low}}t}\,. \tag{5.22}$$

Inserting this into Eq. (5.19) gives

$$\begin{aligned}\mathbf{P}_0 &= \frac{1}{4\pi}\{[1-\varepsilon^{-1}(\omega_{\text{low}})]\boldsymbol{\mathcal{D}}_{\text{low}}e^{-i\omega_{\text{low}}t} + [1-\varepsilon^{-1}(-\omega_{\text{low}})]\boldsymbol{\mathcal{D}}^*_{\text{low}}e^{i\omega_{\text{low}}t}\} \\ &\approx \frac{1}{4\pi}\left(1-\frac{1}{\varepsilon_S}\right)\boldsymbol{\mathcal{D}}\,. \end{aligned} \tag{5.23}$$

If exclusively high-frequency components are contained in the external field, one can deduce in the same manner

$$\mathbf{P}_\infty = \frac{1}{4\pi}\left(1-\frac{1}{\varepsilon_\infty}\right)\boldsymbol{\mathcal{D}}\,. \tag{5.24}$$

Since $\mathbf{P}_0$ also contains an electronic contribution, the orientational polarization follows as

$$\mathbf{P}_{\text{or}} = \mathbf{P}_0 - \mathbf{P}_\infty = \frac{1}{4\pi}\left(\frac{1}{\varepsilon_\infty}-\frac{1}{\varepsilon_S}\right)\boldsymbol{\mathcal{D}}\,. \tag{5.25}$$

The combination

$$c_{\text{Pek}} = \frac{1}{\varepsilon_\infty}-\frac{1}{\varepsilon_S} \tag{5.26}$$

of the inverse dielectric constants is known as the Pekar factor [65]. The dielectric response of a polar medium, characterized by the polarization field $\mathbf{P}$, can be described in terms of the Hamiltonian (3.3) that corresponds to a system of independent harmonic oscillators in which the harmonic modes are motions of the polarization field [64, 94].

5.3. Harmonic field representation of dielectric response

In this section, we briefly show how the response of the polarization field $\mathbf{P}$ can be described by a Hamiltonian for independent harmonic oscillators. Our discussion follows Ref. [94], where H. Fröhlich has calculated this relation for a free electron in the conduction band of an isotropic ionic crystal lattice. In such a lattice the electron is subject to forces due to displacements and deformations of atoms or ions. Such displacements can be described by attaching a displacement vector to each lattice point. Moreover, for electrons with sufficiently low energy the electronic wave function changes only very little in one lattice distance. Therefore, the lattice can be treated as a continuum. The displacement vectors then become a continuous function of position, i.e., they form a vector field [94]. Furthermore, displacements leading to electric polarization have a much stronger interaction with electrons than other types of displacements in ionic crystals. The latter will, therefore, be disregarded [94]. Let $\mathbf{P}(\boldsymbol{r})$ be the electric polarization at the position $\boldsymbol{r}$. In reasonable approximation it suffices to consider two distinct contributions to the complete polarization field, as

discussed in the previous section. In the presence of an external field $\boldsymbol{\mathcal{D}}(\boldsymbol{r}, \boldsymbol{r}_{el})$ due to an electron at position $\boldsymbol{r}_{el}$, the equations of motion for the two polarization field contributions read [94]

$$\ddot{\mathbf{P}}_{\mathrm{or}}(\boldsymbol{r}) + \omega^2 \mathbf{P}_{\mathrm{or}}(\boldsymbol{r}) = \boldsymbol{\mathcal{D}}(\boldsymbol{r}, \boldsymbol{r}_{el})/\gamma \,, \tag{5.27}$$

$$\ddot{\mathbf{P}}_{\infty}(\boldsymbol{r}) + \omega_{\infty}^2 \mathbf{P}_{\infty}(\boldsymbol{r}) = \boldsymbol{\mathcal{D}}(\boldsymbol{r}, \boldsymbol{r}_{el})/\delta \,. \tag{5.28}$$

Here, $\omega \equiv \omega_{\mathrm{low}}$ and ω_∞ correspond to the low- and high-frequency oscillations of the external field, respectively. The constants γ and δ are closely connected with the energy due to the respective displacements (cf. Eq. (5.31)). Comparison of Eqs. (5.27) and (5.28), for the static case ($\ddot{\mathbf{P}}_{\mathrm{or}} = 0, \ddot{\mathbf{P}}_{\infty} = 0$), with Eqs. (5.25) and (5.24) respectively leads to [94]

$$\frac{1}{\gamma} = \frac{\omega^2}{4\pi} \left(\frac{1}{\varepsilon_\infty} - \frac{1}{\varepsilon_S} \right) , \tag{5.29}$$

$$\frac{1}{\delta} = \frac{\omega_\infty^2}{4\pi} \left(1 - \frac{1}{\varepsilon_\infty} \right) . \tag{5.30}$$

The equations of motion (5.27) and (5.28) can be derived from the Lagrangian [94]

$$L = \frac{\gamma}{2} \int \left[\dot{\mathbf{P}}_{\mathrm{or}}^2(\boldsymbol{r}) - \omega^2 {\mathbf{P}_{\mathrm{or}}}^2(\boldsymbol{r}) \right] d^3\boldsymbol{r} + \frac{\delta}{2} \int \left[\dot{\mathbf{P}}_{\infty}^2(\boldsymbol{r}) - \omega_\infty^2 \mathbf{P}_{\infty}^2(\boldsymbol{r}) \right] d^3\boldsymbol{r} + \int \boldsymbol{\mathcal{D}}(\boldsymbol{r}, \boldsymbol{r}_{el}) \left[\mathbf{P}_{\mathrm{or}}(\boldsymbol{r}) + \mathbf{P}_{\infty}(\boldsymbol{r}) \right] d^3\boldsymbol{r} \,, \tag{5.31}$$

by putting

$$\delta L = 0 \,, \tag{5.32}$$

and treating the components of $\mathbf{P}_{\mathrm{or}}(\boldsymbol{r})$ and $\mathbf{P}_{\infty}(\boldsymbol{r})$ as variables. We have omitted the motion of the free electron in Eq. (5.31), since we want to establish a Hamiltonian for the polarization field. The spatial derivatives of the functions $\mathbf{P}_{\mathrm{or}}(\boldsymbol{r})$ and $\mathbf{P}_{\infty}(\boldsymbol{r})$ do not occur in the Lagrangian. Therefore, in a straightforward way the components of these functions at different positions can be taken as different variables and Eq. (5.32) then yields immediately [94]

$$\frac{d}{dt} \frac{\partial L}{\partial \dot{q}} - \frac{\partial L}{\partial q} = 0 \,, \tag{5.33}$$

if q represents any of these variables; the differentiations with respect to them follow by considering the integrals as limits of sums [94]. Equations (5.33) then lead to Eqs. (5.27) and (5.28) for all $\boldsymbol{r}$.

The moment conjugate to q is defined as $\partial L/\partial \dot{q}$ so that $\gamma \dot{\mathbf{P}}_{\mathrm{or}}(\boldsymbol{r})$ and $\delta \dot{\mathbf{P}}_{\infty}$ are conjugate to $\mathbf{P}_{\mathrm{or}}(\boldsymbol{r})$ and $\mathbf{P}_{\infty}(\boldsymbol{r})$, respectively. Hence the Hamiltonian is given by [94]

$$H = \sum_q \frac{\partial L}{\partial \dot{q}} \dot{q} - L = \frac{\gamma}{2} \int \left[\dot{\mathbf{P}}_{\mathrm{or}}^2(\boldsymbol{r}) + \omega^2 {\mathbf{P}_{\mathrm{or}}}^2(\boldsymbol{r}) \right] d^3\boldsymbol{r} + \frac{\delta}{2} \int \left[\dot{\mathbf{P}}_{\infty}^2(\boldsymbol{r}) + \omega_\infty^2 \mathbf{P}_{\infty}^2(\boldsymbol{r}) \right] d^3\boldsymbol{r} - \int \boldsymbol{\mathcal{D}}(\boldsymbol{r}, \boldsymbol{r}_{el}) \left[\mathbf{P}_{\mathrm{or}}(\boldsymbol{r}) + \mathbf{P}_{\infty}(\boldsymbol{r}) \right] d^3\boldsymbol{r} \,. \tag{5.34}$$

In the classical case of an electron at rest, when $\boldsymbol{\mathcal{D}}$ for a single free electron in the crystal is given by

$$\boldsymbol{\mathcal{D}}(\boldsymbol{r}, \boldsymbol{r}_{el}) = -\nabla \frac{e}{|\boldsymbol{r} - \boldsymbol{r}_{el}|}\,, \tag{5.35}$$

H becomes infinite because the integrands in Eq. (5.34) diverge as $\boldsymbol{r} \to \boldsymbol{r}_{el}$ [94]. Therefore, we will neglect the interaction energy between electron and lattice displacements, i.e., the third term in the Hamiltonian (5.34). For a more thorough treatment how to remedy this divergence we refer to Ref. [94].

We proceed by introducing auxiliary complex field vectors $\mathbf{B}(\boldsymbol{r})$ and $\mathbf{C}(\boldsymbol{r})$ such that

$$\mathbf{B}(\boldsymbol{r}) = \left(\frac{\gamma\omega}{2}\right)^{1/2} \left(\mathbf{P}_{\mathrm{or}}(\boldsymbol{r}) + \frac{i}{\omega}\dot{\mathbf{P}}_{\mathrm{or}}(\boldsymbol{r})\right), \tag{5.36}$$

$$\mathbf{B}^{\dagger}(\boldsymbol{r}) = \left(\frac{\gamma\omega}{2}\right)^{1/2} \left(\mathbf{P}_{\mathrm{or}}(\boldsymbol{r}) - \frac{i}{\omega}\dot{\mathbf{P}}_{\mathrm{or}}(\boldsymbol{r})\right), \tag{5.37}$$

$$\mathbf{C}(\boldsymbol{r}) = \left(\frac{\delta\omega_{\infty}}{2}\right)^{1/2} \left(\mathbf{P}_{\infty}(\boldsymbol{r}) + \frac{i}{\omega_{\infty}}\dot{\mathbf{P}}_{\infty}(\boldsymbol{r})\right), \tag{5.38}$$

$$\mathbf{C}^{\dagger}(\boldsymbol{r}) = \left(\frac{\delta\omega_{\infty}}{2}\right)^{1/2} \left(\mathbf{P}_{\infty}(\boldsymbol{r}) - \frac{i}{\omega_{\infty}}\dot{\mathbf{P}}_{\infty}(\boldsymbol{r})\right), \tag{5.39}$$

or

$$\mathbf{P}_{\mathrm{or}}(\boldsymbol{r}) = \left(\frac{1}{2\gamma\omega}\right)^{1/2} \left[\mathbf{B}^{\dagger}(\boldsymbol{r}) + \mathbf{B}(\boldsymbol{r})\right], \tag{5.40}$$

$$\dot{\mathbf{P}}_{\mathrm{or}}(\boldsymbol{r}) = \left(\frac{\omega}{2\gamma}\right)^{1/2} i\left[\mathbf{B}^{\dagger}(\boldsymbol{r}) - \mathbf{B}(\boldsymbol{r})\right], \tag{5.41}$$

$$\mathbf{P}_{\infty}(\boldsymbol{r}) = \left(\frac{1}{2\delta\omega_{\infty}}\right)^{1/2} \left[\mathbf{C}^{\dagger}(\boldsymbol{r}) + \mathbf{C}(\boldsymbol{r})\right], \tag{5.42}$$

$$\dot{\mathbf{P}}_{\infty}(\boldsymbol{r}) = \left(\frac{\omega_{\infty}}{2\delta}\right)^{1/2} i\left[\mathbf{C}^{\dagger}(\boldsymbol{r}) - \mathbf{C}(\boldsymbol{r})\right]. \tag{5.43}$$

With these field vectors we can write the field part H_{field} of the Hamiltonian (5.34) as

$$H_{\mathrm{field}} = \omega \int \mathbf{B}^{\dagger}(\boldsymbol{r})\mathbf{B}(\boldsymbol{r}) d^3\boldsymbol{r} + \omega_{\infty} \int \mathbf{C}^{\dagger}(\boldsymbol{r})\mathbf{C}(\boldsymbol{r}) d^3\boldsymbol{r}\,. \tag{5.44}$$

This is a Hamiltonian for independent harmonic oscillators specified by the continuous index $\boldsymbol{r}$ [64]. When going from the continuous description of Eq. (5.44) to a discrete quantization and considering each of the harmonic oscillators having its own frequency, we finally recognize that the dielectric response of a polar medium can be described in terms of the Hamiltonian (3.3) introduced in Sec. 3.3. For what follows we want to relate the solvent reaction to the spectral density.

5.4. Derivation of the spectral density

In this section we elaborate in more detail the derivation of the spectral density introduced in Eq. (4.19). To this extent, we describe the solvation process by the well-known Onsager model [61], and from that starting point the spectral density will be obtained as laid down by Gilmore and McKenzie in Ref. [62]. The Onsager model is a continuum model where the solvent is treated as a homogeneous dielectric and the solute is treated as a point dipole $\boldsymbol{\mu}$ which is surrounded by a spherical cage of polar solvent molecules with Onsager radius a (see Fig. 5.1), which is typically the size of the solute molecule. Inside the molecular cavity, vacuum is assumed, i.e., it has a dielectric constant of $\varepsilon_c = 1$. The central dipole polarizes the solvent which in turn produces an electric reaction field $\boldsymbol{R}$ acting back on the dipole. This dipole-dipole interaction has the energy $E = -\boldsymbol{\mu} \cdot \boldsymbol{R}$, which typically lowers the total energy and forms a stabilized structure. Although the Onsager model does not include the microscopic details of the system, it does capture the essential physics of the solvation process [62]. Now, for the solute molecule and its interaction with the solvent Gilmore and McKenzie have used basically the same corresponding Hamiltonians introduced for our model in Eqs. (3.1) and (3.5) with the only major difference of the included dipole moment. They assumed that the solute molecule has a permanent dipole moment in both the ground and excited state, given by $\boldsymbol{\mu}_g$ and $\boldsymbol{\mu}_e$, respectively, and that the direction of the dipole moment points in the same direction in these two states. The two parts of the Hamiltonian in their notation then look like

$$H_{\text{solute}} = \frac{1}{2}\varepsilon_0 \sigma_z, \quad H_{\text{int}} = \frac{1}{2}\sigma_z \Delta\mu R + \frac{1}{2}(\mu_e + \mu_g) I_2 R\,, \tag{5.45}$$

with $\Delta\mu = \mu_e - \mu_g$, the 2×2 Pauli matrix σ_z and the 2×2 identity matrix I_2. The reaction field is quantized with its modes ω_m and its amplitudes e_m according to

$$R(t) = \sum_m e_m \left[a_m e^{-i\omega_m t} + a_m^\dagger e^{i\omega_m t} \right] \,, \tag{5.46}$$

where a_m and $a_m^\dagger$ again obey the bosonic commutation relation $\left[a_m, a_n^\dagger\right] = \delta_{m,n}$. The solvent is likewise considered as a bath of independent harmonic oscillators with the total solvent energy expressed analogously to Eq. (3.3). Thus, the full Hamiltonian for a single molecule coupled to the polar solvent can be written as

$$H = \frac{1}{2}\varepsilon_0 \sigma_z + \sum_m \omega_m a_m^\dagger a_m + \sigma_z \sum_m M_m (a_m^\dagger + a_m) + \sum_m \tilde{M}_m (a_m^\dagger + a_m)\,, \tag{5.47}$$

with the redefined couplings $M_m = \frac{1}{2} e_m \Delta\mu$ and $\tilde{M}_m = \frac{1}{2} e_m (\mu_e + \mu_g)$. Apart from the last term, this is the same Hamiltonian as Eq. (3.6) without the contributions from the leads, which is referred to as the independent boson model [84]. The next step is to relate $J(\omega)$ to the zero-temperature fluctuations in the uncoupled environment. To this extent, we first consider the expectation value of the reaction field to vanish,

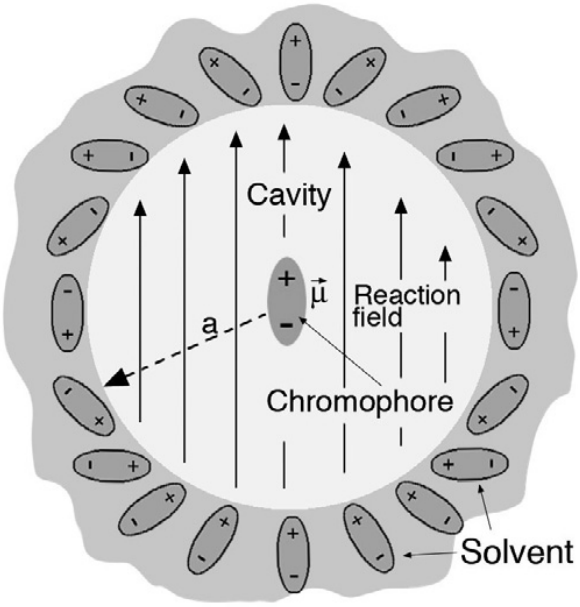

Figure 5.1.: Onsager model of solvation. The molecule is treated as a point dipole inside a vacuum cavity with dielectric constant $\varepsilon_c = 1$ and radius a, which is surrounded by a polar solvent. The dipole polarizes the solvent, which in turn creates an electric reaction field which acts back on the dipole, stabilizing the solvated system. The picture is taken from Ref. [62].

i.e., $\langle R(t)\rangle = 0$, and examine the reaction field fluctuation correlation function $C_R(t)$, defined as

$$C_R(t) = i\langle R(t)R(0)\rangle\theta(t) \equiv i\langle 0|e^{iH_{\rm solv}t}Re^{-iH_{\rm solv}t}R|0\rangle\theta(t)\,, \tag{5.48}$$

where $|0\rangle$ is the ground state of the solvent harmonic oscillators and $\theta(t)$ is the Heaviside step function. In order to see a connection between $C_R(t)$ and $J(\omega)$ we have to look at the Fourier transform of $C_R(t)$, in particular its imaginary part, given by

$$\mathrm{Im}\, C_R(\omega) = \pi \sum_n \delta(\omega - E_n)|\langle 0|R|n\rangle|^2 = \pi \sum_m \delta(\omega - \omega_m)e_m^2\,. \tag{5.49}$$

Here we have included an identity of energy eigenstates $\sum_n |n\rangle\langle n| = 1$, so that $H_{\rm solv}|n\rangle = E_n|n\rangle$, and used the fact that all terms $\langle 0|R|n\rangle$ vanish except for when a single oscillator is singly occupied. These states have energy $E_n = \omega_m$, and $\langle 0|R|m\rangle = e_m$, due to the orthogonality of the solvent states $\langle m|m'\rangle = \delta_{mm'}$. Furthermore, the factor π comes from the one-sided Fourier transform as a result of the Heaviside step function appearing in $C_R(t)$ and writing it by virtue of the delta function. When we compare now Eq. (5.49) with Eq. (4.18) and the corresponding Hamiltonian parts, we find

$$J(\omega) = (\Delta\mu)^2 \mathrm{Im}\, C_R(\omega)\,. \tag{5.50}$$

Now that we have a link between the spectral density and the reaction field fluctuation correlation function, we further want to actually find an expression for the reaction field fluctuations. To this extent, we note that in the Onsager model the reaction field and the central dipole are related via the susceptibility function $\chi(t-t')$ as

$$\boldsymbol{R}(t) = \int_{-\infty}^{t} \mathrm{d}t' \chi(t-t') \boldsymbol{\mu}(t') \,, \tag{5.51}$$

which reflects the fact that the dipole moments of solvent molecules do not adjust instantaneously to the central dipole moment, but rather lag behind the changing dipole in time [95]. The Fourier transform of Eq. (5.51) can be directly obtained utilizing the convolution theorem and reads

$$\boldsymbol{R}(\omega) = \chi(\omega) \boldsymbol{\mu}(\omega) \,. \tag{5.52}$$

To obtain an appropriate expression for $\chi(\omega)$ which is the response of the idealized homogeneous dipolar solvent to the molecular dipole moment, it is necessary to solve the time-dependent electrostatic problem for the system [95, 96]. Taking the center of the dipole as the origin of a coordinate system and choosing the dipole vector in alignment with the $z-$axis, i.e., $\boldsymbol{\mu} = \mu \hat{\boldsymbol{e}}_z$, we are able to solve the Laplace equation $\Delta\Phi = 0$ for the electric potential Φ as the net charge is zero. The resulting solution exploits the spherical symmetry and is $\Phi_i = \sum_{n=0}^{\infty} \left(A_n^{(i)} r^n + B_n^{(i)} r^{-(n+1)} \right) P_n(\cos\theta)$, where P_n are the Legendre polynomials and θ is the angle with respect to the $z-$axis [95]. We label the potential outside the sphere with index $i = 1$ and that inside the sphere with index $i = 2$. The coefficients $A_n^{(i)}$ and $B_n^{(i)}$ are determined from the values of the potential at the boundary ($r = a$), or, when appropriate, from the asymptotic behavior at infinity [97]. That is, the potentials have to fulfill the conditions [97]

$$\left(\Phi_1\right)_{r\to\infty} = 0 \,, \tag{5.53}$$

$$\left(\Phi_1\right)_{r=a} = \left(\Phi_2\right)_{r=a} \,, \tag{5.54}$$

$$\varepsilon \left(\frac{\partial \Phi_1}{\partial r} \right)_{r=a} = \left(\frac{\partial \Phi_2}{\partial r} \right)_{r=a} \,. \tag{5.55}$$

The potentials outside and inside the Onsager sphere then read

$$\Phi_1 = \frac{3}{2\varepsilon + 1} \frac{\mu}{r^2} \cos\theta \,, \tag{5.56}$$

$$\Phi_2 = \frac{\mu}{r^2} \cos\theta - \frac{2(\varepsilon - 1)}{2\varepsilon + 1} \frac{\mu}{a^3} r \cos\theta \,. \tag{5.57}$$

The resulting electric field inside the cavity is a superposition of the dipole field in vacuum and the uniform reaction field $\boldsymbol{R}$ of the form [95, 97]

$$\boldsymbol{R}(\omega) = \frac{1}{4\pi\varepsilon_0 a^3} \frac{2(\varepsilon(\omega) - 1)}{2\varepsilon(\omega) + 1} \boldsymbol{\mu}(\omega) \,. \tag{5.58}$$

Thus, for the case of a point dipole in a sphere with radius a one obtains for the susceptibility function [62, 97]

$$\chi(\omega) = \frac{1}{4\pi\varepsilon_0 a^3} \frac{2(\varepsilon(\omega) - 1)}{2\varepsilon(\omega) + 1}\,, \tag{5.59}$$

where $\varepsilon(\omega)$ is the frequency-dependent dielectric function of the solvent and ε_0 in this case is the vacuum permittivity. As mentioned earlier, we want the spectral density to be in the Debye form, so we use the Debye dielectric relaxation function $\varepsilon(t) = \varepsilon_\infty \delta(t) + \tau_D^{-1}(\varepsilon_S - \varepsilon_\infty)\exp(-t/\tau_D)\theta(t)$ which in Fourier space is given by (see Eq. (5.9))

$$\varepsilon(\omega) = \varepsilon_\infty + \frac{\varepsilon_S - \varepsilon_\infty}{1 - i\omega\tau_D}\,. \tag{5.60}$$

In the high-frequency limit ($\omega \to \infty$), the Debye dielectric function in Eq. (5.60) approaches the corresponding high-frequency value ε_∞, whereas for very low frequencies ($\omega \to 0$) it reaches the corresponding low frequency (static) dielectric constant ε_S [95]. The intermediate, frequency-dependent range is characterized by the Debye relaxation time τ_D, which represents the bulk reorientational relaxation time of the solvent dipoles [62]. The Debye dielectric function can be split into a real and imaginary part $\varepsilon(\omega) = \varepsilon'(\omega) + i\varepsilon''(\omega)$, with

$$\varepsilon'(\omega) = \varepsilon_\infty + \frac{\varepsilon_S - \varepsilon_\infty}{1 + (\omega\tau_D)^2} \quad \text{and} \quad \varepsilon''(\omega) = \frac{(\varepsilon_S - \varepsilon_\infty)\,\omega\tau_D}{1 + (\omega\tau_D)^2}\,. \tag{5.61}$$

Likewise, the susceptibility function $\chi(\omega)$ can be split into a real and imaginary part according to $\chi(\omega) = \chi'(\omega) + i\chi''(\omega)$. There is a relationship between dissipation represented by the imaginary part $\chi''(\omega)$ and the fluctuation correlation spectra $C_R(\omega)$ which is called the fluctuation-dissipation theorem. It is given by [38, 62, 98]

$$\chi''(\omega) = -\frac{i}{2}\left(1 - e^{-\beta\omega}\right) C_R(\omega)\,, \tag{5.62}$$

which reduces to $C_R(\omega) = 2i\chi''(\omega)$ at zero temperature. Note that the use of zero temperature fluctuations is a mathematical derivation only, and provided that the appropriate temperature parameters for the solvent and molecule are used, the resulting spectral density is applicable to all temperatures [67]. By plugging in the Debye formula for the dielectric function given by Eq. (5.60) into Eq. (5.59) and taking the imaginary part $\chi''(\omega)$ to utilize the fluctuation-dissipation theorem, one finally gets to the spectral density of the Onsager model using Eq. (5.50) in the form

$$J(\omega) = \frac{(\Delta\mu)^2}{2\pi\varepsilon_0 a^3} \frac{6(\varepsilon_S - \varepsilon_\infty)}{(2\varepsilon_S + 1)(2\varepsilon_\infty + 1)} \frac{\omega\tau_E}{\omega^2\tau_E^2 + 1}\,, \tag{5.63}$$

where $\tau_E = \frac{2\varepsilon_\infty + 1}{2\varepsilon_S + 1}\tau_D$ [62]. The reorganization energy η is related to the spectral density via [99]

$$\eta = \frac{1}{\pi}\int_0^\infty \mathrm{d}\omega \frac{J(\omega)}{\omega} = \frac{(\Delta\mu)^2}{4\pi\varepsilon_0 a^3} \frac{6(\varepsilon_S - \varepsilon_\infty)}{(2\varepsilon_S + 1)(2\varepsilon_\infty + 1)}\,, \tag{5.64}$$

and together with the cut-off frequency $\omega_c = \frac{1}{\tau_E}$ we can write the spectral density as introduced in Eq. (4.19). When we use the general form of the spectral density given in Eq. (4.18), the reorganization energy can be written as

$$\eta = \sum_m \frac{g_m^2}{\omega_m}\,, \tag{5.65}$$

which is exactly the term by which the molecule energy becomes renormalized after the polaron transformation due to the coupling to the solvent, see Eq. (3.9). A major advantage of the reorganization energy is that it reduces all solvent degrees of freedom to a single number because it is the integral over all bath modes [95].

5.5. Solvent mixtures

In the following we want to take into consideration the influence on the current not only due to one solvent but a mixture composed of two solvents. There exists already a successful theory to describe multicomponent mixtures which is the Maxwell Garnett mixing formula. It describes the permittivity of the effective medium in terms of the permittivities and volume fractions of the individual constituents of the complex medium [100]. We will start, however, with the simplest approach proposed by Gladstone and Dale who expressed a formula for the effective permittivity of a binary mixture given by [66, 101]

$$\varepsilon_{\mathrm{GD}}(\omega) = (1-f)\varepsilon_h(\omega) + f\varepsilon_i(\omega)\,, \tag{5.66}$$

which is proportional and linear to the relative concentrations of a host, $1-f$, and an inclusive solvent, f, with complex, frequency dependent permittivities $\varepsilon_h(\omega)$ and $\varepsilon_i(\omega)$, respectively. We assume each of the constituents to exhibit a dielectric function in the Debye form, i.e.,

$$\varepsilon_h(\omega) = h_\infty + \frac{h_S - h_\infty}{1 - i\omega\tau_h} \quad \text{and} \quad \varepsilon_i(\omega) = i_\infty + \frac{i_S - i_\infty}{1 - i\omega\tau_i}\,, \tag{5.67}$$

with the static (h_S, i_S) and high-frequency (h_∞, i_∞) dielectric constants as well as the Debye relaxation times (τ_h, τ_i) of the host and the inclusive solvent, respectively. From Eqs. (5.50)–(5.62) we see that we can write the spectral density in terms of the real $(\varepsilon'(\omega))$ and imaginary $(\varepsilon''(\omega))$ part of the dielectric function as

$$J(\omega) = \frac{(\Delta\mu)^2}{2\pi\varepsilon_0 a^3} \frac{6\varepsilon''(\omega)}{(2\varepsilon'(\omega)+1)^2 + 4\varepsilon''(\omega)^2}\,. \tag{5.68}$$

In this equation we will replace the dielectric function of a single solvent by the Gladstone-Dale formula as given in Eq. (5.66). Then, by solving for roots of the denominator we can factorize the denominator and write the spectral density with the Gladstone-Dale permittivity as

$$J_{\mathrm{GD}}(\omega) = \frac{\omega D + \omega^3 E}{(\omega^2+\omega_1^2)(\omega^2+\omega_2^2)}\,, \tag{5.69}$$

where

$$D = \frac{(\Delta\mu)^2}{A\pi\varepsilon_0 a^3} 3\left[\tau_i f(i_S - i_\infty) + \tau_h(1-f)(h_S - h_\infty)\right], \tag{5.70}$$

$$E = \frac{(\Delta\mu)^2}{A\pi\varepsilon_0 a^3} 3\left[\tau_h^2\tau_i f(i_S - i_\infty) + \tau_i^2\tau_h(1-f)(h_S - h_\infty)\right], \tag{5.71}$$

and

$$\omega_1 = \sqrt{\frac{B - \sqrt{B^2 - 4AC}}{2A}}, \qquad \omega_2 = \sqrt{\frac{B + \sqrt{B^2 - 4AC}}{2A}}, \tag{5.72}$$

with

$$A = \tau_h^2\tau_i^2\left[2h_\infty(1-f) + 1 + 2fi_\infty\right]^2, \tag{5.73}$$

$$\begin{aligned} B = {} & \tau_h^2[2h_\infty(1-f) + 1 + 2fi_S]^2 + \tau_h\tau_i 8f(1-f)(h_S - h_\infty)(i_S - i_\infty) \\ & + \tau_i^2[2h_S(1-f) + 1 + 2fi_\infty]^2, \end{aligned} \tag{5.74}$$

$$C = [2h_S(1-f) + 1 + 2fi_S]^2. \tag{5.75}$$

When we afterwards calculate the reorganization energy with this spectral density via the relation (5.64), we find

$$\eta_{\mathrm{GD}} = \eta_1 + \eta_2, \tag{5.76}$$

where

$$\eta_1 = \frac{-D + E\omega_1^2}{2\omega_1(\omega_1^2 - \omega_2^2)} \quad \text{and} \quad \eta_2 = \frac{-D + E\omega_2^2}{2\omega_2(\omega_2^2 - \omega_1^2)}. \tag{5.77}$$

Rewriting the last two expressions in terms of D and E, we see

$$D = 2\omega_1\omega_2(\omega_1\eta_2 + \omega_2\eta_1) \quad \text{and} \quad E = 2(\omega_1\eta_1 + \omega_2\eta_2). \tag{5.78}$$

By inserting (5.78) into (5.69) and some trivial algebra, we end up with

$$J_{\mathrm{GD}}(\omega) = 2\eta_1\frac{\omega\omega_1}{(\omega^2 + \omega_1^2)} + 2\eta_2\frac{\omega\omega_2}{(\omega^2 + \omega_2^2)}, \tag{5.79}$$

which resembles a sum of two separate spectral densities in the Debye form. Note, that only for $f = 0$ the reorganization energy as well as the frequency ω_1 become that of the host only, i.e.,

$$\begin{aligned} \eta_{\mathrm{GD}}\Big|_{f=0} = \eta_1 = \eta_h &\equiv \frac{(\Delta\mu)^2}{4\pi\varepsilon_0 a^3}\frac{6(h_S - h_\infty)}{(2h_S + 1)(2h_\infty + 1)}, \\ \omega_1\Big|_{f=0} = \omega_h &\equiv \frac{2h_S + 1}{2h_\infty + 1}\tau_h^{-1}. \end{aligned} \tag{5.80}$$

Likewise, for $f = 1$ only the inclusive solvent remains with

$$\begin{aligned} \eta_{\mathrm{GD}}\Big|_{f=1} = \eta_2 = \eta_i &\equiv \frac{(\Delta\mu)^2}{4\pi\varepsilon_0 a^3}\frac{6(i_S - i_\infty)}{(2i_S+1)(2i_\infty+1)}\,, \\ \omega_2\Big|_{f=1} = \omega_i &\equiv \frac{2i_S+1}{2i_\infty+1}\tau_i^{-1}\,. \end{aligned} \tag{5.81}$$

For f between zero and one, however, all parameters η_1, η_2, ω_1 and ω_2 depend on the high- and low-frequency dielectric constants of the host and inclusive solvent and their respective Debye relaxation times as shown in Eqs. (5.70)–(5.77).

In Fig. 5.2 (a), we show an exemplary plot of the spectral density as a function of the volume fraction f and the frequency ω for a solvent mixture between nitrobenzene and toluene. When pure nitrobenzene is considered ($f = 0$), the spectral density has its peak at the cut-off frequency of nitrobenzene ω_c^{NBZ}, as expected from Eq. (5.80). For nonzero volume fractions the position as well as the height of the peak change according to Eq. (5.79). Additionally, in Fig. 5.2 (b), we show the maximum of the spectral density $J_{\max}$ as well as the reorganization energy η for the solvent mixtures toluene-nitrobenzene, chlorobenzene-nitrobenzene and dimethylformamide-nitrobenzene. It can be observed that only for the mixture between nitrobenzene and toluene $J_{\max}$ is non-monotonous which subsequently results in the non-monotonous behavior of the maximum differential conductance for this mixture, see Fig. 5.7 in Sec. 5.6.4. Furthermore, for nonzero volume fractions both $J_{\max}$ and η can reach values which are higher than the individual ones of each constituent, as observed for toluene-nitrobenzene.

Due to the fact that the spectral density of the composite can be written as a sum of structurally two spectral densities in the Debye form, we can directly write down the exponent of the bath correlation function for a binary solvent mixture as

$$\begin{aligned} W_{\mathrm{GD}}(\tau) =& \frac{2\eta_1}{\beta\omega_1}|\tau| + \frac{4\eta_1\omega_1}{\beta}\sum_{n=1}^{\infty}\frac{e^{-\nu_n|\tau|}-1}{\nu_n\left(\nu_n^2-\omega_1^2\right)} + \frac{\eta_1}{\omega_1}\left(e^{-\omega_1|\tau|}-1\right)\left[\cot\left(\frac{\beta\omega_1}{2}\right) - i\,\mathrm{sgn}(\tau)\right] \\ &+ \frac{2\eta_2}{\beta\omega_2}|\tau| + \frac{4\eta_2\omega_2}{\beta}\sum_{n=1}^{\infty}\frac{e^{-\nu_n|\tau|}-1}{\nu_n\left(\nu_n^2-\omega_2^2\right)} + \frac{\eta_2}{\omega_2}\left(e^{-\omega_2|\tau|}-1\right)\left[\cot\left(\frac{\beta\omega_2}{2}\right) - i\,\mathrm{sgn}(\tau)\right]. \end{aligned} \tag{5.82}$$

With this expression we can calculate the influence of a binary solvent mixture on the tunneling current diagrams appearing in Fig. 4.4, by which we can then, in total, determine the solvent effects on the current by means of Eq. (4.43).

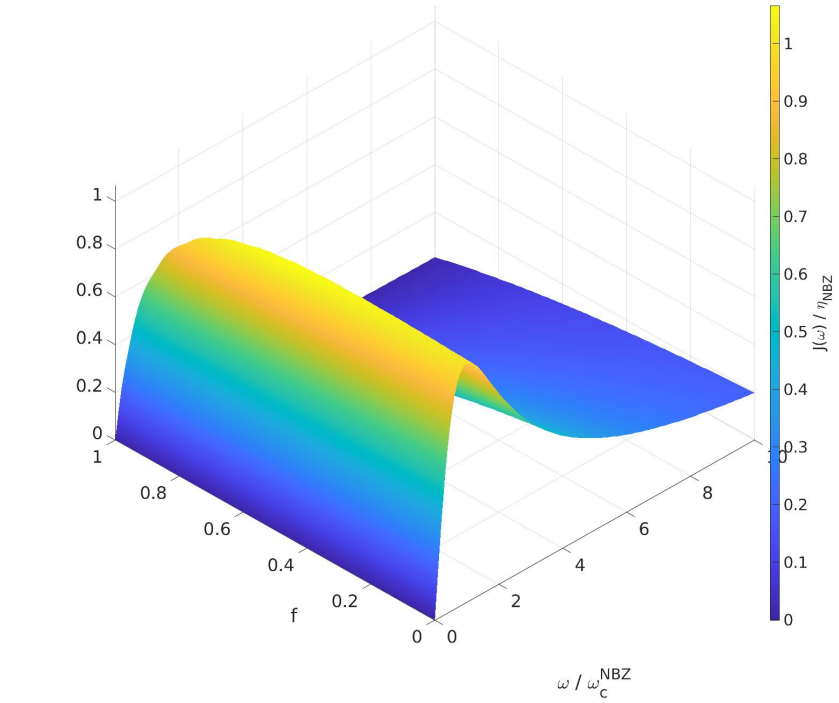

(a) $J(\omega)/\eta_{\mathrm{NBZ}}$

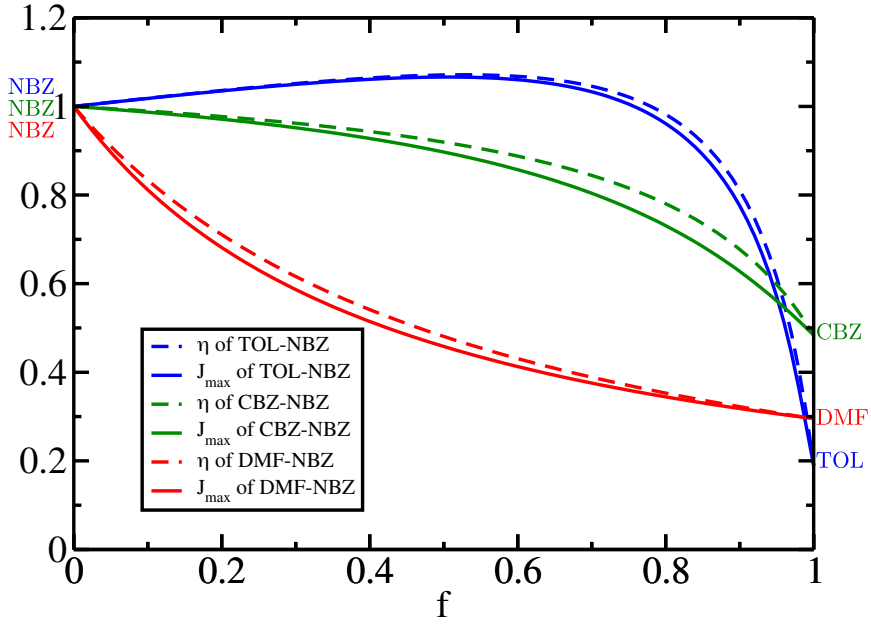

(b) $J_{\mathrm{max}}/\eta_{\mathrm{NBZ}}$ and η/η_{NBZ}

Figure 5.2.: (a) Spectral density $J(\omega)$ normalized to the reorganization energy η_{NBZ} of nitrobenzene as a function of the volume fraction f and the frequency ω (normalized to the cut-off frequency of nitrobenzene ω_c^{NBZ}) for the solvent mixture between nitrobenzene and toluene. (b) Maximum of the spectral density as well as the reorganization energy η for the solvent mixtures toluene-nitrobenzene, chlorobenzene-nitrobenzene and dimethylformamide-nitrobenzene, both normalized to η_{NBZ}. The solvent parameters are taken from Ref. [102].

5.6. Results and discussion

In this section, we present the results generated on the basis of the theoretical analysis described so far. We start by reproducing well-known results within the field of electron transport theory in order to give a general introduction into the possible observations with our model. Specifically, we first have a look at current-voltage plots without any surrounding solvents. In the next step, we introduce several different pure solvents and analyze their influence both on the current as well as on the differential conductance. Following this, we investigate the impact of temperature on electron transfer through the molecule. Finally, we incorporate also binary solvent mixtures in our investigation of electron transport through single-molecule junctions and conclude with a promising comparison to experimental data.

5.6.1. Electron transport without solvent

We consider first the molecule without surrounding solvent ($\eta = 0\,\Gamma$) and examine a typical bias voltage plot with respect to the applied gate voltage, corresponding in this case to the energy level of the molecule. In Fig. 5.3 (a), we can observe a linear dependence between the bias voltage and the molecular energy given at the temperature $T = 0.1\,\Gamma$, which corresponds to room temperature (300 K) with $\Gamma = 250$ meV. When the bias potential has reached twice the value of the molecular energy level a current can flow through the molecule, indicated in yellow for a positive current at positive biases and in blue for a negative current at negative biases. The reason why it has to reach twice the molecular energy level is due to the symmetrically applied bias voltage, that is illustrated in Fig. 5.3 (b). At zero bias the chemical potentials of the leads are aligned and no current can be generated. When a positive or negative bias voltage is applied, one of the lead chemical potentials has to reach the molecular energy in order to generate a current flow and since they are applied symmetrically, i.e., $\mu_L = -\mu_R = eV/2$, this is achieved when the bias voltage is twice the molecular energy. The transition from no current to the onset of current is smoothed out by the temperature-dependent occupation of the Fermi leads.

When more than one energy level of the molecule and electron-electron interactions are considered such bias-gate voltage plots typically show a diamond-shaped pattern, see Fig. 2.4 in Chapter 2. The resulting diamonds are called Coulomb diamonds due to the Coulomb blockade effect. A Coulomb blockade describes the suppression of current flow through the molecule due to the electrostatic (Coulomb) repulsion between electrons occupying the molecule.

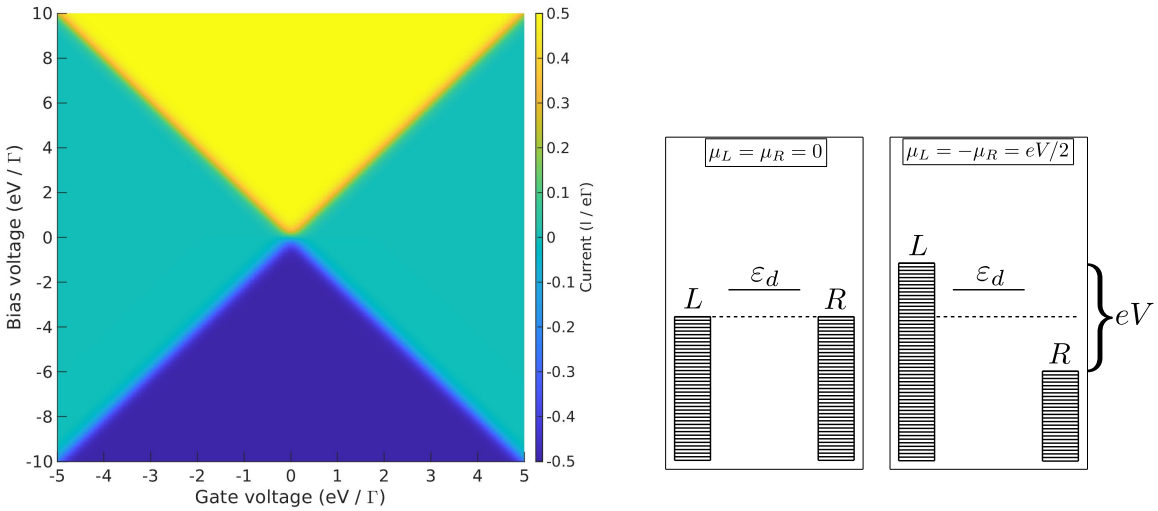

(a) Current at $T = 0.1\,\Gamma$.

(b) Energy level configuration.

Figure 5.3.: (a) Color coded current in dependence of the applied bias voltage with respect to the gate voltage, the latter corresponding to the molecule energy level in this case. The temperature is $T = 0.1\ \Gamma$, which corresponds to room temperature (300 K) with $\Gamma = 250$ meV. (b) The single-level energy of the molecule between the two leads at different bias potentials.

5.6.2. Pure solvents affecting electron transport

We study next how a pure solvent influences the behavior of the current. To this extent, we take a look at a specific value of the molecular energy given by $\varepsilon_d = 1.2\,\Gamma$ and consider a bias voltage window between 0 and 5 Γ.

When we want to compare different solvents by utilizing their experimentally measured dielectric relaxation parameters, we have to transcribe the solvent characteristics, such as the reorganization energy and the cut-off frequency, in units of Γ. To this end, we set $\Gamma = 250\,\text{meV}$ so that a temperature of $T = 0.1\,\Gamma$ corresponds to room temperature (300 K) which is where the dielectric relaxation parameters were measured [102]. In addition to the dielectric parameters of the solvent we need to specify the molecular radius a and the transition dipole moment $\Delta\mu$ of the solute in order to calculate the reorganization energy. We consider a realistic molecular radius $a = 5\,\text{Å}$, and a typical dipole moment change of $\Delta\mu = 5\,\text{D}$ [103–108].

In Fig. 5.4 one can see the current-voltage plot and Fig. 5.5 shows the nonlinear conductance curve of the molecular junction dissolved in the pure solvents toluene (TOL), chlorobenzene (CBZ), ethanol (ETH), butanol (BUT), water (WAT) and nitrobenzene (NBZ). The maximum of the differential conductance is reduced and its width is enhanced when the junction is immersed in a solvent (grey dashed line for the case in absence of a solvent vs. solid curves with a solvent in Fig. 5.5). This is due to the fact that a part of the electric potential energy eV, inducing the electric current, is used

for the reorganization of the solvent. Thus, the slope of the current-voltage response is reduced. Consequently, the larger is the reorganization energy of the solvent, the smaller the conductance maximum becomes.

Once dissolved, the molecular energy level is broadened due to solvent fluctuations which brings the former in resonance with the electronic levels of the leads even if the applied voltage is low. On the other hand, higher level fluctuations lead to off-resonances with lead levels for higher voltages. This additional tunneling broadening occurs via the absorption or emission of (bosonic) solvent polarization modes similar to the broadening dominated by the emission of phonons into a substrate [109]. Franck-Condon steps are not present in our case because the dielectric provides a continuum of modes instead of a single mode (which could be a single molecular vibrational mode) in accordance with the high-temperature regime [69].

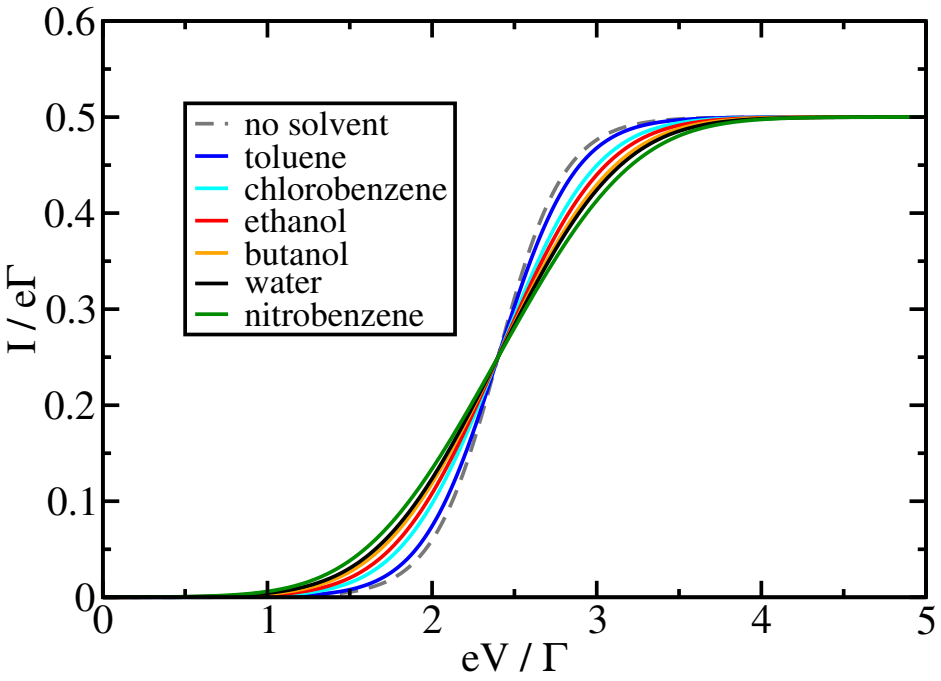

Figure 5.4.: Stationary current I as a function of the bias voltage V in the absence of a solvent (grey dashed line) and with various surrounding pure solvents (solid lines) as indicated. Parameters are $a = 5$ Å, $\Delta\mu = 5$ D, $T = 0.1\ \Gamma$, $\varepsilon_d = 1.2\ \Gamma$ and $\Gamma = 250$ meV.

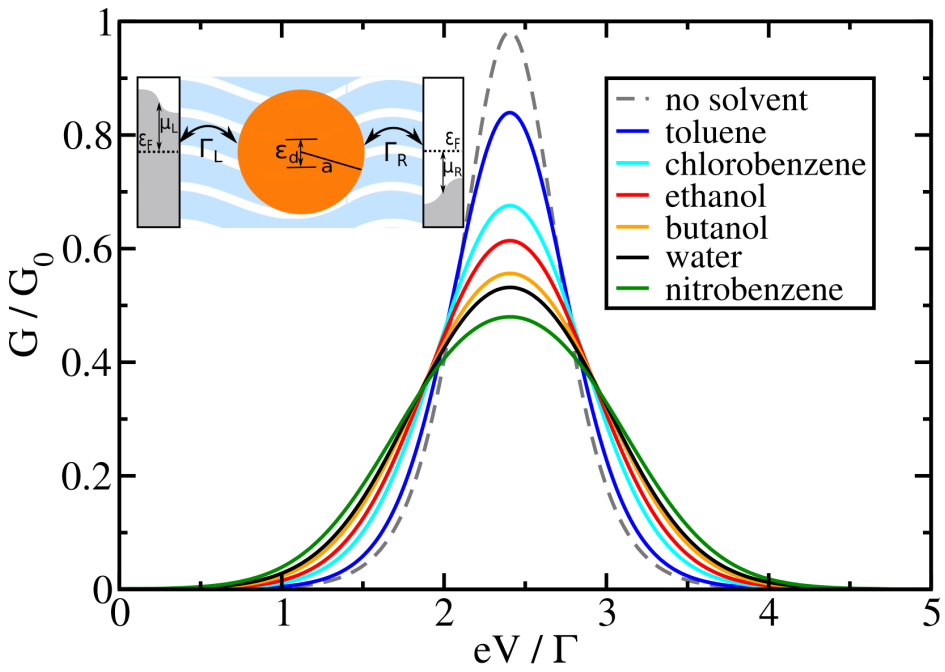

Figure 5.5.: Nonlinear differential conductance $G = dI/dV$ as a function of the bias voltage V in the absence of a solvent (grey dashed line) and with various surrounding pure solvents (solid lines) as indicated. $G_0 = 2e^2/h$ is the conductance quantum. Parameters are $a = 5$ Å, $\Delta\mu = 5$ D, $T = 0.1\ \Gamma$, $\varepsilon_d = 1.2\ \Gamma$ and $\Gamma = 250$ meV. Inset: Sketch of the model of the molecular junction between two metallic leads and surrounded by a dielectric solvent.

5.6.3. Temperature dependence of the differential conductance

Before we continue with the investigation of binary solvent mixtures, we first investigate the influence of temperature on electron transport through the molecule both with and without surrounding solvent. Figure 5.6 portrays the maximum of the nonlinear differential conductance $G_{\max}$, calculated at the bias voltage $eV = 2.4\ \Gamma$, as a function of the temperature T. As expected, $G_{\max}$ is inversely proportional to T. For the case of no surrounding solvent, i.e., for $\eta = 0\ \Gamma$, and in the linear transport regime, i.e., for $V \to 0$, this inverse proportionality is a well known result which can be derived analytically [41, 52, 110, 111] and reads

$$G_{\max} = \frac{e^2}{4k_{\mathrm{B}}T}\frac{\Gamma_L\Gamma_R}{\Gamma_L + \Gamma_R}\ . \tag{5.83}$$

This behavior also holds true when a surrounding solvent is considered, see the colored lines with $\eta \neq 0\ \Gamma$ in Fig 5.6 (a). The main difference is that $G_{\max}$ gets smaller with larger reorganization energies η when compared to the case of no surrounding solvent. This reduction of the nonlinear differential conductance maximum is in accordance with the results presented in Fig. 5.4 (b) for specific solvents, where also solvents with

a larger reorganization energy suppress the peak of G more strongly than solvents with a smaller η. The reason for this reduction is again that a part of the electric potential energy eV is exploited to reorganize the solvent. We additionally show the log-log plot of the $G_{\max}$-T curves in Fig. 5.6 (b) to emphasize the inverse relationship between $G_{\max}$ and T. Here, the curves appear as straight lines with a negative slope indicative of a power function with a negative exponent.

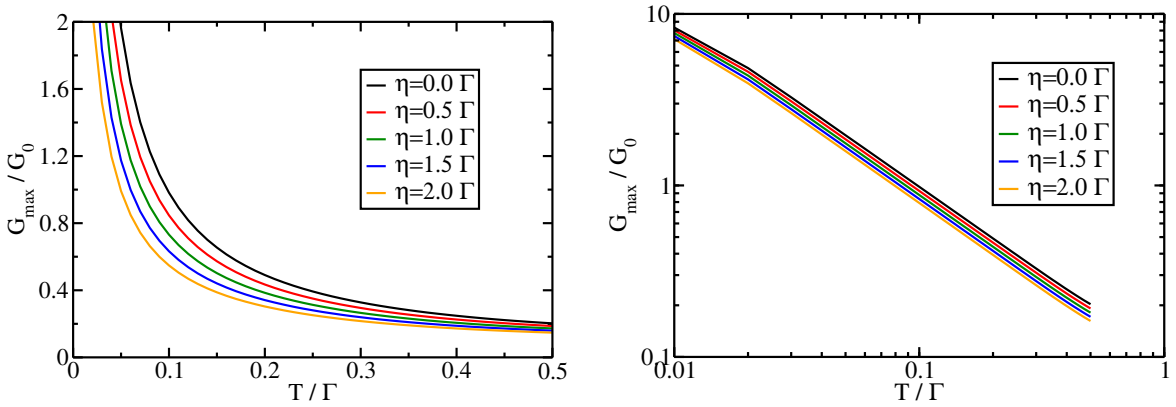

(a) $G_{\max}$ (b) Log-log plot of $G_{\max}$

Figure 5.6.: (a) Maximum of the nonlinear differential conductance as a function of the temperature T in the absence of a solvent (black line) and with a surrounding solvent with a cutoff frequency of $\omega_c = 10\,\Gamma$ and varying reorganization energies (colored lines) as indicated. The value of Γ is $\Gamma = 250\,\text{meV}$, so that a temperature of $T = 0.1\,\Gamma$ corresponds to room temperature (300 K). (b) Log-log plot of (a).

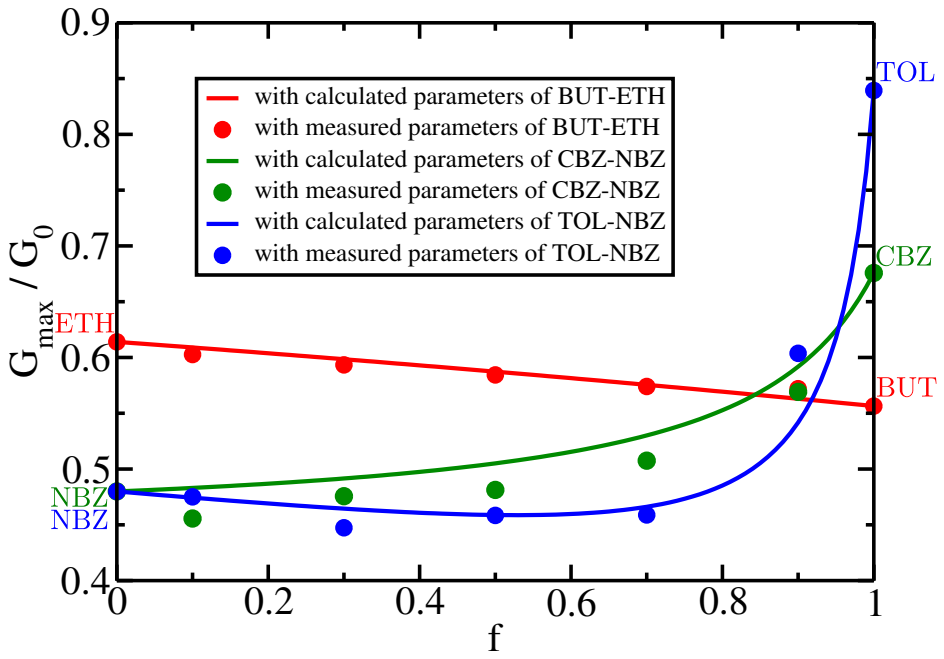

Figure 5.7.: Maximum of the nonlinear differential conductance as a function of the volume fraction f for the binary mixtures between butanol and ethanol, chlorobenzene and nitrobenzene, as well as toluene and nitrobenzene. The solid lines show the results calculated using the effective dielectric parameters of Gladstone-Dale (Eq. (5.66)) in an effective Debye spectral density. In addition, the circles mark the conductance calculated with a single Debye spectral density of the mixture with the directly measured dielectric parameters taken from Ref. [102]. Parameters are $a = 5$ Å, $\Delta\mu = 5$ D, $T = 0.1\ \Gamma$, $\varepsilon_d = 1.2\ \Gamma$, and $\Gamma = 250$ meV.

5.6.4. Influence of binary solvent mixtures on electron transport

Next, we examine the influence of solvent mixtures with a particular eye on the three binary solvent pairs toluene-nitrobenzene (TOL-NBZ), chlorobenzene-nitrobenzene (CBZ-NBZ), and butanol-ethanol (BUT-ETH). To this end, we have calculated the maximum of the differential conductance $G_{\max}$ under variation of the volume fraction f of the mixture. In Fig. 5.7 we start with one pure solvent ($f = 0$) and increase the volume fraction f of the other until the latter solvent is solely present at $f = 1$. We find that $G_{\max}$ is highly sensitive to both the volume fraction and the individual solvents themselves. While the conductance for CBZ-NBZ and BUT-ETH monotonously increases or decreases, respectively, the result for TOL-NBZ shows a non-monotonous behavior. The latter originates from the non-monotonous dependence of the spectral density and reorganization energy of the solvent mixture on the volume fraction, see Fig. 5.2 (b). A signature of mixtures of different dielectric properties.

The reasoning is analogue to the case of pure solvents. Solvent mixtures with higher reorganization energies require a larger part of the electric potential energy, provided

by the bias voltage V, to reorganize than mixtures with smaller reorganization energies. This in turn lowers the slope of the current-voltage response and reduces the conductance maximum for solvent mixtures with larger reorganization energies. Notably, we find an excellent agreement when we compare the dependence of $G_{\max}$ calculated with an effective Gladstone-Dale-Debye solvent mixture of Eq. (5.66) with the differential conductance calculated with a single Debye solvent with the actual measured dielectric parameters of the binary mixture directly as obtained in Ref. [102] (symbols in Fig. 5.7). Hence, the Gladstone-Dale model of dielectric mixtures can be a sensitive tool to directly read off the volume fraction of binary solvent mixtures.

A measure complementary to the maximum of the differential conductance is the full width at half maximum (FWHM) which we have calculated for the solvent mixtures between toluene-nitrobenzene, chlorobenzene-nitrobenzene and dimethylformamide-nitrobenzene. The results are shown in Fig. 5.8. The accuracy of our results is determined by the voltage step size of 0.02 Γ and we have used a cubic spline interpolation to show the general trend without extensively exhausting numerical expenses [69]. It can be nicely observed that the FWHM directly follows the behavior of the spectral density or the reorganization energy when comparing with Fig. 5.2 (b).

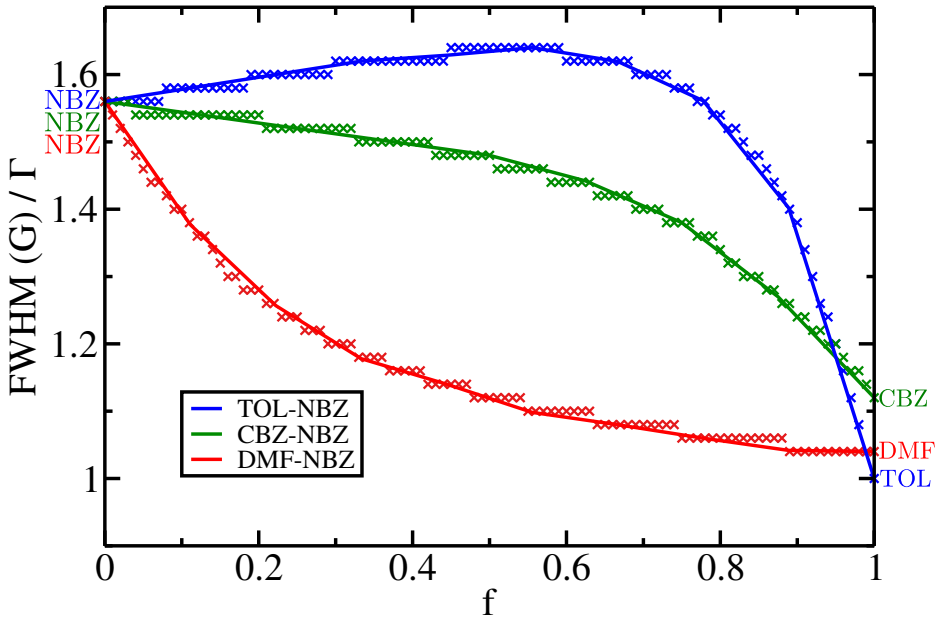

Figure 5.8.: Full width at half maximum of the nonlinear differential conductance as a function of the volume fraction f for the binary solvent mixtures between nitrobenzene-toluene, nitrobenzene-chlorobenzene and nitrobenzene-dimethylformamide. The data points have been calculated with an accuracy determined by the voltage step size of 0.02 Γ and we have used a cubic spline interpolation for the final curves (solid lines). Parameters are $a = 5$ Å, $\Delta\mu = 5$ D, $T = 0.1$ Γ, $\varepsilon_d = 1.2$ Γ and Γ = 250 meV.

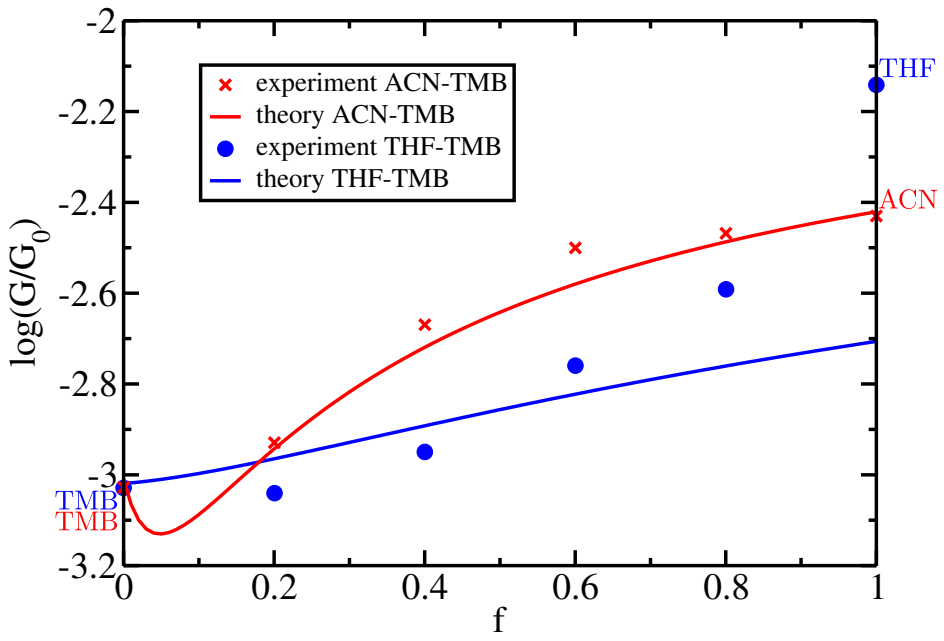

Figure 5.9.: Nonlinear differential conductance of a OPE-SMe molecular junction as a function of the volume fraction f for binary solvent mixtures of ACN and TMB (red) as well as of THF and TMB (blue). Parameters are $a = 5$ Å, $\Delta\mu = 10$ D, $T = 10\ \Gamma$, $\varepsilon_d = 120\ \Gamma$ and $\Gamma = 2.5$ meV. Experimental data are taken from Ref. [27].

5.6.5. Comparison to experimental data

In this section, we compare the experimental results of the differential conductance of Ref. [27] with our theoretical results. In the experiment, the electronic conductance of oligophenylethynylene-sulfurmethyl (OPE-SMe) placed between two gold electrodes and additionally embedded in a solvent has been measured for varying volume fractions of different solvent mixtures. The nonlinear differential conductance of this single-molecule junction can be tuned by nearly an order of magnitude when varying the polarity of the solvent. To recover the experimental data by our model we use the Debye dielectric function while utilizing the static dielectric constants ε_S and the dielectric relaxation times τ_D from literature (see Table B.1) for the three investigated solvents 1,3,5-trimethylbenzene (TMB), tetrahydrofuran (THF), and acetonitrile (ACN) and adjust the high-frequency dielectric constants ε_∞ as fitting parameters. In Ref. [27], the length of the molecular junction has been determined by the break-junction technique to be stable around 1 nm. Thus, we choose a radius of $a = 5$ Å. Moreover, we set the dipole moment change to $\Delta\mu = 10$ D, which is in the typical range of OPE-SMe molecular junctions [103–108], and $\Gamma = 2.5$ meV so that a temperature of $T = 10\ \Gamma$ corresponds to room temperature (300 K).

Figure 5.9 depicts the logarithm of the differential conductance calculated at a voltage corresponding to the molecule energy of $\varepsilon_d = 120\ \Gamma$ and normalized to the conductance quantum $G_0 = 2e^2/h$ for varying volume fractions between the host sol-

vent TMB and the two inclusions THF and ACN, respectively. A very good agreement between theory and experiment is achieved for the solvent mixture between TMB and ACN (red color in Fig. 5.9). For TMB and THF (blue color in Fig. 5.9), a good alignment between experiment and theory is obtained for volume fractions below 0.8.

In order to explore the mechanism of solvent gating on the charge transport, control experiments with other bridge molecules, which did not exhibit a significant solvent induced shift on the conductance, have been reported in Ref. [27]. In addition, the local density of states (LDOS) has been calculated by means of DFT calculations for all investigated molecules [27]. Only for OPE-SMe, the LDOS was found to be mainly localized on the molecular bridge itself, while for the other molecules, the LDOS was shown to be delocalized almost equally over the gold electrodes as well as the molecular bridge. Hence, only for OPE-SMe, strong LDOS localization on the molecule implies a weak hybridization coupling between the molecule and the electrodes together with a strong influence of the solvent, in agreement with the assumption of sequential tunneling as scope of this thesis. However, the precise form of the investigated molecules as well as the spatial distribution of the LDOS on the molecule do not follow a perfect spherical geometry, which we assume in our model. Hence, deviations between our calculations and the experimental data, such as for the conductance of THF, can occur for these reasons.

Moreover, the influence of the solvent on the transmission spectra for OPE-SMe was investigated [27]. The solvent effect on the spectral shift is almost twice as pronounced for ACN as compared to THF, which further supports the very good agreement of our results for ACN [69]. The less pronounced spectral shift for THF in comparison to ACN might be directly related to the polarity of the solvents which is roughly twice as large for ACN compared to THF [103]. A more polar solvent in turn might lead to a stronger influence on the electron density distribution of the solute, and thus, to a stronger localization on the bridge molecule [112].

Chapter 6.

Time dependent transport under an ac voltage

The calculations with the dc current can be generalized to the case of ac-driven leads. Indeed, we show that we may utilize the ac-driving to determine the impact of a hydration shell surrounding the molecule. To do so, we extend the procedure of the calculations presented for the dc case. We start with the determination of the stationary current driven by an ac field. We assume that the time-dependence of the electrostatic potentials is periodic in time with period $T = 2\pi/\omega_{ac}$. This implies a periodicity of the irreducible self-energies and of the stationary probability distribution as well as the tunneling current in the stationary state [35]. Therefore, as a next step, we Fourier expand the master equation which subsequently becomes a numerically conveniently tractable algebraic equation. Finally, we incorporate the hydration shell by determining a spectral density which includes necessary information to characterize the shell. Let us start with the derivation of the current under ac drive.

6.1. Stationary current under ac drive

The ac voltage is explicitly included in the energies of the lead electrons $\varepsilon_{k,r}(t) = \varepsilon_{k,r} + eV_r\cos(\omega_{ac}t)$, with the amplitude $V_L = -V_R = V_{ac}$ and the frequency ω_{ac}, respectively. By using the unitary transformation $U(t) = e^{-i\int_{t_0}^{t}\mathrm{d}\tau\sum_{k,r}eV_r\cos(\omega_{ac}\tau)c_{k,r}^{\dagger}c_{k,r}}$, the time dependence of the single particle energies $\varepsilon_{k,r}(t)$ is transferred to the tunneling amplitudes $t_{k,r}(t) = t_{k,r}\exp(-i\int_{t_0}^{t}\mathrm{d}\tau eV_r\cos(\omega_{ac}\tau))$. The appearing exponential can be expanded via the Jacobi-Anger expansion

$$e^{ix\sin\theta} = \sum_{n=-\infty}^{\infty} J_n(x)e^{in\theta}\ , \tag{6.1}$$

where $J_n(x)$ are the ordinary Bessel functions of the first kind. For the calculation of the irreducible self-energies Σ the tunneling amplitudes appear as products $t_{k,r}(t')t_{k,r}^{*}(t)$, which leads to exponentials of the form

$$e^{\pm i\int_{t'}^{t}\mathrm{d}\tau eV_r\cos(\omega_{ac}\tau)} = \sum_{mn} d_{mn}^{r}e^{\pm im\omega_{ac}t}e^{\mp in\omega_{ac}t'}\ , \tag{6.2}$$

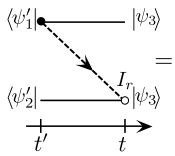

$$= +i\frac{\Gamma}{2\beta}\langle\psi_3|d|\psi_1'\rangle\langle\psi_2'|d^\dagger|\psi_3\rangle\sum_{mp} d^r_{mm-p}e^{ip\omega_{ac}t}\frac{e^{i(\omega_{\psi_1'\psi_3}+(m-p)\omega_{ac})\tau}e^{-W(+\tau)}e^{-i\mu_r(\tau-\frac{i}{B})}}{\sinh\left(\frac{\pi}{\beta}\left(\tau-\frac{i}{B}\right)\right)}$$

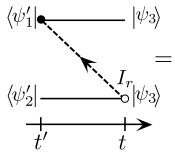

$$= -i\frac{\Gamma}{2\beta}\langle\psi_3|d^\dagger|\psi_1'\rangle\langle\psi_2'|d|\psi_3\rangle\sum_{mp} d^r_{mm-p}e^{-ip\omega_{ac}t}\frac{e^{i(\omega_{\psi_1'\psi_3}-(m-p)\omega_{ac})\tau}e^{-W(+\tau)}e^{+i\mu_r(\tau-\frac{i}{B})}}{\sinh\left(\frac{\pi}{\beta}\left(\tau-\frac{i}{B}\right)\right)}$$

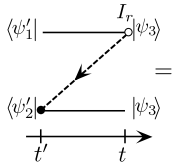

$$= +i\frac{\Gamma}{2\beta}\langle\psi_2'|d^\dagger|\psi_3\rangle\langle\psi_3|d|\psi_1'\rangle\sum_{mp} d^r_{mm-p}e^{-ip\omega_{ac}t}\frac{e^{i(\omega_{\psi_3\psi_2'}-(m-p)\omega_{ac})\tau}e^{-W(-\tau)}e^{+i\mu_r(\tau+\frac{i}{B})}}{\sinh\left(\frac{\pi}{\beta}\left(\tau+\frac{i}{B}\right)\right)}$$

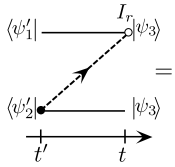

$$= -i\frac{\Gamma}{2\beta}\langle\psi_2'|d|\psi_3\rangle\langle\psi_3|d^\dagger|\psi_1'\rangle\sum_{mp} d^r_{mm-p}e^{ip\omega_{ac}t}\frac{e^{i(\omega_{\psi_3\psi_2'}+(m-p)\omega_{ac})\tau}e^{-W(-\tau)}e^{-i\mu_r(\tau+\frac{i}{B})}}{\sinh\left(\frac{\pi}{\beta}\left(\tau+\frac{i}{B}\right)\right)}$$

Figure 6.1.: The four tunneling current diagrams which contribute to sequential tunneling in the ac-driven case.

with the coefficients

$$d^r_{mn} = J_m\left(\frac{eV_r}{\omega_{ac}}\right)J_n\left(\frac{eV_r}{\omega_{ac}}\right). \tag{6.3}$$

Utilizing Eq. (6.2) to determine the stationary current for the ac-driven case we see that Eq. (4.42) turns into

$$\begin{aligned}\langle I_r(t)\rangle = -e\sum_{\psi_1'\psi_2'\psi_3}\int_{t_0}^{t}\mathrm{d}\tau P^{\psi_1'}_{\psi_2'}(t)\sum_k|t_{k,r}|^2\sum_{mn}d^r_{mn}\\ \times\Big\{e^{i(\varepsilon_{\psi_1'}-\varepsilon_{\psi_3})\tau}e^{-W(+\tau)}\Big(e^{-i\omega_{ac}t(m-n)-in\omega_{ac}\tau}e^{i\varepsilon_{k,r}\tau}f_r^+(\varepsilon_{k,r})\langle\psi_3|d^\dagger|\psi_1'\rangle\langle\psi_2'|d|\psi_3\rangle\\ - e^{i\omega_{ac}t(m-n)+in\omega_{ac}\tau}e^{-i\varepsilon_{k,r}\tau}f_r^-(\varepsilon_{k,r})\langle\psi_3|d|\psi_1'\rangle\langle\psi_2'|d^\dagger|\psi_3\rangle\Big)\\ + e^{i(\varepsilon_{\psi_3}-\varepsilon_{\psi_2'})\tau}e^{-W(-\tau)}\Big(e^{-i\omega_{ac}t(m-n)-in\omega_{ac}\tau}e^{i\varepsilon_{k,r}\tau}f_r^-(\varepsilon_{k,r})\langle\psi_2'|d^\dagger|\psi_3\rangle\langle\psi_3|d|\psi_1'\rangle\\ - e^{i\omega_{ac}t(m-n)+in\omega_{ac}\tau}e^{-i\varepsilon_{k,r}\tau}f_r^+(\varepsilon_{k,r})\langle\psi_2'|d|\psi_3\rangle\langle\psi_3|d^\dagger|\psi_1'\rangle\Big)\Big\}.\end{aligned} \tag{6.4}$$

Here, we recognize that the terms contributing to the irreducible self-energy no longer depend only on the time difference $\tau = t - t'$ but additionally maintain a time-dependence due to the applied periodic ac drive. Nevertheless, we can still perform the integral over τ and find for the irreducible self-energy in the stationary limit, i.e., for $t_0 \to -\infty$, that

$$\Sigma^{I_r\psi_1'\psi_3}_{\psi_2'\psi_3}(t) = \int_{t_0}^{t} \mathrm{d}\tau \Sigma^{I_r\psi_1'\psi_3}_{\psi_2'\psi_3}(t-\tau,t) = \sum_p \Sigma^{I_r\psi_1'\psi_3,p}_{\psi_2'\psi_3} e^{ip\omega_{ac}t} \,. \tag{6.5}$$

The four tunneling current diagrams which contribute to sequential tunneling now have the form as depicted in Fig. 6.1. In the same fashion we can write the irreducible self-energies of the reduced density matrix as

$$\Sigma^{\psi_1'\psi_1}_{\psi_2'\psi_2}(t) = \int_{t_0}^{t} \mathrm{d}\tau \Sigma^{\psi_1'\psi_1}_{\psi_2'\psi_2}(t-\tau,t) = \sum_m \Sigma^{\psi_1'\psi_1,m}_{\psi_2'\psi_2} e^{im\omega_{ac}t} \,, \tag{6.6}$$

and the master equation for the ac-driven case becomes

$$\frac{\partial}{\partial t} P^{\psi_1}_{\psi_2}(t) = i\left(\varepsilon_{\psi_2} - \varepsilon_{\psi_1}\right) P^{\psi_1}_{\psi_2}(t) - \sum_{\psi_1',\psi_2'} P^{\psi_1'}_{\psi_2'}(t) \Sigma^{\psi_1'\psi_1}_{\psi_2'\psi_2}(t) \,. \tag{6.7}$$

The tunneling diagrams of the self-energy from the reduced density matrix adjust accordingly as presented in Fig. 6.2.

6.2. Fourier expansion of the master equation and numerical implementation

We use the periodicity of the irreducible self-energies and Fourier expand the master equation. In particular,

$$P^{\psi_1}_{\psi_2}(t) = \sum_k P^{\psi_1,k}_{\psi_2} e^{ik\omega_{ac}t} \,. \tag{6.8}$$

When we insert this expression into Eq. (6.7) together with Eq. (6.6) and use the orthogonality of the complex exponentials, we arrive at the Fourier expanded master equation

$$0 = i(\varepsilon_{\psi_2} - \varepsilon_{\psi_1} - k\omega_{ac}) P^{\psi_1,k}_{\psi_2} + \sum_{\psi_1'\psi_2',q} P^{\psi_1',q}_{\psi_2'} \Sigma^{\psi_1'\psi_1,k-q}_{\psi_2'\psi_2} \,. \tag{6.9}$$

For the numerical implementation we introduce the number M of Fourier modes which are maximally taken into account, i.e., the Fourier sums run from $-M$ to $+M$. Furthermore, we define the probability vector $\vec{P} = [\vec{P}^{\psi}_{\psi}, \vec{P}^{\psi_1}_{\psi_2}]^T$, where $\vec{P}^{\psi}_{\psi}$ and $\vec{P}^{\psi_1}_{\psi_2}$ are $2M+1$ dimensional vectors carrying the different Fourier modes for the diagonal and

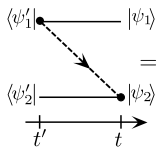

$$= -i\frac{\Gamma}{2\beta}\langle\psi_1|d|\psi_1'\rangle\langle\psi_2'|d^\dagger|\psi_2\rangle \sum_{r,mp} d^r_{mm-p} e^{ip\omega_{ac}t} \frac{e^{i(\omega_{\psi_1'\psi_1}+(m-p)\omega_{ac})\tau} e^{-W(+\tau)} e^{-i\mu_r(\tau-\frac{i}{B})}}{\sinh\left(\frac{\pi}{\beta}\left(\tau-\frac{i}{B}\right)\right)}$$

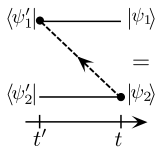

$$= -i\frac{\Gamma}{2\beta}\langle\psi_1|d^\dagger|\psi_1'\rangle\langle\psi_2'|d|\psi_2\rangle \sum_{r,mp} d^r_{mm-p} e^{-ip\omega_{ac}t} \frac{e^{i(\omega_{\psi_1'\psi_1}-(m-p)\omega_{ac})\tau} e^{-W(+\tau)} e^{+i\mu_r(\tau-\frac{i}{B})}}{\sinh\left(\frac{\pi}{\beta}\left(\tau-\frac{i}{B}\right)\right)}$$

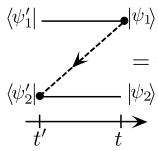

$$= +i\frac{\Gamma}{2\beta}\langle\psi_1|d|\psi_1'\rangle\langle\psi_2'|d^\dagger|\psi_2\rangle \sum_{r,mp} d^r_{mm-p} e^{-ip\omega_{ac}t} \frac{e^{i(\omega_{\psi_2\psi_2'}-(m-p)\omega_{ac})\tau} e^{-W(-\tau)} e^{+i\mu_r(\tau+\frac{i}{B})}}{\sinh\left(\frac{\pi}{\beta}\left(\tau+\frac{i}{B}\right)\right)}$$

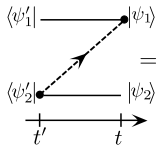

$$= +i\frac{\Gamma}{2\beta}\langle\psi_1|d^\dagger|\psi_1'\rangle\langle\psi_2'|d|\psi_2\rangle \sum_{r,mp} d^r_{mm-p} e^{ip\omega_{ac}t} \frac{e^{i(\omega_{\psi_2\psi_2'}+(m-p)\omega_{ac})\tau} e^{-W(-\tau)} e^{-i\mu_r(\tau+\frac{i}{B})}}{\sinh\left(\frac{\pi}{\beta}\left(\tau+\frac{i}{B}\right)\right)}$$

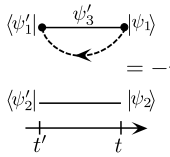

$$= -i\frac{\Gamma}{2\beta}\langle\psi_1|d|\psi_3'\rangle\langle\psi_3'|d^\dagger|\psi_1'\rangle\delta_{\psi_2'\psi_2} \sum_{r,mp} d^r_{mm-p} e^{-ip\omega_{ac}t} \frac{e^{i(\omega_{\psi_1'\psi_3'}-(m-p)\omega_{ac})\tau} e^{-W(+\tau)} e^{+i\mu_r(\tau-\frac{i}{B})}}{\sinh\left(\frac{\pi}{\beta}\left(\tau-\frac{i}{B}\right)\right)}$$

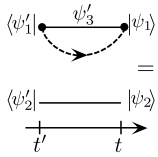

$$= -i\frac{\Gamma}{2\beta}\langle\psi_1|d^\dagger|\psi_3'\rangle\langle\psi_3'|d|\psi_1'\rangle\delta_{\psi_2'\psi_2} \sum_{r,mp} d^r_{mm-p} e^{ip\omega_{ac}t} \frac{e^{i(\omega_{\psi_1'\psi_3'}+(m-p)\omega_{ac})\tau} e^{-W(+\tau)} e^{-i\mu_r(\tau-\frac{i}{B})}}{\sinh\left(\frac{\pi}{\beta}\left(\tau-\frac{i}{B}\right)\right)}$$

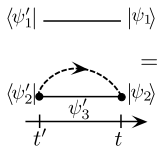

$$= +i\frac{\Gamma}{2\beta}\langle\psi_2'|d|\psi_3'\rangle\langle\psi_3'|d^\dagger|\psi_2\rangle\delta_{\psi_1'\psi_1} \sum_{r,mp} d^r_{mm-p} e^{ip\omega_{ac}t} \frac{e^{i(\omega_{\psi_3'\psi_2'}+(m-p)\omega_{ac})\tau} e^{-W(-\tau)} e^{-i\mu_r(\tau+\frac{i}{B})}}{\sinh\left(\frac{\pi}{\beta}\left(\tau+\frac{i}{B}\right)\right)}$$

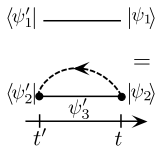

$$= +i\frac{\Gamma}{2\beta}\langle\psi_2'|d^\dagger|\psi_3'\rangle\langle\psi_3'|d|\psi_2\rangle\delta_{\psi_1'\psi_1} \sum_{r,mp} d^r_{mm-p} e^{-ip\omega_{ac}t} \frac{e^{i(\omega_{\psi_3'\psi_2'}-(m-p)\omega_{ac})\tau} e^{-W(-\tau)} e^{+i\mu_r(\tau+\frac{i}{B}}}{\sinh\left(\frac{\pi}{\beta}\left(\tau+\frac{i}{B}\right)\right)}$$

Figure 6.2.: Tunneling diagrams of the irreducible self-energy of the reduced density matrix in the ac-driven case.

off-diagonal elements of the reduced density matrix, respectively. The two possible states of our model are $\{|\psi\rangle\} = \{|0\rangle, |1\rangle\}$. Thus, the dimension of $\vec{P}$ is $d = 4(2M+1)$. The master equation in Fourier representation is an algebraic equation which can be written in a matrix vector notation as

$$0 = R \cdot \vec{P} = \begin{pmatrix} R_{00}^{00} & R_{10}^{10} & R_{10}^{00} & R_{00}^{10} \\ R_{01}^{01} & R_{11}^{11} & R_{11}^{01} & R_{01}^{11} \\ R_{01}^{00} & R_{11}^{10} & R_{11}^{00} & R_{01}^{10} \\ R_{00}^{01} & R_{10}^{11} & R_{10}^{01} & R_{00}^{11} \end{pmatrix} \cdot \begin{pmatrix} \vec{P}_0^0 \\ \vec{P}_1^1 \\ \vec{P}_1^0 \\ \vec{P}_0^1 \end{pmatrix} , \tag{6.10}$$

with a $d \times d$ matrix R. Within the Fourier subspace, the elements of R read

$$\left(R_{\psi_2'\psi_2}^{\psi_1'\psi_1}\right)_{k,q} = i(\varepsilon_{\psi_2} - \varepsilon_{\psi_1} - q\omega_{ac})\delta_{qk}\delta_{\psi_1'\psi_1}\delta_{\psi_2'\psi_2} + \Sigma_{\psi_2'\psi_2}^{\psi_1'\psi_1,k-q} . \tag{6.11}$$

In order that the probability is conserved at any time t, it has to hold that

$$\sum_{\psi_n} P_{\psi_n}^{\psi_n,k} = \delta_{k0} . \tag{6.12}$$

Then, one sees that

$$\begin{aligned} \mathrm{Tr}\left[\rho_{\mathrm{mol}}(t)\right] &= \sum_{\psi_n} \langle\psi_n|\rho_{\mathrm{mol}}(t)|\psi_n\rangle = \sum_{\psi_n} P_{\psi_n}^{\psi_n}(t) \\ &= \sum_{\psi_n}\sum_{k} P_{\psi_n}^{\psi_n,k} e^{ik\omega_{ac}t} = \sum_{k} \delta_{k0} e^{ik\omega_{ac}t} \\ &= 1 . \end{aligned} \tag{6.13}$$

Furthermore, since the density matrix needs to be a positive semidefinite operator, it has to hold that

$$\langle\psi_n|\rho_{\mathrm{mol}}(t)|\psi_n\rangle \geq 0 , \quad \forall t, \psi_n , \tag{6.14}$$

leading to

$$P_{\psi_n}^{\psi_n,k} = 0 , \quad \text{if } k \neq 0 , \tag{6.15}$$

$$P_{\psi_n}^{\psi_n,k} \geq 0 , \quad \text{if } k = 0 . \tag{6.16}$$

Since the vector $\vec{P}$ in Eq. (6.10) represents the density matrix it can not be the null vector. Thus, the matrix R is not only in general complex, non-symmetric and non-diagonalizable but also has to be singular, i.e., $\det R = 0$. This means that $\vec{P}$ is an eigenvector of R with eigenvalue 0. Therefore, the Fourier components $P_{\psi_2}^{\psi_1,k}$ of the reduced density matrix can readily be obtained by numerically solving the eigenvalue problem given by Eq. (6.10), while ensuring conservation of probability.

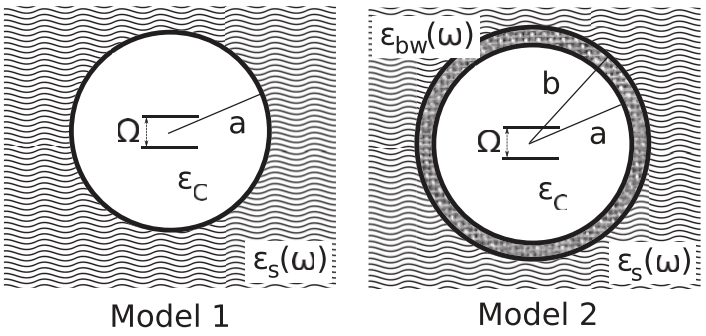

Figure 6.3.: Two models of solvation. Model 1 is the Onsager model as shown in Fig. 5.1. Model 2 additionally incorporates a hydration shell with radius b and dielectric function $\varepsilon_{\mathrm{bw}}(\omega)$. The picture is taken from Ref. [113].

Finally, we obtain the stationary current by inserting the numerically calculated expressions (6.5) and (6.8) into Eq. (4.40) which yields

$$\begin{aligned}\langle I_r(t)\rangle &= -e \sum_{\psi_1'\psi_2'\psi_3} P^{\psi_1'}_{\psi_2'}(t)\Sigma^{I_r\psi_1'\psi_3}_{\psi_2'\psi_3}(t) \\ &= -e \sum_{\psi_1'\psi_2'\psi_3}\sum_{kq} P^{\psi_1',q}_{\psi_2'}\Sigma^{I_r\psi_1'\psi_3,k-q}_{\psi_2'\psi_3} e^{ik\omega_{ac}t} \\ &= \sum_k I_r^k e^{ik\omega_{ac}t},\end{aligned} \tag{6.17}$$

where, in the last line, the current under the applied ac voltage is written in the form of a Fourier expansion where the Fourier-components are given by

$$I_r^k = -e \sum_{\psi_1'\psi_2'\psi_3}\sum_{q} P^{\psi_1',q}_{\psi_2'}\Sigma^{I_r\psi_1'\psi_3,k-q}_{\psi_2'\psi_3}. \tag{6.18}$$

This result is used to investigate the influence of the solvent and different extensions of the hydration shell on the current under an applied ac voltage.

6.3. Spectral density of the hydration shell

The inclusion of the bridging molecule into the (bulk) solvent alters the interacting network between the solvent molecules in proximity of the introduced molecule. Thus the solvent molecules surrounding the central molecule form a hydration shell with a more rigid water structure and a pronounced slowing down of structure fluctuations as well as rotational motion and a concomitant increase of H-bond lifetimes [68]. In order to incorporate hydration shell effects on the quantum transport we expand our model in such a way that the Onsager sphere introduced in Sec. 5.4 now contains a shell of thickness $(b-a)$, where b denotes the outer sphere radius and a is the

inner sphere radius, see Fig. 6.3. The new contribution now stems from the dielectric function associated with the bound water shell $\varepsilon_{\mathrm{bw}}(\omega)$ which is different than either the surrounding solvent dielectric function $\varepsilon_s(\omega)$ as well as the dielectric constant of vacuum $\varepsilon_c = 1$ inside the cavity. From the considerations in Sec. 5.4 we know that we can write the spectral density as

$$J(\omega) = 2\left(\Delta\mu\right)^2 \mathrm{Im}\left[\chi\left(\omega\right)\right] \ . \tag{6.19}$$

The susceptibility function $\chi(\omega)$ for a point dipole in a sphere containing a hydration shell of thickness $(b-a)$ can be derived in analogy to the derivation of Eq. (5.59). Our derivation follows Ref. [67]. Due to the spherical symmetry, the electric potentials in the cavity Φ_c, the shell Φ_{bw} and the bulk water Φ_s can be expressed in terms of spherical harmonics [63, 67, 97]

$$\Phi_i = \sum_{n=0}^{\infty} \left(A_n^{(i)} r^n + B_n^{(i)} r^{-(n+1)}\right) P_n(\cos\theta)\,, \tag{6.20}$$

as in Sec. 5.4. We recall that P_n are the Legendre polynomials and θ is the angle with respect to the $z-$axis, i.e., the axis of the dipole $\boldsymbol{\mu} = \mu\hat{\boldsymbol{e}}_z$. At the dielectric boundaries (and in general), the electric potential as well as the electric displacement must be continuous. Therefore, we can apply the boundary conditions [67]

$$\left(\Phi_s\right)_{r\to\infty} = 0\,, \tag{6.21}$$

$$\Phi_\mu = \frac{\mu}{r^2}\cos\theta\,, \tag{6.22}$$

$$\left(\Phi_{\mathrm{bw}}\right)_{r=b} = \left(\Phi_s\right)_{r=b}\ , \tag{6.23}$$

$$\left(\Phi_c\right)_{r=a} = \left(\Phi_{\mathrm{bw}}\right)_{r=a}\ , \tag{6.24}$$

$$\varepsilon_c \left(\frac{\partial\Phi_c}{\partial r}\right)_{r=a} = \varepsilon_{\mathrm{bw}} \left(\frac{\partial\Phi_{\mathrm{bw}}}{\partial r}\right)_{r=a}\ , \tag{6.25}$$

$$\varepsilon_{\mathrm{bw}} \left(\frac{\partial\Phi_{\mathrm{bw}}}{\partial r}\right)_{r=b} = \varepsilon_s \left(\frac{\partial\Phi_s}{\partial r}\right)_{r=b}\ . \tag{6.26}$$

The first condition is that the potential must go to zero at infinity. This means that all coefficients from the bulk environment with positive powers of r must vanish, that is, $A_n^{(s)} = 0$ for all n.

The second condition is the field from a point dipole. As this is the only free charge in the cavity, this is the only source term (inverse power of r) that will contribute to the potential Φ [67]. Since $P_1(\cos\theta) = \cos\theta$, only the $n = 1$ term is involved. Therefore, $B_{n=1}^{(c)} = \mu$ and $B_{n\neq1}^{(c)} = 0$. (Nothing is said about $A_n^{(c)}$.) The final terms describe the continuity of the potential and its derivative over the boundary. The first condition gives [67]

$$\sum_{n=0}^{\infty} \left(A_n^{(\mathrm{bw})} b^n + B_n^{(\mathrm{bw})} b^{-(n+1)}\right) P_n(\cos\theta) = \sum_{n=0}^{\infty} B_n^{(s)} b^{-(n+1)} P_n(\cos\theta)\,. \tag{6.27}$$

Because the Legendre polynomials P_n are orthogonal, we can consider each term of this sum as being equal, therefore

$$A_n^{(\mathrm{bw})} b^n + B_n^{(\mathrm{bw})} b^{-(n+1)} = B_n^{(s)} b^{-(n+1)} \,. \tag{6.28}$$

In a similar way, the remaining boundary conditions can be applied to produce a set of linear equations on the coefficients $A_n^{(i)}$ and $B_n^{(i)}$. We have six boundary conditions and six variables (each, of course, a function of n), and therefore, we are able to solve for all parameters. However, we are only interested in the field inside of the cavity and, in particular, the unknown part $A_n^{(c)}$. We find that all of the $A_n^{(c)}$ values are zero except for $n = 1$. Thus, the potential due to the surface charges is given by $\Phi_{c,\mathrm{surf}} = A_1^{(c)} r^1 P_1(\cos\theta) = -\chi \mu r \cos\theta$, where we find with $\varepsilon_c = 1$ [67]

$$\chi(\omega) = \frac{1}{4\pi\varepsilon_0 a^3} \frac{(\varepsilon_{\mathrm{bw}} + 2)(\varepsilon_s - \varepsilon_{\mathrm{bw}})a^3 + (\varepsilon_{\mathrm{bw}} - 1)(2\varepsilon_s + \varepsilon_{\mathrm{bw}})b^3}{2(\varepsilon_{\mathrm{bw}} - 1)(\varepsilon_s - \varepsilon_{\mathrm{bw}})a^3 + (2\varepsilon_{\mathrm{bw}} + 1)(2\varepsilon_s + \varepsilon_{\mathrm{bw}})b^3} \,. \tag{6.29}$$

In this expression we have omitted the frequency dependence of the complex dielectric functions for better clarity. The actual electric field in the cavity due to the surface charges but not the dipole itself, i.e., the reaction field, is then $\boldsymbol{R}(\omega) = \chi(\omega)\boldsymbol{\mu}(\omega)$, which will be a constant throughout the cavity, parallel to the dipole, and proportional to the dipole moment μ [67]. With Eq. (6.19) we can then directly write the spectral density for a point dipole in a sphere containing a hydration shell of thickness $(b - a)$ as

$$J_2(\omega) = \frac{(\Delta\mu)^2}{2\pi\varepsilon_0 a^3} \mathrm{Im}\left[\frac{(\varepsilon_{\mathrm{bw}} + 2)(\varepsilon_s - \varepsilon_{\mathrm{bw}})a^3 + (\varepsilon_{\mathrm{bw}} - 1)(2\varepsilon_s + \varepsilon_{\mathrm{bw}})b^3}{2(\varepsilon_{\mathrm{bw}} - 1)(\varepsilon_s - \varepsilon_{\mathrm{bw}})a^3 + (2\varepsilon_{\mathrm{bw}} + 1)(2\varepsilon_s + \varepsilon_{\mathrm{bw}})b^3}\right] \,. \tag{6.30}$$

We assume that the hydration shell is thin compared to the radius of the inner sphere and perform a Taylor expansion of the spectral density in the relative shell thickness $(b - a)/a \ll 1$. This yields [67]

$$J_2(\omega) = J_1(\omega) + J_{\mathrm{bw}}(\omega) \,, \tag{6.31}$$

where $J_1(\omega)$ represents the spectral density of a molecule inside a cavity of radius a surrounded by a bulk solvent in the absence of a hydration shell, as previously encountered in Eq. (5.63). The second term $J_{\mathrm{bw}}(\omega)$ can be identified with the contribution to the spectral density of the bound water layer for which we get

$$J_{\mathrm{bw}}(\omega) = \frac{(\Delta\mu)^2}{2\pi\varepsilon_0 a^3} \mathrm{Im}\left[\frac{3}{\varepsilon_{\mathrm{bw}}} \frac{(2\varepsilon_s + \varepsilon_{\mathrm{bw}})(\varepsilon_{\mathrm{bw}} - \varepsilon_s)}{(2\varepsilon_s + 1)^2} \frac{(b - a)}{a}\right] \,. \tag{6.32}$$

If we further consider frequencies much smaller than the inverse bulk solvent relaxation time $1/\tau_s$, we can approximate the dielectric function of the bulk solvent by its static value, i.e., $\varepsilon_s(\omega) \approx \varepsilon_{s,S}$, and the spectral density becomes

$$J_{\mathrm{bw}}(\omega) = \frac{3\,(\Delta\mu)^2}{2\pi\varepsilon_0 a^3} \frac{(b - a)}{a} \frac{1}{(2\varepsilon_{s,S} + 1)^2} \mathrm{Im}\left[\left(1 + \frac{2\varepsilon_{s,S}}{\varepsilon_{\mathrm{bw}}}\right)(\varepsilon_{\mathrm{bw}} - \varepsilon_{s,S})\right] \tag{6.33}$$

$$= \frac{3\,(\Delta\mu)^2}{2\pi\varepsilon_0 a^3} \frac{(b - a)}{a} \frac{1}{(2\varepsilon_{s,S} + 1)^2} \left(1 + \frac{2\varepsilon_{s,S}^2}{|\varepsilon_{\mathrm{bw}}(\omega)|^2}\right) \mathrm{Im}\left[\varepsilon_{\mathrm{bw}}(\omega)\right] \,. \tag{6.34}$$

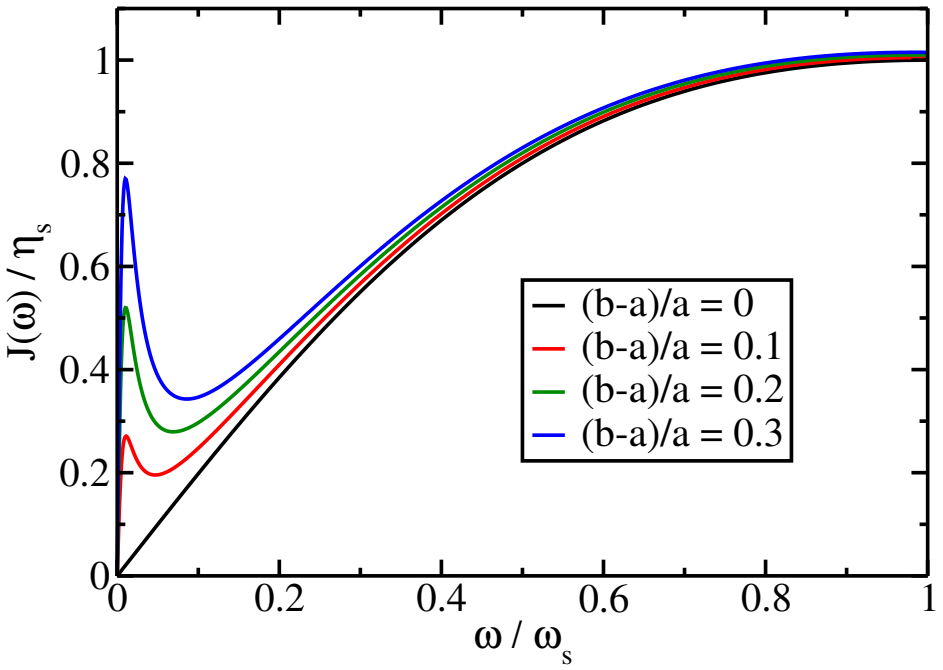

Figure 6.4.: Spectral density $J(\omega)$ normalized to the reorganization energy η_s of bulk water as a function of the frequency ω (normalized to the cut-off frequency of water ω_s) for various relative hydration shell thicknesses as indicated. The cut-off frequency of the hydration shell is $\omega_\mathrm{bw} = 10^{-2}\omega_\mathrm{s}$.

By additionally approximating the absolute square with the static value squared, i.e., $|\varepsilon_\mathrm{bw}(\omega)|^2 \approx \varepsilon^2_{\mathrm{bw},S}$, and using the Debye form for the bound water dielectric function, i.e., $\mathrm{Im}\left[\varepsilon_\mathrm{bw}(\omega)\right] = (\varepsilon_{\mathrm{bw},S} - \varepsilon_{\mathrm{bw},\infty})(\omega\tau_\mathrm{bw}/(1+\omega^2\tau^2_\mathrm{bw}))$, the final expression for the spectral density of the bound water turns into [67, 113]

$$J_\mathrm{bw}(\omega) = \frac{3\,(\Delta\mu)^2}{2\pi\varepsilon_0 a^3}\frac{(b-a)}{a}\frac{(\varepsilon^2_{\mathrm{bw},S} + 2\varepsilon^2_{s,S})(\varepsilon_{\mathrm{bw},S} - \varepsilon_{\mathrm{bw},\infty})}{\varepsilon^2_{\mathrm{bw},S}(2\varepsilon_{s,S}+1)^2}\frac{\omega\tau_\mathrm{bw}}{1+\omega^2\tau^2_\mathrm{bw}}\ . \tag{6.35}$$

In this form it resembles the spectral density of the bulk solvent and likewise can be expressed as

$$J_\mathrm{bw}(\omega) = 2\eta_\mathrm{bw}\frac{\omega\omega_\mathrm{bw}}{\omega^2+\omega^2_\mathrm{bw}}\ , \tag{6.36}$$

with the bound water cut-off frequency $\omega_\mathrm{bw} = 1/\tau_\mathrm{bw}$ and reorganization energy

$$\eta_\mathrm{bw} = \frac{3\,(\Delta\mu)^2}{4\pi\varepsilon_0 a^3}\frac{(b-a)}{a}\frac{(\varepsilon^2_{\mathrm{bw},S} + 2\varepsilon^2_{s,S})(\varepsilon_{\mathrm{bw},S} - \varepsilon_{\mathrm{bw},\infty})}{\varepsilon^2_{\mathrm{bw},S}(2\varepsilon_{s,S}+1)^2}\ . \tag{6.37}$$

In order to further simplify this expression, we take a closer look at the involved relaxation times and dielectric constants. For bulk water at room temperature, $\varepsilon_{s,S} = 78.3$, $\varepsilon_{s,\infty} = 4.21$, and $\tau_s = 8.2$ ps [62, 114, 115]. The dielectric properties of the hydration shell are less clear, but in general, a higher structural order of the water

molecules in the first few layers around the solute implies weaker fluctuations and, thus, $\varepsilon_{s,S} \gg \varepsilon_{\mathrm{bw},S}$ [63, 67, 68, 113]. This reflects the fact, that the water molecules are stronger bound in a hydrogen network and are less polarizable. Due to this enhanced interaction in the hydration shell, the relaxation time is significantly slower, such that $\tau_{\mathrm{bw}} \gg \tau_s$ [63, 67, 68, 113]. Furthermore, the high-frequency dielectric constants are generally smaller than the static ones, i.e., $\varepsilon_{s,S} \gg \varepsilon_{s,\infty}$, and $\varepsilon_{\mathrm{bw},S} \gg \varepsilon_{\mathrm{bw},\infty}$ [67, 113], because the dielectric response is weaker at high frequencies. Hence, we use these relations and set $\tau_{\mathrm{bw}} = 10\tau_s$ to obtain

$$\frac{(\varepsilon_{\mathrm{bw},S}^2 + 2\varepsilon_{s,S}^2)(\varepsilon_{\mathrm{bw},S} - \varepsilon_{\mathrm{bw},\infty})}{\varepsilon_{\mathrm{bw},S}^2(2\varepsilon_{s,S}+1)^2} \approx \frac{1}{2\varepsilon_{\mathrm{bw},S}} \ . \tag{6.38}$$

Compared to the factor of the reorganization energy, Eq. (5.64), of bulk water

$$\frac{2(\varepsilon_{\mathrm{s},S} - \varepsilon_{\mathrm{s},\infty})}{(2\varepsilon_{\mathrm{s},S}+1)(2\varepsilon_{\mathrm{s},\infty}+1)} \approx \frac{1}{2\varepsilon_{\mathrm{s},\infty}} \ , \tag{6.39}$$

we see that

$$\eta_{\mathrm{bw}} \approx \frac{\varepsilon_{\mathrm{s},\infty}}{\varepsilon_{\mathrm{bw},S}} \frac{(b-a)}{a} \eta_{\mathrm{water}} \ . \tag{6.40}$$

In this expression we see that the reorganization energy of the shell can be increased compared to the bulk water reorganization energy by increasing either the relative shell thickness or the ratio between the high-frequency dielectric parameter of bulk water and the static dielectric parameter of bound water.

In Fig. 6.4, we show an exemplary plot of the spectral density for water with various relative hydration shell thicknesses. The two contributions to the spectral density can be clearly observed by the two separated peaks when the hydration shell is present (colored lines). Without the hydration shell only one peak appears at the cut-off frequency of the bulk water ω_{s} (black line). Therefore, an increase in the shell thickness only increases the bound water part of the spectral density which in this case has its peak at $\omega_{\mathrm{bw}} = 10^{-2}\omega_{\mathrm{s}}$. Although the spectral density of the form (6.31) is only valid for thin hydration shells $(b-a)/a \ll 1$, we also show $J(\omega)$ for larger values of $(b-a)/a$ in Fig. 6.4 to illustrate the leading contribution from the hydration shell. Interestingly, one observes a strong impact on $J(\omega)$ already in the limit $(b-a)/a \ll 1$ which signals the electrodynamically collective response of the strongly bound water in the shell. Clearly, as follows from Eq. (6.40), the slope of $J(\omega)$ at low frequencies depends linearly on the relative hydration shell thickness $(b-a)/a$.

6.4. Results and discussion

In the following, we present the results for the current through the single-molecule junction driven by an ac voltage. Like we did for the dc case, we begin by discussing results without any surrounding solvents. In Fig. 6.5 (a) the zeroth and first Fourier

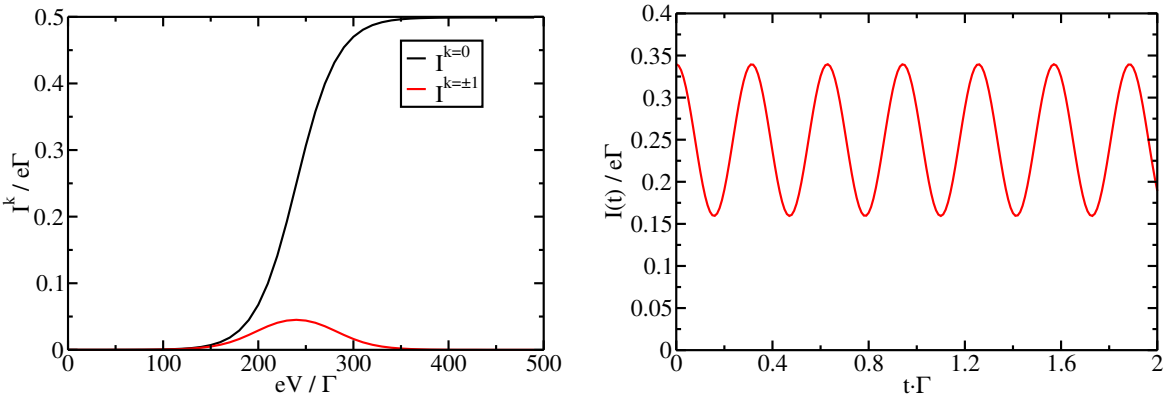

(a) I^k (b) $I(t)$

Figure 6.5.: (a) Zeroth and first Fourier component of the stationary current with respect to the applied dc voltage. (b) Stationary current as a function of the time t at a dc voltage of $eV_{dc} = 240\ \Gamma$. Parameters are $\varepsilon_d = 120\ \Gamma$, $eV_{ac} = 10\ \Gamma$, $\omega_{ac} = 20\ \Gamma$, $T = 10\ \Gamma$, and $\Gamma = 2.5$ meV.

component of the stationary current are illustrated as a function of the applied dc voltage. The amplitude and frequency of the ac voltage are $eV_{ac} = 10\,\Gamma$ and $\omega_{ac} = 20\,\Gamma$, respectively. It can be nicely seen that the zeroth Fourier component of the current corresponds to the dc current as observed in Fig. 5.4 (a). We note, that the scaling of the parameters is different by a factor of 100 between Figs. 6.5 and 5.4.

In addition to the dc part of the current we observe a peak of the first Fourier component where the dc voltage reaches the energy level of the molecule, i.e., at $eV_{dc} = 240\ \Gamma$. Since the first negative $I^{k=-1}$ and positive $I^{k=+1}$ Fourier components are the same in this case the time-dependent current at $eV_{dc} = 240\ \Gamma$ then has a form of a cos-function, see Fig. 6.5 (b). The time-dependent current oscillates around the dc current value $I^{k=0}(eV_{dc} = 240\ \Gamma) \approx 0.25\ \Gamma$ with twice the amplitude of the first Fourier component $I^{k=1}(eV_{dc} = 240\ \Gamma) \approx 0.04\ \Gamma$.

When the molecular junction is embedded in the same solvents as investigated for the nonlinear differential conductance in the dc case (see Fig. 5.4 (b)), the maximum value of the first Fourier component decreases in a similar fashion, see Fig. 6.6. Accordingly, a part of the electric potential energy eV is used for the reorganization of the solvent. Solvents with larger reorganization energies suppress the maximum value of the first Fourier component of the current more strongly than solvents with smaller reorganization energies. Notice, that the ac voltage in Fig. 6.6 has been doubled compared to Fig. 6.5, i.e., $eV_{ac} = 20\ \Gamma$.

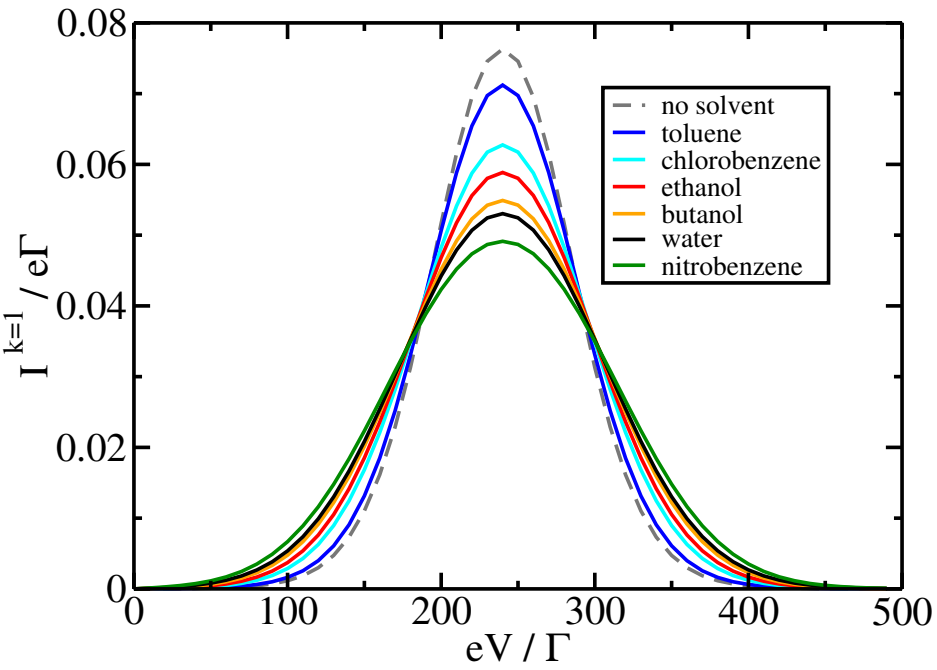

Figure 6.6.: First Fourier component of the stationary current as a function of the dc voltage. Parameters are $\varepsilon_d = 120\ \Gamma$, $eV_{ac} = 20\ \Gamma$, $\omega_{ac} = 20\ \Gamma$, $T = 10\ \Gamma$, and $\Gamma = 2.5$ meV.

6.4.1. Hydration shell effects in ac-driven single-molecule junctions

In experimental setups of metal-molecule-metal junctions it is oftentimes favorable to operate in the linear transport regime (small applied dc voltages) to distinguish solvent and hydration shell effects from other nonlinear effects like the negative differential resistance due to the interplay between two or more conduction channels accessible by a finite applied dc voltage. Having this in mind, we use a different control parameter than the applied dc voltage, i.e., the ac voltage frequency ω_{ac}, to study the influence of the solvent with and without hydration shell. We fix the dc voltage to $\mu_L = \mu_R = eV_{dc} = 0$ and set the molecular energy level to $\varepsilon_d = 0$. Given this symmetry of our model where the leads' Fermi levels align with the molecular level in the absence of an applied voltage, all even Fourier components of the ac current vanish and only the odd ones are nonzero. Additionally, the zeroth Fourier component of the current also vanishes due to the fact that we are in the linear transport regime with $V_{dc} = 0$, since it corresponds to the dc current.

In Fig. 6.7, we show the first Fourier component $I^{k=1}$ of the stationary current both in the absence of a solvent and for water with various relative hydration shell thicknesses. $I^{k=1}$ is only induced by the applied ac voltage so that in the limit $\omega_{ac}/\Gamma \to 0$ no potential difference can be build up across the molecule in the relevant charge transfer time scale Γ^{-1} and $I^{k=1}$ goes to zero. The $I^{k=1}$-ω_{ac} curve goes through a maximum

close to the frequency $\omega_{ac} = eV_{ac} = 10\ \Gamma$, which can be attributed to the Bessel functions appearing in Eq. (6.4), because the product of the zeroth and first Bessel function is maximal when the argument eV_{ac}/ω_{ac} is close to one. These two Bessel functions are the main contributors to the first Fourier component of the stationary current for frequencies at or above $\omega_{ac} = eV_{ac}$ because all higher Bessel functions are significantly smaller in that frequency range. Put differently, the energy supplied by the ac voltage $(\hbar)\omega_{ac}$ matches the electric energy eV_{ac} by the (time-dependent) voltage sweep across the molecule. Higher ac frequencies ω_{ac} lead to an energetic mismatch and $I^{k=1}$ declines. Similar observations are found in the photon assisted current in single molecular junctions where $I^{k=1}$ is the related current induced when electrons exchange a single energy quantum, i.e., a photon with the oscillating ac field [116].

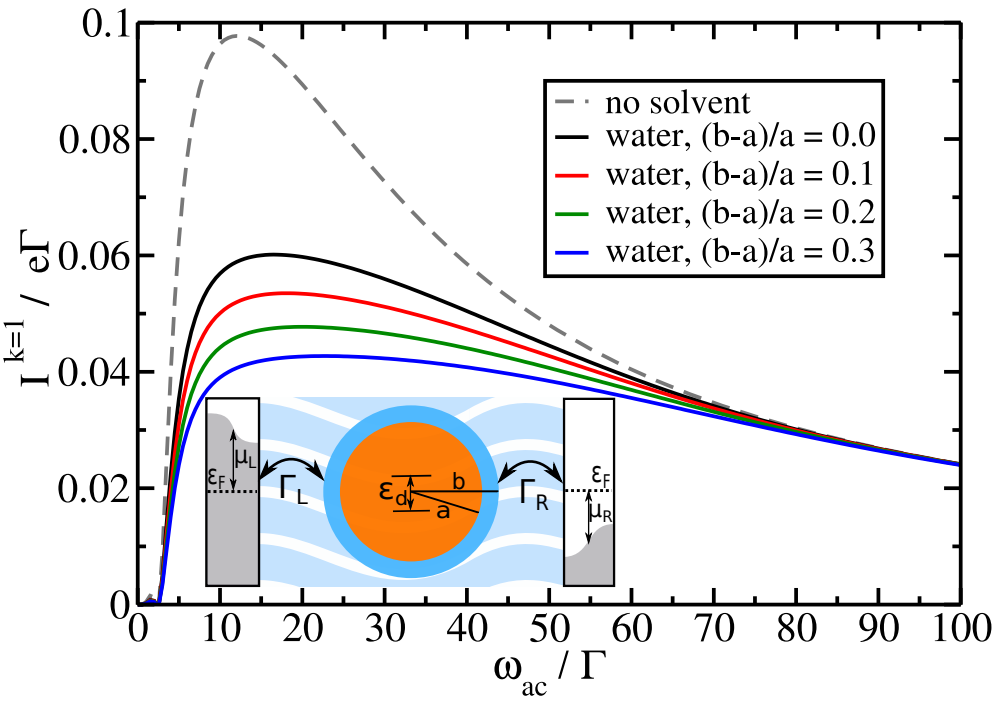

Figure 6.7.: First Fourier component of the stationary current $I^{k=1}$ as a function of the ac frequency ω_{ac} in the absence of a solvent (grey dashed line) and for water with various relative hydration shell thicknesses (solid lines). Parameters are $a = 5$ Å, $\Delta\mu = 5$ D, $T = 10\ \Gamma$, $\varepsilon_d = 0\ \Gamma$, $eV_{ac} = 10\ \Gamma$ and $\Gamma = 2.5$ meV.

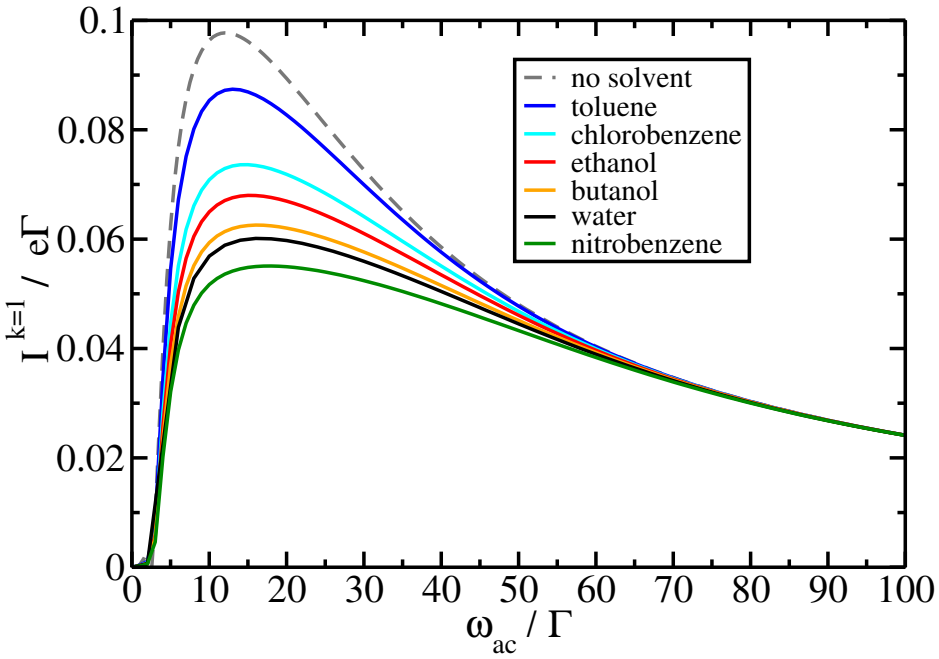

Figure 6.8.: First Fourier component of the stationary current $I^{k=1}$ as a function of the ac frequency ω_{ac} in the absence of a solvent (grey dashed line) and for different pure solvents (solid lines) as indicated. Parameters are $a = 5$ Å, $\Delta\mu = 5$ D, $T = 10$ Γ, $\varepsilon_d = 0$ Γ, $eV_{ac} = 10$ Γ and Γ = 2.5 meV.

When water is considered as a solvent surrounding the molecule then the $I^{k=1}$-ω_{ac} curves significantly decrease, see Fig. 6.7. This is due to the fact that a part of the electric potential energy of the ac drive is used for the reorganization of the solvent. Even more energy is needed to reorganize the solvent when we additionally consider the hydration shell. That is why the maximum current $I^{k=1}_{\max}$ decreases further with an increase of the hydration shell as depicted in Fig. 6.7 (a). Furthermore, we notice that the $I^{k=1}$ values for different ω_{ac} in a given window ($\sim$ 10–70 Γ) decline differently when increasing the shell thickness. This behavior reflects the distinct coupling of the molecular level to different polarization modes captured by the spectral density (see Fig. 6.4). We additionally portray $I^{k=1}$ in Fig. 6.8 with respect to ω_{ac} for the same parameters as in Fig. 6.7, but for various different solvents. The trend of the $I^{k=1}$-ω_{ac} curves is similar to the $I^{k=1}$-V_{dc} curves in Fig. 6.6 when it comes to the variation of the solvent. That is, solvents with larger reorganization energies suppress the maximum value of the first Fourier component of the current more strongly than solvents with smaller reorganization energies. The explanation is again that a part of the electric energy is used for the reorientation of the solvent.

In Fig. 6.9, we show $I^{k=1}_{\max}$ with respect to the relative shell thickness $(b - a)/a$ and observe that it is consistent with an exponential decrease. Such an exponential decrease of $I^{k=1}_{\max}$ with respect to the shell thickness could be expected from the real part of $W(t)$ from Eq. (4.17) where the spectral density $J(\omega)$ enters. The dominant term in $J(\omega)$ is the reorganization energy of the shell η_{bw} which is directly proportional to its

relative thickness $(b-a)/a$ (see Eq. (6.40)). Note, that deviations from that behavior may occur due to the exact calculations of the time integral over the self-energy in Eq. (6.5). The decline of $I^{k=1}_{\max}$ directly reflects the enhanced collective response of the strongly bound molecules in the hydration shell.

Interestingly, the position $\omega_{ac}(I^{k=1}_{\max})$ at which $I^{k=1}$ is maximal is also influenced by the shell and shifts to higher frequencies when compared to the case without hydration shell, see Fig. 6.10. Since the contribution from the irreducible self-energy (4.42) to the current is maximal when the imaginary part of the exponent vanishes the observed increase of $\omega_{ac}(I^{k=1}_{\max})$ with a growing hydration-shell can be related to the increasing imaginary part of $W(t)$ in Eq. (4.17) which makes the imaginary part in the exponent in Eq. (6.4) smaller [70].

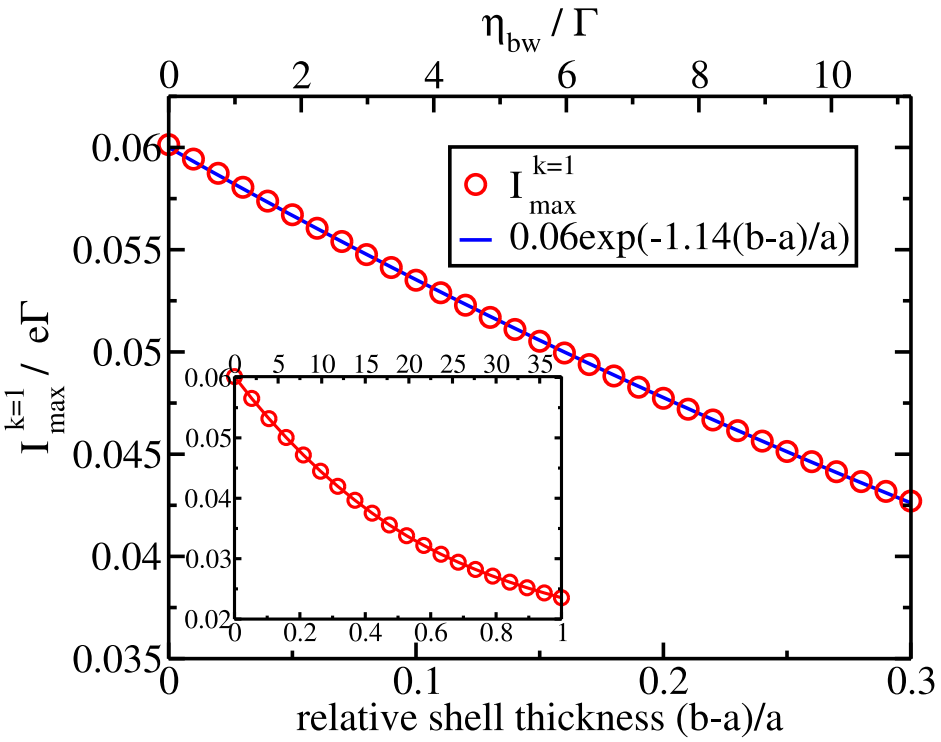

Figure 6.9.: Maximum of the first Fourier component of the stationary current $I^{k=1}_{\max}$ as a function of the relative shell thickness $(b-a)/a$. Parameters are $a = 5$ Å, $\Delta\mu = 5$ D, $T = 10\ \Gamma$, $\varepsilon_d = 0\ \Gamma$, $eV_{ac} = 10\ \Gamma$ and $\Gamma = 2.5$ meV. The inset shows the trend for larger relative shell thicknesses within the expansion of Eq. (6.31). The blue line is a fit to an exponential function as indicated.

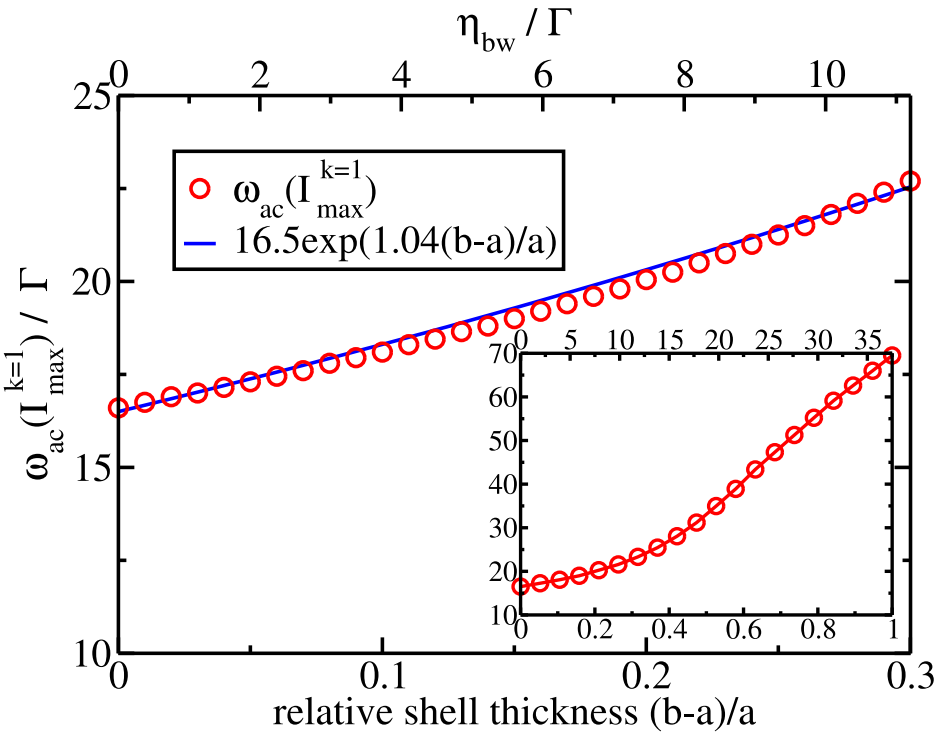

Figure 6.10.: Frequency $\omega_{ac}(I^{k=1}_{\max})$ position at $I^{k=1}_{\max}$ as a function of the relative shell thickness $(b-a)/a$. Parameters are $a = 5$ Å, $\Delta\mu = 5$ D, $T = 10\ \Gamma$, $\varepsilon_d = 0\ \Gamma$, $eV_{ac} = 10\ \Gamma$ and $\Gamma = 2.5$ meV. The insets show the trend for larger relative shell thicknesses within the expansion of Eq. (6.31). The blue line is a fit to an exponential function as indicated.

6.4.2. Higher order Fourier components of the current

In Fig. 6.11, we show the third Fourier component $I^{k=3}$ of the stationary current both in the absence of a solvent and for water with various relative hydration shell thicknesses. $I^{k=3}$ shows a similar behavior with increasing hydration shell thicknesses as $I^{k=1}$ in Fig. 6.7. Note, however, that the magnitude of the value of this Fourier component is much smaller than $I^{k=1}$ due to the chosen small amplitude of our model. Furthermore, we show $I^{k=3}$ only for frequencies at or above $\omega_{ac} = eV_{ac} = 10\ \Gamma$ because we consider only the first three Bessel functions which contribute mainly to the third Fourier component of the stationary current and all higher Bessel functions are significantly smaller in that frequency range.

In Fig. 6.12, we also illustrate the second $I^{k=2}$ and third $I^{k=3}$ Fourier components of the stationary current as a function of the dc voltage in the absence of a solvent. But this time again for a molecular energy level of $\varepsilon_d = 120\ \Gamma$, ac voltage $eV_{ac} = 20\ \Gamma$, and ac frequency $\omega_{ac} = 20\ \Gamma$, as in Fig. 6.6 for $I^{k=1}$. It can be nicely observed that the second Fourier component is antisymmetric around the resonance point of $eV_{dc} = 240\ \Gamma$, where the dc voltage reaches the energy level of the molecule. In contrast to this, the third Fourier component is symmetric around $eV_{dc} = 240\ \Gamma$, like $I^{k=1}$ in

Fig. 6.6. Furthermore, the odd Fourier components have their maximum around the resonance point whereas the even ones are zero at that point. This is in accordance with our results in the linear transport regime, i.e., for $eV_{dc} = 0\ \Gamma$ and $\varepsilon_d = 0\ \Gamma$.

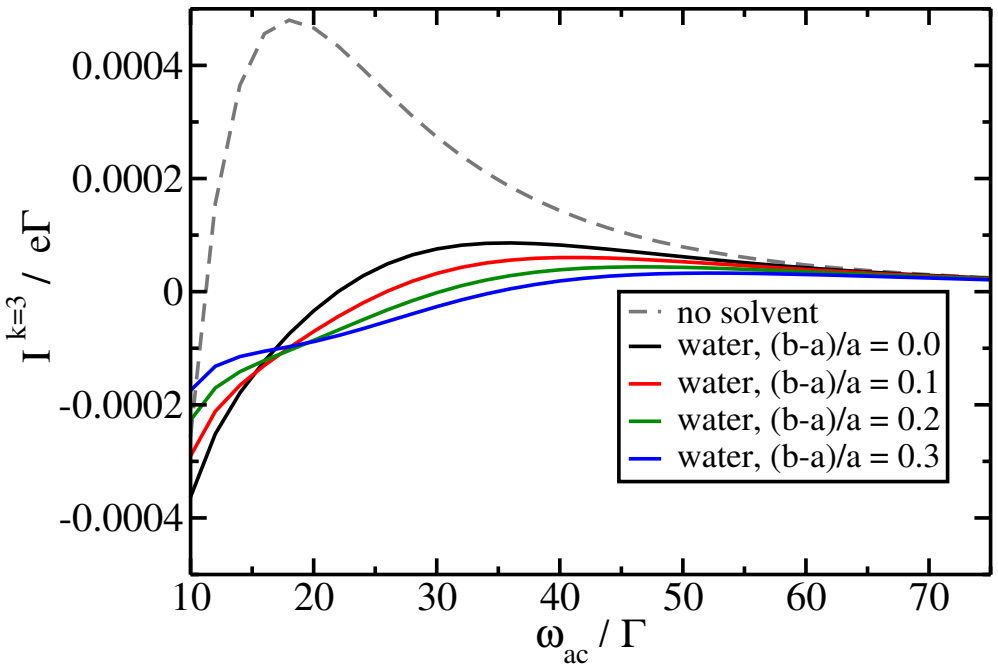

Figure 6.11.: Third Fourier component of the stationary current $I^{k=3}$ as a function of the ac frequency ω_{ac} in the absence of a solvent (grey dashed line) and for water with various relative hydration shell thicknesses (solid lines) as indicated. Parameters are $a = 5$ Å, $\Delta\mu = 5$ D, $T = 10\ \Gamma$, $\varepsilon_d = 0\ \Gamma$, $eV_{ac} = 10\ \Gamma$, and $\Gamma = 2.5$ meV.

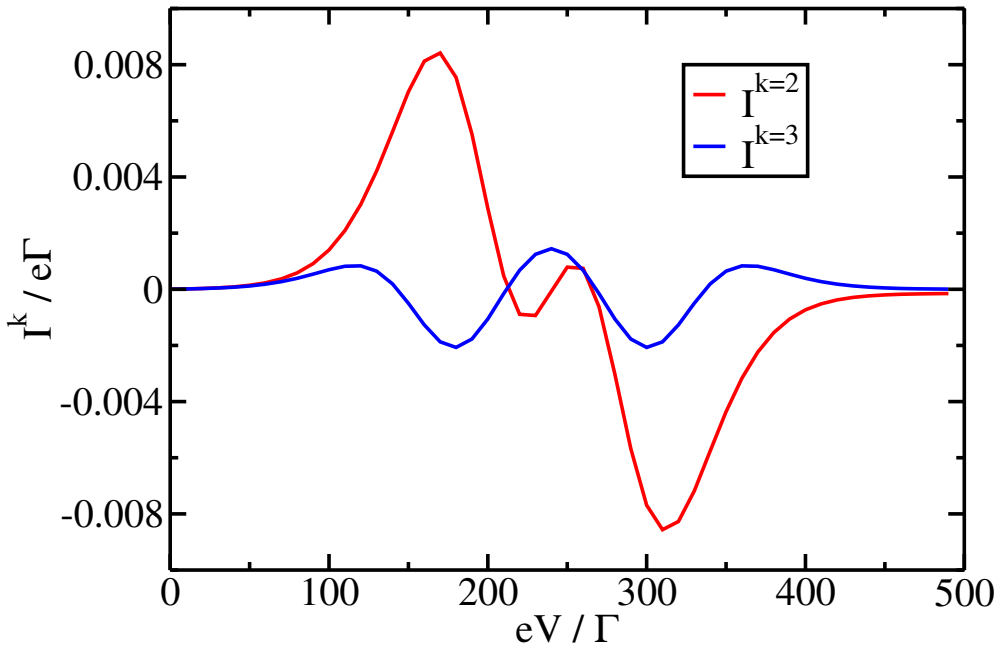

Figure 6.12.: Second $I^{k=2}$ and third $I^{k=3}$ Fourier component of the stationary current as function of the dc voltage V_{dc} in the absence of a solvent. Parameters are $\varepsilon_d = 120\ \Gamma$, $eV_{ac} = 20\ \Gamma$, $\omega_{ac} = 20\ \Gamma$, $T = 10\ \Gamma$, and $\Gamma = 2.5$ meV.

6.4.3. Application to binary solvent mixtures

With the same methodology as in Sec. 5.6.4 for the nonlinear differential conductance we next investigate the first-order Fourier component $I^{k=1}$ under an ac voltage with frequency $\omega_{ac} = 10\ \Gamma$ and amplitude $eV_{ac} = 10\ \Gamma$ as a function of the volume fraction f for the binary mixtures between butanol and ethanol, chlorobenzene and nitrobenzene, as well as toluene and nitrobenzene. Notably, we find the same qualitative behavior for $I^{k=1}$ with respect to f, Fig. 6.13, as for the nonlinear differential conductance, see Fig. 5.7. $I^{k=1}$ is also highly influenced by the volume fraction f of the additional solvent. The $I^{k=1}$-f behavior likewise depends on the specific binary mixture and reflects the non-monotonous characteristics of the dielectric function Eq. (5.66). The main difference is that we are here again in the linear transport regime, i.e., $eV_{dc} = 0\ \Gamma$ and $\varepsilon_d = 0\ \Gamma$, and still find that $I^{k=1}$ is highly sensitive to both the volume fraction and the individual solvents themselves [70].

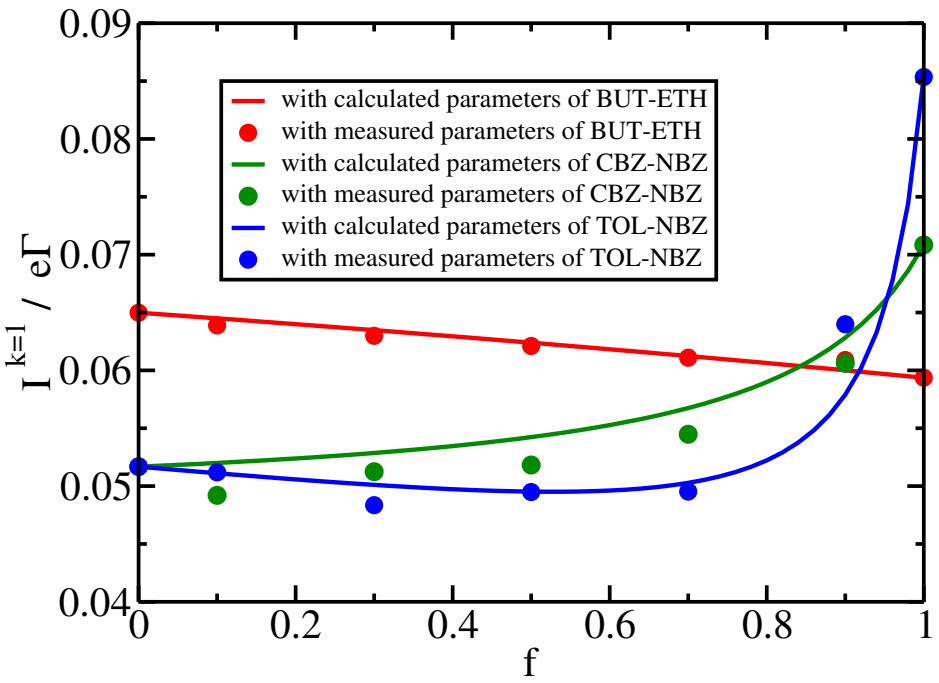

Figure 6.13.: First Fourier component of the stationary current as a function of the volume fraction f for the binary mixtures between butanol and ethanol, chlorobenzene and nitrobenzene, as well as toluene and nitrobenzene. The solid lines show the results calculated using the effective dielectric parameters of Gladstone-Dale in an effective Debye spectral density. In addition, the circles mark the current calculated with a single Debye spectral density of the mixture with the directly measured dielectric parameters taken from Ref. [102]. Parameters are $a = 5$ Å, $b = 0$, $\Delta\mu = 5$ D, $T = 10\ \Gamma$, $\varepsilon_d = 0\ \Gamma$, $eV_{ac} = 10\ \Gamma$, $\omega_{ac} = 10\ \Gamma$ and $\Gamma = 2.5$ meV.

Chapter 7.

Summary and outlook

In this thesis, we have investigated the interplay between molecular electronic conduction and the response of a polar solvent environment. A setup of a molecular junction immersed in solution offers a promising ground for molecular electronics devices, in particular sensors and switches. As sensors such devices are sensitive to small changes of concentrations of target species dissolved in a polar solvent, while as switches they are controlled by the bias and gate voltage. We provide a theory to calculate the charge current through a molecular junction surrounded by a polar solvent. For the calculation of the tunneling current we utilize a quantum mechanical real-time diagrammatic technique in the regime of sequential charge tunneling, which includes the electrostatic molecule-solvent coupling in the single electron transfer nonperturbatively. This technique is based on the Liouville-von Neumann equation and allows to solve the quantum master equation of the reduced density matrix of the molecule in a perturbative manner in the tunnel coupling to the leads. The lowest order of this perturbation corresponds to the sequential tunneling regime and is the main contribution to the current when the molecule-lead coupling is weak and the temperature or the bias voltage are comparably large. For larger tunnel coupling or low temperature and transport voltage higher-order processes, so-called cotunneling contributions, will have significant effects on the transport characteristics and in general need to be taken into account under these conditions. In this thesis, we have concentrated on sequential tunneling only.

For the incorporation of the solvent, we have used an approach by Gilmore and McKenzie. Based on the Onsager model of solvation, this approach offers the determination of the solvent spectral density which enters the irreducible self-energy of the quantum master equation. Using a Debye dielectric function, the solvent can thereby be characterized by its dielectric constants and the Debye relaxation time. In addition to the investigation of pure solvents, we use the Gladstone-Dale approach to determine an effective dielectric function and propose an expression for the resulting spectral density of the polarization fluctuations of binary solvent mixtures. We believe that this approach could be also relevant for optical absorption spectroscopy of solutes in solvent mixtures. Utilizing the measured dielectric constants of pure solvents as well as their respective relaxation times together with tuning the volumetric fraction, we have obtained a very good agreement of the nonlinear differential conductance either calculated by the proposed model and experimentally measured conductance values.

We have observed that the maximum of the differential conductance gets reduced and its width is enhanced when the junction is immersed in a solvent. This is due to the fact that a part of the electric potential energy, inducing the electric current, is used for the reorganization of the solvent. Therefore, the larger the reorganization energy of the solvent is, the smaller the conductance maximum becomes. Furthermore, the additional tunneling broadening occurs via the absorption or emission of (bosonic) solvent polarization modes similar to the broadening dominated by the emission of phonons into a substrate. The examined nonmonotonous behavior of the differential conductance with respect to the volume fraction for certain solvent mixtures subsequently results from the nonmonotonous behavior of the spectral density of these mixtures. Franck-Condon steps are not present in our case because the dielectric provides a continuum of modes instead of a single mode (which could be a single molecular vibrational mode) in accordance with the high-temperature regime.

In order to investigate novel transport characteristics while staying in the linear transport regime (linear response to a small external static voltage), we introduce a time-dependent ac voltage. By Fourier expanding the quantum master equation, the electric current can then be expressed by its Fourier components. We have calculated the Fourier components of the current in dependence of the ac frequency in order to investigate the influence of a hydration shell on the transport characteristics. Similar to the solvation description of solvent mixtures, the spectral density of the hydration shell can be captured via an extended Onsager model where the shell properties, i.e., its thickness or its dielectric function, directly enter. Here our main results are calculations of the Fourier components of the current with respect to the hydration shell thickness. Interestingly, the Fourier components of the charge current for different applied ac voltage frequencies portray a nonlinear behavior when altering the thickness of the hydration shell. The hydration shell is formed around the central molecule which alters the interacting network between the solvent molecules in proximity of the junction molecule. Due to a more rigid water structure and a pronounced slowing down of structure fluctuations as well as rotational motion of the water molecules in the hydration shell more energy is needed to reorganize the shell in comparison to the bulk solvent further away from the bridging molecule. That is why the maximum value of the Fourier components of the current decreases with an increase of the hydration shell thickness. Like in the dc case for solvent mixtures this is due to the fact that a part of the electric potential energy of the ac drive is used for the reorganization of the (bulk) solvent and, additionally, the hydration shell. Furthermore, we notice that the Fourier components of the current for different ac frequencies decline differently in a certain frequency window when increasing the shell thickness. This behavior reflects the distinct coupling of the molecular level to different polarization modes captured by the spectral density.

We find that by comparing the results of no solvent and water as a solvent both with and without hydration shell we can determine the thickness of the shell through the current under ac drive. The relative shell thickness can be read off, for example, by the exponential-like decline of the first Fourier component of the current. We have also applied the same methodology as for the investigation of the hydration shell to the

inspection of binary solvent mixtures. Notably, we find the same qualitative behavior for the first Fourier component of the current with respect to the volume fraction as for the nonlinear differential conductance in the dc case. The main difference is that we are here in the linear transport regime and still find that the current is highly sensitive to both the volume fraction and the individual solvents themselves. As a consequence, a possible application is provided by a prototype molecular junction under ac drive, measuring the volume fraction of a binary solvent mixture. Therefore, in total, the proposed theoretical methodology may be applied for a molecular sensor to determine the thickness of a hydration shell or the volume fraction of a solvent mixture with high sensitivity.

Possible extensions of the model are manifold and, given the rich field of molecular electronics, can provide exciting prospects for future research. One extension that directly comes into mind is the combination of the investigated influences of solvent mixtures and the incorporation of a shell. In that case not only a hydration shell build out of water molecules could be considered but a generalized theory could be developed which contains a solvation shell from the constituents of the solvent mixture. The spectral density of such a solvation shell will depend on the volume fraction of the mixture in addition to the volume fraction dependence of the spectral density of the mixture itself.

Speaking of solvent mixtures, our model incorporates only binary solvent mixtures. A further possible extension is, thus, to allow an arbitrary number of solvents in the mixture. There exists already a successful theory to describe multicomponent mixtures which is the Maxwell Garnett mixing formula. It describes the permittivity of the effective medium in terms of the permittivities and volume fractions of the individual constituents of the complex medium [100]. With the Maxwell Garnett mixing formula it should, in principle, be possible to find a spectral density for a multicomponent mixture. Not only the inclusion of more than two solvents could be regarded for the investigation of transport characteristics of molecular junctions.

Also the addition of salt ions could be taken into account. Like in the case of the Maxwell Garnett mixing formula, an effective dielectric function can be derived which contains not only the permittivities and volume fractions of the individual liquids but also considers the polarizability of the ionic species, by properly accounting for the volume change upon mixing [117]. Furthermore, solvent miscibility is a fundamental property that governs the applications of liquid mixtures [118]. While we have investigated only miscible solvent mixtures it remains unclear whether the theoretical methodology provides a valid means to describe immiscible solvents. Further possible extensions of the model could be the inclusion of solvent viscosity [119] or current noise [120]. Spin-dependent transport [121] is yet another important field of research. The spin degree of freedom can readily be included in the model Hamiltonian. Considering a coupling specific to the spin, such as, e.g., an external magnetic field or spin-orbit coupling, also magnetic effects can be studied within this theoretical framework. Accompanying the inclusion of spin, more than a single energy level of the molecule could be incorporated. Additionally, higher-order tunneling, such as cotunneling, can be investigated in a systematic way by calculating the quantum master

equation to second (or higher) order in the tunnel coupling. The inclusion of asymmetric tunnel barriers [122] could further be incorporated. The results of the ac-driven current can be easily extended to photon-assisted electron transport [116] in molecular wires given its mathematical form as under ac driving.

The list of possible extensions as well as investigations of novel transport characteristics could go on for several pages. This demonstrates, on the one hand, the versatility and broad range of application that the theoretical methodology offers. On the other hand, it shows the rich and exciting field of research that molecular electronics provides.

Appendix A.

Contour integral of the bosonic correlation function exponent

Here, we apply complex analysis to evaluate the frequency integral of the exponent $W(\tau)$ of the bosonic correlation function. To this extent, we utilize the theorem of residues for the contour integral. Let us start with the imaginary part $W''(\tau)$, for which we have to calculate the integral according to Eq. (4.25)

$$\int_0^\infty \mathrm{d}\omega \frac{\cos(\omega\tau_1)}{\omega^2+\omega_c^2} = \frac{1}{2}\int_{-\infty}^\infty \mathrm{d}\omega \frac{\cos(\omega\tau_1)}{\omega^2+\omega_c^2} \ . \tag{A.1}$$

Here, we have used, as a first step, that the integrand is an even function of ω. For the remaining integral we want to make use of the residue theorem. To this extent, we choose a closed contour in $\mathbb{C}$ and a complex function $f(z)$ which is related to our initial integrand. Let C be the closed contour with mathematically positive orientation in the upper half of the complex plane, as shown in red in Fig. A.1. It consists of two parts, the line segment on the real axis which runs from minus R to plus R and the semicircular arch C_R with radius R, where R is a large positive real number which we will later send to infinity in order to calculate our integral.

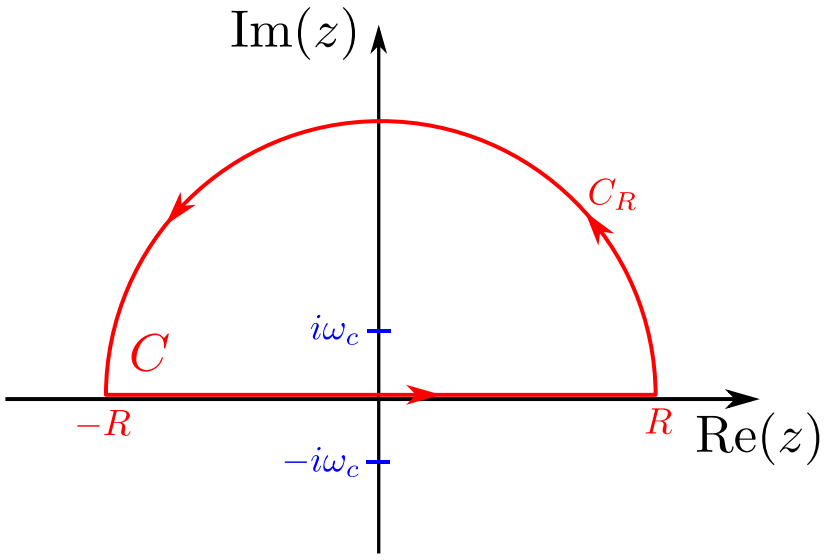

Figure A.1.: The closed contour C encloses the pole $z_1 = i\omega_c$ of $f(z)$.

To proceed, we want to calculate the contour integral

$$\oint_C \mathrm{d}z f(z) = \oint_C \mathrm{d}z \frac{e^{iz\tau_1}}{z^2+\omega_c^2} = \oint_C \mathrm{d}z \frac{e^{iz\tau_1}}{(z-i\omega_c)(z+i\omega_c)} \tag{A.2}$$

of the complex function $f(z)$ along the contour C. Since $f(z)$ is analytic everywhere on and within C except for the single isolated singularity $z_1 = i\omega_c$, we can apply the theorem of residues to calculate the contour integral which results in

$$\oint_C \mathrm{d}z f(z) = 2\pi i \mathrm{Res}(f(z), z_1)\,. \tag{A.3}$$

Here, $\mathrm{Res}(f(z), z_1)$ is the residue of $f(z)$ at z_1, which in this case is given by

$$\mathrm{Res}(f(z), z_1) = \lim_{z\to z_1}(z-z_1)f(z) = \lim_{z\to i\omega_c}(z-i\omega_c)\frac{e^{iz\tau_1}}{(z-i\omega_c)(z+i\omega_c)} = \frac{e^{-\omega_c\tau_1}}{2i\omega_c}\ . \tag{A.4}$$

We note that $f(z)$ has also a second isolated singularity $z_2 = -i\omega_c$, but since it is not enclosed by the contour, it does not contribute to the contour integral. Now that we have found the value of the complex contour integral, we want to make use of it for our initial real integral. When looking at the two parts of the contour integral, we can split the full contour and write

$$\oint_C \mathrm{d}z f(z) = \int_{-R}^{R} \mathrm{d}\omega f(\omega) + \int_{C_R} \mathrm{d}z f(z)\ , \tag{A.5}$$

where the first term on the right hand side stems from the line segment and the second term corresponds to the semicircular arch. Notice that, since the line segment runs from $-R$ to R along the real axis, we have replaced the complex variable by the real quantity ω for that part.

Let us have a look how the two separate parts look like. Starting with the line part, we get

$$\int_{-R}^{R} \mathrm{d}\omega f(\omega) = \int_{-R}^{R} \mathrm{d}\omega \frac{e^{i\omega\tau_1}}{\omega^2+\omega_c^2} = \int_{-R}^{R} \mathrm{d}\omega \frac{\cos(\omega\tau_1)}{\omega^2+\omega_c^2} + i\int_{-R}^{R} \mathrm{d}\omega \frac{\sin(\omega\tau_1)}{\omega^2+\omega_c^2}\ , \tag{A.6}$$

where we have used Euler's identity. We see that the imaginary part consists of an integrand which is odd in ω and therefore will be zero, because we integrate an odd function over an interval which is symmetric around the origin. When we then take the limit $R\to\infty$ in Eq. (A.6), we end up with our desired integral given in Eq. (A.1). What remains to be calculated is the integral over the semicircular arch. To do so, we first parameterize the path along the semicircular arch by $z = Re^{i\theta}$ with $\theta\in[0,\pi]$ and $\mathrm{d}z = iRe^{i\theta}\mathrm{d}\theta$. Then, the integral becomes

$$\int_{C_R} \mathrm{d}z f(z) = \int_0^{\pi} \mathrm{d}\theta iRe^{i\theta}\frac{e^{iR\tau_1 e^{i\theta}}}{R^2e^{2i\theta}+\omega_c^2}\ . \tag{A.7}$$

Next, we show that this integral approaches zero as R approaches infinity. We estimate the upper and lower bound by looking at the absolute value of the integral and use the triangle inequality. Since

$$\left| iRe^{i\theta} \frac{e^{iR\tau_1 \cos(\theta)} e^{-R\tau_1 \sin(\theta)}}{R^2 e^{2i\theta} + \omega_c^2} \right| = \frac{Re^{-R\tau_1 \sin(\theta)}}{|R^2 e^{2i\theta} + \omega_c^2|} \leq \frac{R}{R^2 - \omega_c^2} \, , \tag{A.8}$$

where we have utilized Euler's identity again. For the first equality, we have used the fact, that R, τ_1, and $\sin(\theta)$ are real positive values (for $\theta \in [0, \pi]$) and therefore the absolute value brackets of the nominator can be omitted. For the last inequality, we have employed the reverse triangle inequality for the denominator, i.e., $\left|R^2 e^{2i\theta} - (-\omega_c^2)\right| \geq \left|\left|R^2 e^{2i\theta}\right| - |\omega_c^2|\right|$, and also utilized that R is an arbitrarily large real number greater than ω_c. Thus, the absolute value brackets of the denominator can also be omitted. In total, we see that the absolute value of the integral over the semicircular arch is restricted by

$$0 \leq \left| \int_{C_R} \mathrm{d}z f(z) \right| \leq \frac{R}{R^2 - \omega_c^2} \int_0^\pi \mathrm{d}\theta = \frac{\pi R}{R^2 - \omega_c^2} \, , \tag{A.9}$$

and thus $\int_{C_R} \mathrm{d}z f(z) \to 0$ as $R \to \infty$. Finally, by putting everything together, we see that in the limit $R \to \infty$ of Eq. (A.5) together with Cauchy's residue theorem (A.3), we get an expression for our initial integral over ω, viz

$$\lim_{R\to\infty} \oint_C \mathrm{d}z f(z) = \lim_{R\to\infty} \left(\int_{-R}^{R} \mathrm{d}\omega f(\omega) + \int_{C_R} \mathrm{d}z f(z) \right) = \int_{-\infty}^{\infty} \mathrm{d}\omega \frac{\cos(\omega\tau_1)}{\omega^2 + \omega_c^2} = \frac{\pi}{\omega_c} e^{-\omega_c \tau_1} \, . \tag{A.10}$$

In the same manner, we can calculate the integral over the frequency ω for the real part of the bosonic correlation function exponent from Eq. (4.24). The only major difference of this part is the coth function for which we have to calculate additional residues in order to determine the contour integral. It turns out that these residues are given by the sum over the Matsubara frequencies appearing in Eq. (4.26). We further notice that the real part of $W(\tau)$ not only is an even function in ω but also in τ and the imaginary part is an odd function in τ, leading to the fact that $W(-\tau) = W^*(\tau)$. Thus, Eq. (A.10) should be the same whether we have $+\tau$ or $-\tau$. Consequently, we get the absolute value of τ in Eqs. (4.26) and (4.27) and the imaginary part obtains the signum function, see also Eq. (3.274) in Ref. [65].

Appendix B.

Dielectric solvent parameters

In Tab. B.1, we list the magnitudes of the static (ε_S) and high-frequency (ε_∞) dielectric constants as well as the dielectric relaxation times (τ_D) of the solvents considered in Section 5.6 and Section 6.4. The parameter values have been taken from literature, as indicated by the references in square brackets in the table.

Solvent	ε_S	ε_∞	τ_D (ps)
1,3,5-trimethylbenzene (TMB)	2.27 [123]	1.2	30.2 [124]
Toluene (TOL)	2.7 [102]	2.3 [102]	17.3 [102]
Chlorobenzene (CBZ)	6.2 [102]	3.3 [102]	16.8 [102]
Tetrahydrofuran (THF)	6.8 [125]	3.0	3.93 [125]
Butanol (BUT)	19.0 [102]	3.8 [102]	482 [102]
Ethanol (ETH)	25.4 [102]	4.9 [102]	168 [102]
Nitrobenzene (NBZ)	35.7 [102]	3.3 [102]	44.5 [102]
Acetonitrile (ACN)	35.8 [126]	8.5	3.37 [126]
Dimethylformamide (DMF)	38.5 [102]	10 [102]	14.6 [102]
Water (WAT)	78.4 [115]	5.2 [115]	8.27 [115]
Formamide (FOR)	110 [102]	5.3 [102]	35.9 [102]

Table B.1.: Magnitudes of the static and high-frequency dielectric constants as well as the dielectric relaxation times. The respective references are given in square brackets.

Bibliography

[1] F. Evers, R. Korytár, S. Tewari, and J. M. van Ruitenbeek, "Advances and challenges in single-molecule electron transport," *Rev. Mod. Phys.*, vol. 92, p. 035001, Jul 2020.

[2] M. Ratner, "A brief history of molecular electronics," *Nature nanotechnology*, vol. 8, no. 6, pp. 378–381, 2013.

[3] A. Aviram and M. A. Ratner, "Molecular rectifiers," *Chem. Phys. Lett.*, vol. 29, no. 2, pp. 277–283, 1974.

[4] K. S. Kwok and J. C. Ellenbogen, "Moletronics: Future electronics," *Mater. Today*, vol. 5, no. 2, pp. 28–37, 2002.

[5] L. Wang, L. Wang, L. Zhang, and D. Xiang, *Advance of Mechanically Controllable Break Junction for Molecular Electronics*, pp. 45–86. Cham: Springer International Publishing, 2019.

[6] R. Landauer, "Spatial variation of currents and fields due to localized scatterers in metallic conduction," *IBM Journal of research and development*, vol. 1, no. 3, pp. 223–231, 1957.

[7] R. Landauer, "Electrical resistance of disordered one-dimensional lattices," *Philosophical magazine*, vol. 21, no. 172, pp. 863–867, 1970.

[8] M. Büttiker, Y. Imry, R. Landauer, and S. Pinhas, "Generalized many-channel conductance formula with application to small rings," *Physical Review B*, vol. 31, no. 10, p. 6207, 1985.

[9] M. Büttiker, "Four-terminal phase-coherent conductance," *Physical review letters*, vol. 57, no. 14, p. 1761, 1986.

[10] M. Büttiker, "Symmetry of electrical conduction," *IBM Journal of Research and Development*, vol. 32, no. 3, pp. 317–334, 1988.

[11] R. Landauer, "Conductance determined by transmission: probes and quantised constriction resistance," *Journal of Physics: Condensed Matter*, vol. 1, no. 43, p. 8099, 1989.

[12] J. K. Sowa and R. A. Marcus, "On the theory of charge transport and entropic effects in solvated molecular junctions," *The Journal of Chemical Physics*, vol. 154, no. 3, 2021.

[13] J. K. Sowa, J. A. Mol, G. A. D. Briggs, and E. M. Gauger, "Beyond marcus theory and the landauer-büttiker approach in molecular junctions: A unified framework," *The Journal of chemical physics*, vol. 149, no. 15, 2018.

[14] H. Park, J. Park, A. K. Lim, E. H. Anderson, A. P. Alivisatos, and P. L. McEuen, "Nanomechanical oscillations in a single-C 60 transistor," *Nature*, vol. 407, no. 6800, pp. 57–60, 2000.

[15] X. Qiu, S. Rousseva, G. Ye, J. C. Hummelen, and R. C. Chiechi, "In operando modulation of rectification in molecular tunneling junctions comprising reconfigurable molecular self-assemblies," *Advanced Materials*, vol. 33, no. 4, p. 2006109, 2021.

[16] S. Y. Quek, M. Kamenetska, M. L. Steigerwald, H. J. Choi, S. G. Louie, M. S. Hybertsen, J. Neaton, and L. Venkataraman, "Mechanically controlled binary conductance switching of a single-molecule junction," *Nature Nanotechnology*, vol. 4, no. 4, pp. 230–234, 2009.

[17] S.-L. Lv, C. Zeng, Z. Yu, J.-F. Zheng, Y.-H. Wang, Y. Shao, and X.-S. Zhou, "Recent advances in single-molecule sensors based on stm break junction measurements," *Biosensors*, vol. 12, no. 8, p. 565, 2022.

[18] Z. Li, M. Smeu, S. Afsari, Y. Xing, M. A. Ratner, and E. Borguet, "Single-Molecule Sensing of Environmental pH—an STM Break Junction and NEGF-DFT Approach," *Angew. Chem. Int. Ed.*, vol. 53, no. 4, pp. 1098–1102, 2014.

[19] J. K. Sowa, J. A. Mol, and E. M. Gauger, "Marcus theory of thermoelectricity in molecular junctions," *J. Phys. Chem. C*, vol. 123, no. 7, pp. 4103–4108, 2019.

[20] N. A. Zimbovskaya, "Seebeck effect in molecular junctions," *Journal of Physics: Condensed Matter*, vol. 28, p. 183002, apr 2016.

[21] H. Kirchberg and A. Nitzan, "Energy transfer and thermoelectricity in molecular junctions in non-equilibrated solvents," *J. Chem. Phys.*, vol. 156, no. 9, p. 094306, 2022.

[22] I. Bunker, R. T. Ayinla, and K. Wang, "Single-molecule chemical reactions unveiled in molecular junctions," *Processes*, vol. 10, no. 12, p. 2574, 2022.

[23] H. Kirchberg, P. Nalbach, C. Bressler, and M. Thorwart, "Spectroscopic signatures of the dynamical hydrophobic solvation shell formation," *J. Phys. Chem. B*, vol. 123, no. 9, pp. 2106–2113, 2019. PMID: 30731041.

[24] D. Laage, T. Elsaesser, and J. T. Hynes, "Water dynamics in the hydration shells of biomolecules," *Chem. Rev.*, vol. 117, no. 16, pp. 10694–10725, 2017. PMID: 28248491.

[25] H. Kirchberg and M. Thorwart, "Time-resolved probing of the nonequilibrium structural solvation dynamics by the time-dependent stokes shift," *J. Phys. Chem. B*, vol. 124, no. 27, pp. 5717–5722, 2020. PMID: 32515195.

[26] K. Luka-Guth, S. Hambsch, A. Bloch, P. Ehrenreich, B. M. Briechle, F. Kilibarda, T. Sendler, D. Sysoiev, T. Huhn, A. Erbe, and E. Scheer, "Role of solvents in the electronic transport properties of single-molecule junctions," *Beilstein J. Nanotechnol.*, vol. 7, no. 1, pp. 1055–1067, 2016.

[27] Z. Tang, S. Hou, Q. Wu, Z. Tan, J. Zheng, R. Li, J. Liu, Y. Yang, H. Sadeghi, J. Shi, *et al.*, "Solvent-molecule interaction induced gating of charge transport through single-molecule junctions," *Sci. Bull.*, vol. 65, no. 11, pp. 944–950, 2020.

[28] V. Fatemi, M. Kamenetska, J. Neaton, and L. Venkataraman, "Environmental control of single-molecule junction transport," *Nano Lett.*, vol. 11, no. 5, pp. 1988–1992, 2011.

[29] E. Leary, H. Höbenreich, S. J. Higgins, H. Van Zalinge, W. Haiss, R. J. Nichols, C. Finch, I. Grace, C. Lambert, R. McGrath, and J. Smerdon, "Single-molecule solvation-shell sensing," *Phys. Rev. Lett.*, vol. 102, no. 8, p. 086801, 2009.

[30] S. Yeganeh, M. Galperin, and M. A. Ratner, "Switching in molecular transport junctions: polarization response," *J. Am. Chem. Soc.*, vol. 129, no. 43, pp. 13313–13320, 2007.

[31] H. Schoeller and G. Schön, "Mesoscopic quantum transport: Resonant tunneling in the presence of a strong coulomb interaction," *Physical Review B*, vol. 50, no. 24, p. 18436, 1994.

[32] J. König, H. Schoeller, and G. Schön, "Resonant tunneling and coulomb oscillations," *Europhys. Lett.)*, vol. 31, no. 1, p. 31, 1995.

[33] J. König, H. Schoeller, and G. Schön, "Zero-bias anomalies and boson-assisted tunneling through quantum dots," *Phys. Rev. Lett.*, vol. 76, pp. 1715–1718, 1996.

[34] J. König, J. Schmid, H. Schoeller, and G. Schön, "Resonant tunneling through ultrasmall quantum dots: Zero-bias anomalies, magnetic-field dependence, and boson-assisted transport," *Phys. Rev. B*, vol. 54, pp. 16820–16837, 1996.

[35] H. Schoeller, *Transport Theorie für wechselwirkende Quantenpunkte*. Habilitation thesis, Karlsruhe Institut für Technologie, Karlsruhe, 1997.

[36] R. Feynman and F. Vernon, "The theory of a general quantum system interacting with a linear dissipative system," *Annals of Physics*, vol. 24, pp. 118–173, 1963.

[37] A. Caldeira and A. J. Leggett, "Quantum tunnelling in a dissipative system," *Ann. Phys.*, vol. 149, no. 2, pp. 374–456, 1983.

[38] U. Weiss, *Quantum dissipative systems*, vol. 13. Singapore: World scientific, 2008.

[39] G. Binnig, H. Rohrer, C. Gerber, and E. Weibel, "Surface studies by scanning tunneling microscopy," *Physical review letters*, vol. 49, no. 1, p. 57, 1982.

[40] G. Binnig, H. Rohrer, C. Gerber, and E. Weibel, "Vacuum tunneling," *Physica B+ C*, vol. 109, pp. 2075–2077, 1982.

[41] E. Scheer and J. C. Cuevas, *Molecular Electronics: An Introduction To Theory And Experiment*, vol. 15. World Scientific, 2017.

[42] R. Wiesendanger, *Scanning probe microscopy and spectroscopy: methods and applications*. Cambridge university press, 1994.

[43] M. Rief, M. Gautel, F. Oesterhelt, J. M. Fernandez, and H. E. Gaub, "Reversible unfolding of individual titin immunoglobulin domains by afm," *science*, vol. 276, no. 5315, pp. 1109–1112, 1997.

[44] N. Agraıt, A. L. Yeyati, and J. M. Van Ruitenbeek, "Quantum properties of atomic-sized conductors," *Physics Reports*, vol. 377, no. 2-3, pp. 81–279, 2003.

[45] C. Muller, J. Van Ruitenbeek, and L. De Jongh, "Experimental observation of the transition from weak link to tunnel junction," *Physica C: Superconductivity*, vol. 191, no. 3-4, pp. 485–504, 1992.

[46] J. Moreland and J. Ekin, "Electron tunneling experiments using nb-sn "break"junctions," *Journal of applied physics*, vol. 58, no. 10, pp. 3888–3895, 1985.

[47] J. Chen, M. Reed, A. Rawlett, and J. Tour, "Large on-off ratios and negative differential resistance in a molecular electronic device," *science*, vol. 286, no. 5444, pp. 1550–1552, 1999.

[48] H. Park, A. K. Lim, A. P. Alivisatos, J. Park, and P. L. McEuen, "Fabrication of metallic electrodes with nanometer separation by electromigration," *Applied Physics Letters*, vol. 75, no. 2, pp. 301–303, 1999.

[49] M. L. Perrin, E. Burzurí, and H. S. van der Zant, "Single-molecule transistors," *Chem. Soc. Rev.*, vol. 44, no. 4, pp. 902–919, 2015.

[50] J. Park, A. N. Pasupathy, J. I. Goldsmith, C. Chang, Y. Yaish, J. R. Petta, M. Rinkoski, J. P. Sethna, H. D. Abruña, P. L. McEuen, *et al.*, "Coulomb blockade and the kondo effect in single-atom transistors," *Nature*, vol. 417, no. 6890, pp. 722–725, 2002.

[51] D. A. Ryndyk *et al.*, "Theory of quantum transport at nanoscale," *Springer Series in Solid-State Sciences*, vol. 184, p. 9, 2016.

[52] J. M. Thijssen and H. S. Van der Zant, "Charge transport and single-electron effects in nanoscale systems," *physica status solidi (b)*, vol. 245, no. 8, pp. 1455–1470, 2008.

[53] L. P. Kadanoff and G. A. Baym, *Quantum Statistical Mechanics Green's Function Methods in Equilibrium Problems*. Benjamin, 1962.

[54] L. V. Keldysh *et al.*, "Diagram technique for nonequilibrium processes," *Sov. Phys. JETP*, vol. 20, no. 4, pp. 1018–1026, 1965.

[55] G. Eliashberg, "Inelastic electron collisions and nonequilibrium stationary states in superconductors," *Sov Phys JETP*, vol. 34, no. 3, pp. 668–676, 1972.

[56] Y. Meir and N. S. Wingreen, "Landauer formula for the current through an interacting electron region," *Physical review letters*, vol. 68, no. 16, p. 2512, 1992.

[57] N. S. Wingreen, A.-P. Jauho, and Y. Meir, "Time-dependent transport through a mesoscopic structure," *Physical Review B*, vol. 48, no. 11, p. 8487, 1993.

[58] A.-P. Jauho, N. S. Wingreen, and Y. Meir, "Time-dependent transport in interacting and noninteracting resonant-tunneling systems," *Phys. Rev. B*, vol. 50, pp. 5528–5544, Aug 1994.

[59] J. König, H. Schoeller, and G. Schön, "Cotunneling and renormalization effects for the single-electron transistor," *Physical Review B*, vol. 58, no. 12, p. 7882, 1998.

[60] J. König, H. Schoeller, and G. Schön, "Cotunneling at resonance for the single-electron transistor," *Physical review letters*, vol. 78, no. 23, p. 4482, 1997.

[61] L. Onsager, "Electric moments of molecules in liquids," *J. Am. Chem. Soc.*, vol. 58, no. 8, pp. 1486–1493, 1936.

[62] J. Gilmore and R. H. McKenzie, "Spin boson models for quantum decoherence of electronic excitations of biomolecules and quantum dots in a solvent," *J. Physics: Condens. Mat.*, vol. 17, no. 10, p. 1735, 2005.

[63] H. G. A. Kirchberg, *Theory of dynamical solvent and guest-host correlated quantum dynamics*. PhD thesis, Staats-und Universitätsbibliothek Hamburg Carl von Ossietzky, 2020.

[64] A. Nitzan, *Chemical Dynamics in Condensed Phases*. Oxford: Oxford University Press, 2006.

[65] V. May and O. Kühn, *Charge and Energy Transfer Dynamics in Molecular Systems*. Weinheim: Wiley-VCH, 2011.

[66] J. Gladstone and T. P. Dale, "Researches on the refraction, dispersion, and sensitiveness of liquids," *P. R. Soc. London*, pp. 317–343, 1863.

[67] J. Gilmore and R. H. McKenzie, "Quantum dynamics of electronic excitations in biomolecular chromophores: role of the protein environment and solvent," *J. Phys. Chem. A*, vol. 112, no. 11, pp. 2162–2176, 2008.

[68] D. Laage, T. Elsaesser, and J. T. Hynes, "Water dynamics in the hydration shells of biomolecules," *Chemical Reviews*, vol. 117, no. 16, pp. 10694–10725, 2017.

[69] G. Gurski, H. Kirchberg, P. Nalbach, and M. Thorwart, "Single-molecule junctions sensitive to binary solvent mixtures," *Physical Review B*, vol. 106, no. 7, p. 075413, 2022.

[70] G. Gurski, H. Kirchberg, P. Nalbach, and M. Thorwart, "Hydration shell effects in ac-driven single-molecule junctions," *Physical Review B*, vol. 107, no. 16, p. 165413, 2023.

[71] L. P. Kouwenhoven, C. M. Marcus, P. L. McEuen, S. Tarucha, R. M. Westervelt, and N. S. Wingreen, "Electron transport in quantum dots," *Mesoscopic electron transport*, pp. 105–214, 1997.

[72] J. König, *Quantum Fluctuations in the Single-Electron Transistor*. PhD thesis, Universität Karlsruhe, 1998.

[73] Y. V. Nazarov and Y. M. Blanter, *Quantum transport: introduction to nanoscience*. Cambridge university press, 2009.

[74] J. Brüggemann, *Spin-polarized Transport in Nanoelectromechanical Systems*. PhD thesis, Staats-und Universitätsbibliothek Hamburg Carl von Ossietzky, 2015.

[75] K. Moth-Poulsen, *Handbook of single-molecule electronics*. Florida: CRC Press, 2016.

[76] R. Patel, Y. Agrawal, and R. Parekh, "Single-electron transistor: review in perspective of theory, modelling, design and fabrication," *Microsystem Technologies*, vol. 27, pp. 1863–1875, 2021.

[77] "Quantum dot." `https://www.sciencedaily.com/terms/quantum_dot.htm`. Accessed: 06-July-2020.

[78] M. A. Kastner, "Artificial atoms," *Phys. Today*, vol. 46, pp. 24–24, 1993.

[79] R. Ashoori, "Electrons in artificial atoms," *Nature*, vol. 379, no. 6564, pp. 413–419, 1996.

[80] J. Zhang, A. M. Kuznetsov, I. G. Medvedev, Q. Chi, T. Albrecht, P. S. Jensen, and J. Ulstrup, "Single-molecule electron transfer in electrochemical environments," *Chem. Rev.*, vol. 108, no. 7, pp. 2737–2791, 2008.

[81] P. Hyldgaard, S. Hershfield, J. H. Davies, and J. W. Wilkins, "Resonant tunneling with an electron-phonon interaction," *Ann. Phys.*, vol. 236, no. 1, pp. 1–42, 1994.

[82] E. Pavarini, E. Koch, R. Scalettar, and R. Martin, *The Physics of Correlated Insulators, Metals, and Superconductors*. Jülich: Forschungszentrum Jülich, 2017.

[83] I. Lang and Y. A. Firsov, "Kinetic theory of semiconductors with low mobility," *Sov. Phys. JETP*, vol. 16, no. 5, p. 1301, 1963.

[84] G. D. Mahan, *Many-particle physics*. New York: Springer Science & Business Media, 2000.

[85] J. Koch, *Quantum transport through single-molecule devices*. PhD thesis, Freie Universität Berlin, 2006.

[86] V. A. Leyton Ortega, *Quantum noise in nonlinear nanoscale systems out of equilibrium*. PhD thesis, Universität Hamburg, 2012.

[87] J. König, J. Schmid, H. Schoeller, and G. Schön, "Resonant tunneling through ultrasmall quantum dots: Zero-bias anomalies, magnetic-field dependence, and boson-assisted transport," *Phys. Rev. B*, vol. 54, no. 23, p. 16820, 1996.

[88] L. Valkunas, D. Abramavicius, and T. Mancal, *Molecular excitation dynamics and relaxation: quantum theory and spectroscopy*. Weinheim: John Wiley & Sons, 2013.

[89] M. Thoss, H. Wang, and W. H. Miller, "Self-consistent hybrid approach for complex systems: Application to the spin-boson model with debye spectral density," *J. Chem. Phys.*, vol. 115, no. 7, pp. 2991–3005, 2001.

[90] S. Kohler, J. Lehmann, and P. Hänggi, "Driven quantum transport on the nanoscale," *Physics Reports*, vol. 406, no. 6, pp. 379–443, 2005.

[91] S. Mukamel, *Principles of nonlinear optical spectroscopy*. New York: Oxford university press, 1995.

[92] I. S. Gradshteyn and I. M. Ryzhik, *Table of Integrals, Series, and Products*. Boston: Elsevier, 2007.

[93] N. Mann, *Nonequilibrium Fluctuations and Phase Transitions in Hybrid Quantum Systems*. PhD thesis, Universität Hamburg, 2019.

[94] H. Fröhlich, "Electrons in lattice fields," *Advances in Physics*, vol. 3, no. 11, pp. 325–361, 1954.

[95] H. G. A. Kirchberg, *Theory of dynamical solvent and guest-host correlated quantum dynamics*. PhD thesis, Universität Hamburg, 2020.

[96] C.-P. Hsu, X. Song, and R. Marcus, "Time-dependent stokes shift and its calculation from solvent dielectric dispersion data," *J. Phys. Chem. B*, vol. 101, no. 14, pp. 2546–2551, 1997.

[97] C. J. F. Böttcher and P. Bordewijk, *Theory of electric polarization*, vol. 1. Amsterdam: Elsevier Science Limited, 1973.

[98] R. Kubo, "The fluctuation-dissipation theorem," *Rep. Prog. Phys.*, vol. 29, no. 1, p. 255, 1966.

[99] C.-P. Hsu, "Reorganization energies and spectral densities for electron transfer problems in charge transport materials," *Phys. Chem. Chem. Phys.*, vol. 22, no. 38, pp. 21630–21641, 2020.

[100] V. A. Markel, "Introduction to the Maxwell Garnett approximation: tutorial," *JOSA A*, vol. 33, no. 7, pp. 1244–1256, 2016.

[101] E. Tuncer, Y. V. Serdyuk, and S. M. Gubanski, "Dielectric mixtures: electrical properties and modeling," *IEEE Transactions on Dielectrics and Electrical Insulation*, vol. 9, no. 5, pp. 809–828, 2002.

[102] J. Lou, T. A. Hatton, and P. E. Laibinis, "Effective dielectric properties of solvent mixtures at microwave frequencies," *J. Phys. Chem. A*, vol. 101, no. 29, pp. 5262–5268, 1997.

[103] C. Reichardt and T. Welton, *Solvents and solvent effects in organic chemistry*. Weinheim: Wiley-VCH Verlag & Co. KGaA, 2011.

[104] L. J. Richter, C. S.-C. Yang, P. T. Wilson, C. A. Hacker, R. D. van Zee, J. J. Stapleton, D. L. Allara, Y. Yao, and J. M. Tour, "Optical characterization of oligo(phenylene-ethynylene) self-assembled monolayers on gold," *J. Phys. Chem. B*, vol. 108, no. 33, pp. 12547–12559, 2004.

[105] Y. Li, J. Zhao, and G. Yin, "Theoretical investigations of oligo(phenylene ethylene) molecular wire: Effects from substituents and external electric field," *Comp. Mater. Sci.*, vol. 39, no. 4, pp. 775–781, 2007.

[106] K. Selvaraju, M. Jothi, and P. Kumaradhas, "Exploring the charge density distribution and the electrical characteristics of oligo phenylene ethylene molecular nanowire using quantum chemical and charge density analysis," *Comput. Theor. Chem.*, vol. 996, pp. 1–10, 2012.

[107] H. Lissau, R. Frisenda, S. T. Olsen, M. Jevric, C. R. Parker, A. Kadziola, T. Hansen, H. S. J. van der Zant, M. Brøndsted Nielsen, and K. V. Mikkelsen, "Tracking molecular resonance forms of donor–acceptor push–pull molecules

by single-molecule conductance experiments," *Nat. Commun.*, vol. 6, no. 1, p. 10233, 2015.

[108] R. Frisenda, S. Tarkuc, E. Galan, M. L. Perrin, R. Eelkema, F. C. Grozema, and H. S. J. van der Zant, "Electrical properties and mechanical stability of anchoring groups for single-molecule electronics," *Beilstein J. Nanotechnol.*, vol. 6, pp. 1558–1567, 2015.

[109] S. Braig and K. Flensberg, "Vibrational sidebands and dissipative tunneling in molecular transistors," *Phys. Rev. B*, vol. 68, no. 20, p. 205324, 2003.

[110] C. W. Beenakker, "Theory of coulomb-blockade oscillations in the conductance of a quantum dot," *Physical Review B*, vol. 44, no. 4, p. 1646, 1991.

[111] H. Bruus and K. Flensberg, *Many-body quantum theory in condensed matter physics: an introduction.* Oxford: Oxford University Press, 2004.

[112] A. Rondi, Y. Rodriguez, T. Feurer, and A. Cannizzo, "Solvation-driven charge transfer and localization in metal complexes," *Acc. Chem. Res.*, vol. 48, no. 5, pp. 1432–1440, 2015.

[113] P. Nalbach, A. Achner, M. Frey, M. Grosser, C. Bressler, and M. Thorwart, "Hydration shell effects in the relaxation dynamics of photoexcited fe-ii complexes in water," *J. Chem. Phys.*, vol. 141, no. 4, p. 044304, 2014.

[114] R. Buchner, J. Barthel, and J. Stauber, "The dielectric relaxation of water between 0 c and 35 c," *Chemical Physics Letters*, vol. 306, no. 1-2, pp. 57–63, 1999.

[115] U. Kaatze, "Complex permittivity of water as a function of frequency and temperature," *J. Chem. Eng. Data*, vol. 34, no. 4, pp. 371–374, 1989.

[116] G. Platero and R. Aguado, "Photon-assisted transport in semiconductor nanostructures," *Phys. Rep.*, vol. 395, no. 1-2, pp. 1–157, 2004.

[117] N. An, B. Zhuang, M. Li, Y. Lu, and Z.-G. Wang, "Combined theoretical and experimental study of refractive indices of water–acetonitrile–salt systems," *The Journal of Physical Chemistry B*, vol. 119, no. 33, pp. 10701–10709, 2015.

[118] B. Zhuang, G. Ramanauskaite, Z. Y. Koa, and Z.-G. Wang, "Like dissolves like: A first-principles theory for predicting liquid miscibility and mixture dielectric constant," *Science Advances*, vol. 7, no. 7, p. eabe7275, 2021.

[119] M. F. Gelin and D. S. Kosov, "A model for dynamical solvent control of molecular junction electronic properties," *J. Chem. Phys.*, vol. 154, no. 4, p. 044107, 2021.

[120] H. Kirchberg and A. Nitzan, "Noise and thermodynamic uncertainty relation in "underwater" molecular junctions," *The Journal of Chemical Physics*, vol. 157, no. 18, 2022.

[121] Z. Ning, Y. Zhu, J. Wang, and H. Guo, "Quantitative analysis of nonequilibrium spin injection into molecular tunnel junctions," *Physical review letters*, vol. 100, no. 5, p. 056803, 2008.

[122] H. Inokawa and Y. Takahashi, "A compact analytical model for asymmetric single-electron tunneling transistors," *IEEE Transactions on Electron Devices*, vol. 50, no. 2, pp. 455–461, 2003.

[123] J. Crossley and S. Walker, "Dielectric studies. Part XVIII. Dipole moments and relaxation times of some symmetrically substituted alkylbenzenes," *Can. J. Chem.*, vol. 46, no. 6, pp. 847–851, 1968.

[124] S. Vaish and N. Mehrotra, "Correlation of NMR spin lattice and dielectric relaxation times of some methyl benzenes," *Indian J. Pure Ap. Phy.*, vol. 37, pp. 881–884, 1999.

[125] A. Chaudhari, P. Khirade, R. Singh, S. Helambe, N. Narain, and S. Mehrotra, "Temperature dependent dielectric relaxation study of tetrahydrofuran in methanol and ethanol at microwave frequency using time domain technique," *J. Mol. Liq.*, vol. 82, no. 3, pp. 245–253, 1999.

[126] J. Barthel, M. Kleebauer, and R. Buchner, "Dielectric relaxation of electrolyte solutions in acetonitrile," *J. Solution Chem.*, vol. 24, no. 1, pp. 1–17, 1995.

Acknowledgment

First, I would like to express my gratitude to Prof. Dr. Michael Thorwart for offering me the opportunity to be part of his group and providing me with this interesting topic for my PhD-project. His support, sheer patience and motivating words gave me strength throughout the whole PhD-period.

I also want to thank Prof. Dr. Peter Nalbach for his support especially in the beginning and during important stages of this project. His helpful hints and advices amid challenging tasks were spot-on so I could proceed and stay target-oriented in the course of this work.

My special thanks are expressed to Dr. Henning Kirchberg for many fruitful discussions via zoom during his stay in the USA. Thanks to our regular zoom-meetings and his insightful suggestions I was able to stay on track and gain deeper knowledge in this very broad field of research. His feedback and recurring questions forced me to dig deeper and gain a better understanding of the discussed topics. I also thank him for proofreading this thesis.

For proofreading and helpful hints I am also obliged to Dr. Thore Posske.

Furthermore, I thank Dr. Niklas Mann for his help and support at the beginning of my PhD-project. Especially his shared program code, which I extended and adjusted for my simulations, provided me an excellent introduction to the numerical implementation of the theoretical model.

To all members of the group, I want to express warm thanks and appreciation for interesting talks at the group seminars as well as for the discussions about everything and anything during lunch break. Especially the group retreat to Kloster Kirchberg and the cozy Christmas parties with self-made Chinese food, Feuerzangenbowle, or a very special Rudolph for dinner will be remembered.

I thank Cindy Horn for keeping me company throughout the bigger part of this project. Ty wiesz, co dla mnie znaczysz.

Finally, I thank my family and friends for their constant support and understanding.

Eidesstattliche Versicherung / Declaration on oath

Hiermit versichere ich an Eides statt, die vorliegende Dissertationsschrift selbst verfasst und keine anderen als die angegebenen Hilfsmittel und Quellen benutzt zu haben.

Hamburg, den 8. Dezember 2023

Gregor Gurski

Publikationsliste / List of publications

G. Gurski, H. Kirchberg, P. Nalbach, and M. Thorwart, "Single-molecule junctions sensitive to binary solvent mixtures," *Physical Review B*, vol. **106**, no. 7, p. 075413, 2022.

G. Gurski, H. Kirchberg, P. Nalbach, and M. Thorwart, "Hydration shell effects in ac-driven single-molecule junctions," *Physical Review B*, vol. **107**, no. 16, p. 165413, 2023.